Functionalized Hybrid Ceramic Membranes for Organic Solvent Nanofiltration

Amirilargani, Mohammad

DOI
10.4233/uuid:2c3f8d00-ca74-4028-a02b-050922ba7aa3

Publication date
2019

Document Version
Final published version

Citation (APA)
Amirilargani, M. (2019). *Functionalized Hybrid Ceramic Membranes for Organic Solvent Nanofiltration*. [Dissertation (TU Delft), Delft University of Technology]. https://doi.org/10.4233/uuid:2c3f8d00-ca74-4028-a02b-050922ba7aa3

Functionalized Hybrid Ceramic Membranes for Organic Solvent Nanofiltration

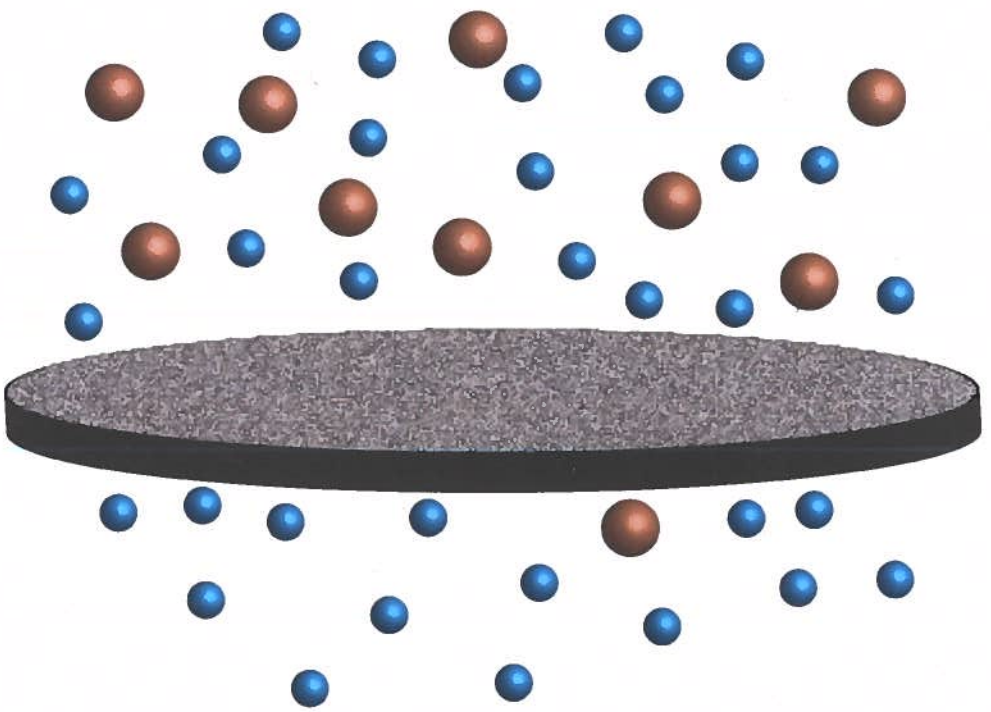

Mohammad Amirilargani

Propositions accompanying the PhD thesis:

Functionalized Hybrid Ceramic Membranes for Organic Solvent Nanofiltration

By Mohammad Amirilargani

1. Unintended scientific observations trigger to open up horizons (Chapter 2 of this thesis).

2. Separation performances of membranes are often poisoned by non-recognised adsorption, making them unreliable (Chapters 2 and 4 of this thesis)

3. Simple equipment having limited sources of errors provides more clarity on the complexity behind the data.

4. Emotional intelligence is a key component for successful academic collaborations.

5. "We cannot solve our problems with the same way of thinking used when we created them". *Albert Einstein*

6. The yield of a successful polymerization reaction is related to the hours of night rest of the experimentalist performing the reaction.

7. A simple Friday afternoon experiment lasts at least one week.

8. Permanent contracts should be conditional, based on employee performance.

9. Scientists are directly responsible for of the socio-economic impacts of their discoveries.

10. "Art is a lie that makes you realise truth" by *Pablo Picasso* is well applicable in engineering where computer simulations often surprisingly predict or confirm experimental data.

These propositions are regarded as opposable and defendable, and have been approved as such by the promotor, Prof. dr. E.J.R. Sudhölter and copromotor, Dr. L.C.P.M. de Smet

Functionalized Hybrid Ceramic Membranes for Organic Solvent Nanofiltration

Proefschrift

ter verkrijging van de graad van doctor

aan de Technische Universiteit Delft,

op gezag van de Rector Magnificus prof. dr. ir. T.H.J.J. van der Hagen,

voorzitter van het College voor Promoties,

in het openbaar te verdedigen op

donderdag 10 oktober 2019 om 12:30 uur

door

Mohammad AMIRILARGANI

Master of Science in Chemical Engineering, Iran University of Science and Technology, Iran

Geboren te Noshahr, Iran

Dit proefschrift is goedgekeurd door de promotoren
Prof. dr. E.J.R. Sudhölter en dr. ir. L.C.P.M. de Smet

Samenstelling van de promotiecommissie:

Rector Magnificus	Voorzitter
Prof. dr. E.J.R. Sudhölter	Technische Universiteit Delft, promotor
Dr. ir. L.C.P.M. de Smet	Wageningen University & Research, copromotor

Onafhankelijke leden

Prof. dr. J.H. van Esch	Technische Universiteit Delft
Prof. dr. J.J.C. Geerlings	Technische Universiteit Delft
Prof. dr. S.J. Picken	Technische Universiteit Delft
Prof. dr. A.P.H.J. Schenning	Technische Universiteit Eindhoven

Overig lid

Prof. dr. A.J.A. Winnubst	Universiteit Twente/University of Science and Technology of China

This research work was part of the research program entitled 'Modular Functionalized Ceramic Nanofiltration Membranes' (BL-20-10), which was conducted within the framework of the Institute for Sustainable Process Technology (ISPT) and was jointly financed by the Netherlands Organization for Scientific Research (NWO) and ISPT.

Proefschrift, Technische Universiteit Delft
Met samenvatting in het Nederlands
ISBN: 978-94-6384-066-8

Ontwerp omslag: Mohammad Amirilargani
Gedrukt door Ipskamp Printing, Enschede

To my family

"Mindfulness is a pause, the space between stimulus and response: that's where choice lies."
Tara Brach

Table of Contents

Chapter 1

Introduction to organic solvent nanofiltration (OSN) membranes and surface modification techniques

This chapter is an adapted version of the review paper:

M. Amirilargani, M. Sadrzadeh, E.J.R. Sudhölter, L.C.P.M. de Smet, *Chem. Eng. J.*, 289 **(2016)** 562-582.

Organic solvent nanofiltration (OSN) is an emerging technology in which membranes are used for organic solvents purification. Fields of applications range from pharmacy, catalyst regeneration, to oil and solvent treatments. A major challenge is to maintain a high stability of these (modified) membranes under different feed and process conditions. Tailoring the selective layer of OSN membranes is the main approach to develop functionalized membranes, which show stable and high rejections and permeabilities. During the past decade, methods such as grafting, light-induced modification, plasma treatment, and modification by polyelectrolytes have been intensively studied. This chapter gives an overview of surface modification of different types of polymeric and ceramic OSN membranes. The most crucial surface layer properties that affect the OSN membranes properties are described in detail. In addition, different surface modification methods and their effects on solute rejection and solvent permeability are reviewed and compared.

1.1 General Introduction

Nowadays chemical separations are playing crucial roles in processes of the chemical, petrochemical, pharmaceutical and food industries [1]. Membrane-based separation processes have attracted significant attention in industrial applications due to their distinct advantages over traditional separation processes like distillation and extraction. This is primarily due to their better separation performance, the lower size and costs of the equipment used, and a much improved energy efficiency [2-4]. Nanofiltration (NF) membranes with separation properties between those of ultrafiltration (UF) and reverse osmosis (RO) membranes (pore size < 0.5 nm), were first explored in the late 1980's [5, 6]. Although NF membranes have been widely applied for water and wastewater treatment processes [7], their application for organic solvent nanofiltration (OSN), sometimes also referred to as solvent-resistant nanofiltration (SRNF) or organophilic NF, is a rather new technology [1]. OSN has a great potential to be employed in a wide range of processes related to, *e.g.* food [8-10], fine chemical [11-13], pharmaceutical [14-16] and petrochemical industries [17-19] for the treatment of organic solvents. Within the Scopus database a total number of 335 papers in indexed journals was found on keywords related to the topic of OSN membranes starting from 2009 (Figure 1.1). More than two third of these papers appeared over the last five years, showing the growing interest in OSN membranes.

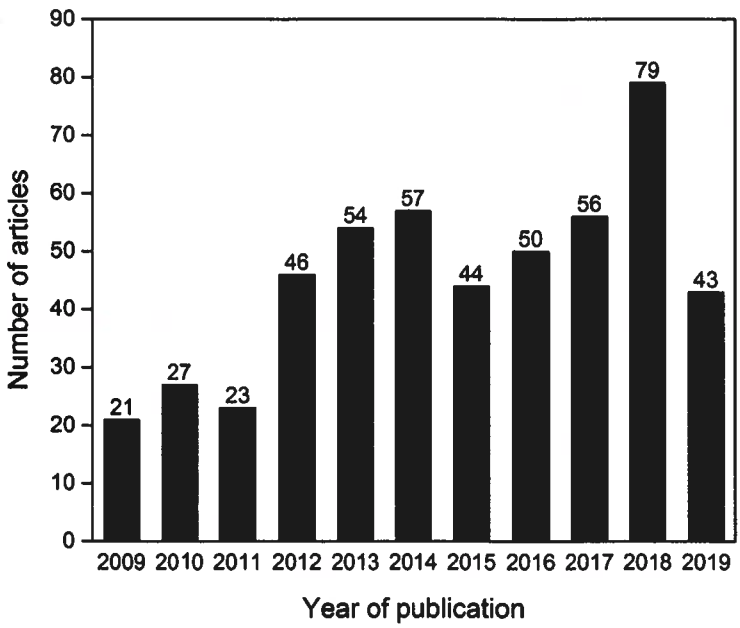

Figure 1.1 Record of the number of publications in indexed journals containing the keywords "organic solvent nanofiltration" or "solvent resistant nanofiltration" or "organophilic nanofiltration" in title, abstract and keywords between 2009 and 2019. (Source: Scopus, searched on 14 June, 2019).

The compatibility of these membranes under extreme operating conditions like harsh and aggressive media, elevated pH and high temperatures, while maintaining a reasonable long-term separation performance and reproducibility is the main challenge in the further development of OSN membranes. In such membranes, solute discrimination occurs in the surface (top) layer at the molecular level. The final performance is determined by solute/solvent interactions with the membrane top layer [6]. In addition, it is well established that solvent-membrane surface interactions, which can vary with solvent composition, play a key role in the permeation properties of NF membranes [20, 21]. Hence, specific modification of the membrane selective layer becomes important in order to obtain the desired high-performance OSN membranes. In addition, exploring novel and viable approaches to synthesize thermally/chemically stable OSN membranes is another challenging research area. Indeed, during the last decade, several techniques were employed to improve the separation properties of OSN membranes (mainly polymeric membranes) without sacrificing their permeation properties.

1.2 The concept of organic solvent nanofiltration

OSN is an energy-efficient and sustainable separation process that allows the separation of organic mixtures by simply applying a pressure gradient over the membrane [22]. About one decade ago, Mulder [23] classified membranes based on the pressure required for the separation. According to this classification, a pressure between 5 to 20 bar is applied for NF membranes. However, nowadays, most of the NF membranes are employed at higher pressure up to 40 bar [1].

Both organic (polymeric) and inorganic materials have been widely used for the preparation of OSN membranes. The mechanical, chemical and thermal stability of these materials is one of the most important factors having a crucial impact on the final performance of OSN membranes [22]. Solvent stability and swelling resilience of polymer materials significantly affect the performance of OSN membranes. In general, polymers lose their physical integrity in contact with the organic solvent due to their tendency to swell or dissolve [2, 24]. However, polymeric OSN membranes must demonstrate continuous long-time operation stability in harsh solvents, while preserving their separation properties. Hence, development of new polymeric materials with superior resistance towards organic solvents such as polyimides [25, 26], poly(1-trimethylsilyl-1-propyne) (PTMSP) [27-29] and polymers with intrinsic microporosity (PIMs) [27, 30] has become one of the most interesting research areas in the field of current membrane science and technology. Several overviews of extensively used polymeric materials for the preparation of OSN membrane are presented elsewhere [1, 2, 6, 14].

Tsuru *et al.* [31, 32] prepared the first ceramic OSN membrane from silica-zirconia. Titania, made by a sol-gel method, was also used to fabricate OSN membranes [33]. Utilizing ceramic materials for the preparation of OSN membranes have a great potential due to several advantages over polymeric

materials, such as a primarily high solvent stability, and their resistance to compaction, and swelling. However, the high costs of ceramic membranes and their low organic solvent rejection properties limit their application in OSN [34]. Hence, surface modification and functionalization techniques have been performed to adjust the surface chemistry (hydrophilicity/hydrophobicity) of ceramic NF membranes in order to improve their separation performance.

In addition to the examples mentioned above, also hybrid organic/inorganic membranes exist. For example, mixed matrix membranes (MMMs), consist of inorganic fillers dispersed in a polymer matrix, have been studied for gas separation purposes [35]. Also, thin film nanocomposite (TFN) membranes, containing dispersed nanoparticles, on a porous support have received a growing research interest in recent years [36].

1.3 Surface layer properties influencing the OSN membrane performance

Surface (top layer) properties of membranes such as surface charge, hydrophilicity/hydrophobicity and surface roughness are the most important factors affecting permeation and separation performances of OSN membranes [1, 37]. These characteristics determine the affinity of the membrane selective layer towards solvent/solute. In order to synthesize high-performance OSN membranes, surface properties must be tuned based on the properties of solvent and/or solute. To have a better understanding of the mutual interactions between membranes and solvent/solute, we briefly review the membrane surface properties in the next paragraph with a focus on surface charge (Section 1.3.1), surface hydrophilicity/hydrophobicity (Section 1.3.2) and surface roughness (Section 1.3.3). These different surface properties are summarized schematically in Figure 1.2.

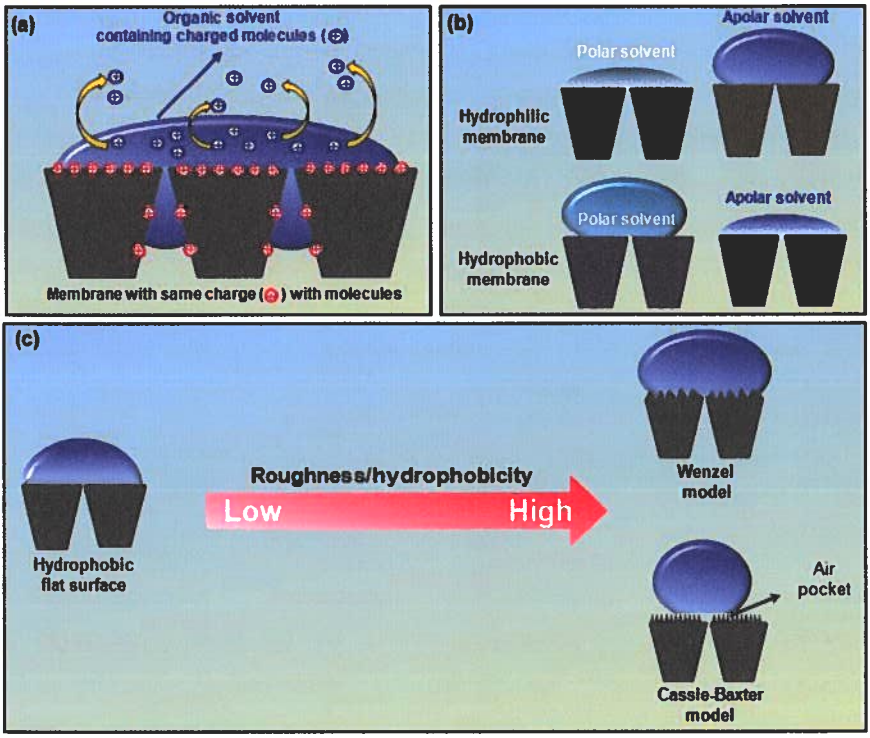

Figure 1.2 Surface layer properties that influence the performance of OSN membranes: (a) surface charge, (b) hydrophilic/hydrophobic properties, and (c) surface roughness.

1.3.1 Surface charge

Depending on the interaction between the membrane and solvent/solute, the effective membrane surface charge could be an dominant factor that influences the membrane performance using charged solutes [38]. Based on the Debye–Hückel theory [39] the thickness of an electrical double layer around an ion is proportional to the square root of the dielectric constant of the surrounding medium. This means that in solvents with a higher dielectric constants, the charge effects are exerted over a longer distance. In the case of polar solvents such as methanol (MeOH) and *iso*-propyl alcohol (IPA) with dielectric constants (ε_r) of 32.6 and 18.3, respectively, the influence of charge is more significant compared to apolar solvents such as toluene with $\varepsilon_r = 2.38$ [40, 41].

In NF membranes, the sieving effect (size exclusion) is the key factor for rejection behavior of uncharged organic molecules, while the separation performance for charged molecules is dominated by electro-static effects [42]. For example, Ahmadiannamini *et al.* [43] studied polyelectrolyte multilayer (PEM) membranes with top layers having different types of charge in combination with

charged solutes. Donnan exclusion (exclusion of ions of the same charge) was found to be the main factor in explaining the high rejections for PEM membrane/solute combinations having the same type of charge. On the contrary, they observed a surprisingly high value of rejection for the PEM membranes with positively charged capping layers for the separation of negatively charged Rose Bengal (RB) dye molecules IPA. They concluded that the negatively charged RB strongly binds to the membrane surface and formed an extra layer that neutralizes the positive surface charge and in this way improved the rejection of RB from IPA due to the Donnan exclusion. Marchetti *et al.* [21] explained that solute-membrane affinity is a function of the chemical nature of the molecules, electro-static (Donnan potential) interactions between solute and membrane charge, composition of the solvent mixture and concentration of salts/ions. Donnan effects were extensively studied in aqueous systems [44] and also these electro-static interactions have been studied for OSN membranes [38, 45, 46].

Contradictory findings are reported in the literature on the correlation between the membrane rejection and solute charge properties. Bhanushali *et al.* [45] observed higher rejection of both negatively (Orange II, *MW* = 350 Da) and positively (Safranin O, *MW* = 350 Da) charged solutes compared to an electrical neutral solute (Solvent Blue 35, *MW* = 350 Da) all in MeOH and using a hydrophobic MPF-60 membrane and attributed this to the solute/membrane charge effects. In contrast, Zhao and Yuan [38] observed higher rejections of neutral molecules (Soybean Daidzin) over charged solutes (Crystal violet and Acid blue 25) in MeOH using a hydrophilic Desal-DK membrane. They concluded that the rejection results strongly depend on the interaction between the type of solvent (polarity), solute (charge), and membrane (hydrophilicity). It is worth noting that charge effects become a decisive factor in determining the rejection of the molecules in NF membranes, when the molecular size of the organic molecules are much smaller than the membrane pores [38, 47]. Even in this case the charge of both membrane surface and organic molecule are essential. Van der Bruggen *et al.* [47] proposed that for a negatively charged membrane, the Donnan exclusion of negatively charged solutes from the membrane increases the rejection, while positively charged solutes might even experience a lower rejection than neutral molecules of similar size. Overall, the solute and membrane charges can increase or decrease the rejection because of electro-static interactions.

It should be highlighted that the mechanism of the surface charge in organic solvents strongly depends on the type of solvent [48]. For instance, acid-base interactions are the main reason for surface charge formation in protic solvents such as alcohols similar to those in water and involving protons as the potential-determining ion. It was observed that the relative acidity of the liquids and the surface hydroxyl groups are the key factors to define the value of surface charge in the diluted solutions. Otherwise, electron donor-electron acceptor interactions determine the surface charge in dipolar aprotic liquids, like dimethyl sulfoxide (DMSO) and dimethyl formamide (DMF).

1.3.2 Surface hydrophilicity/hydrophobicity

The solvent wettability can influence the overall performance of OSN membranes. For example, the combination of the solvent polarity and the hydrophilicity of the membrane determines the permeation properties of alcohols and alkanes through a hydrophilic RO membrane (Osmonics DS11) and a hydrophobic NF membrane (MPF-50) [49]. It has been demonstrated that the permeability of polar solvents in hydrophilic membranes was 8–10 times higher than that of non-polar solvents, whereas in hydrophobic membranes the permeability of non-polar solvents was 2-4 times higher than for polar solvents.

Zhao and Yuan [38] reported higher rejection of neutral molecules in water than in organic solvents for hydrophilic NF membranes, while in the case of hydrophobic membranes the opposite trend was observed. This result matches well with studies of Yang *et al.* [46] and Geens *et al.* [50] that report on rejections of charged and neutral molecules being lower in organic solvents than in water for only hydrophilic membranes, but not for hydrophobic membranes. The "hydration/solvation" mechanism was proposed to explain this behaviour, which affects the relative solute-membrane *versus* solvent-membrane molecular affinity [46]. In highly hydrophobic membranes the interaction with water molecules is very low (*i.e.* no hydration of the membrane) and the solvation of the pores of the membrane with MeOH decreases the effective pore size, thus leading to a higher rejection in organic solvents than in water. However, for hydrophilic membranes the solvation by water (hydration) becomes more significant than solvation by organic solvents, resulting in a smaller effective pore size in water compared to organic solvents. In two separate studies, Zhao and Yuan [38] and Yang *et al.* [46] also reported negligible charge effects during NF of charged solutes in MeOH. These results clearly show that the interaction between the solute–membrane–solvent is different in aqueous and organic systems.

Over the past 10 years the research group of Van der Bruggen published a number of interesting studies covering the investigation of OSN membrane wetting effects on the separation/permeation properties [50-55]. They observed that apolar solvents with a low surface tension showed higher (lower) flux by using hydrophobic (hydrophilic membranes). On the other hand, polar solvents with a high surface tension yielded lower (higher) flux by applying hydrophobic (hydrophilic) membranes.

It should be highlighted that the interaction between a membrane surface and solvent is strongly dependent on the hydrophilicity/hydrophobicity and surface tension respectively [49, 51-53, 55, 56]. As a consequence of weaker interactions between solvent/solute and the surface of hydrophobic membranes, it has been demonstrated that using solvents with a higher surface tension results in higher fluxes through hydrophilic membranes, but lower fluxes through hydrophobic membranes.

In another study, Van Gestel *et al.* [54] showed that the modification of membranes with higher molecular weight silanes (C_8 silane) enhanced the n-hexane permeability more significantly as

compared to lower molecular weight silanes (C_1 silane). They attributed this to the formation of more hydrophobic pores with a higher affinity toward n-hexane or cyclohexane by attachment of a longer alkyl chain to the walls of the pores. As an important remark we note that a large variety of surface modification methods using silane chemistry do exist [57, 58], and that care should be taken on the preparation conditions when one aims for the formation of a true, high-quality monolayer rather than thicker layers with a higher roughness that may be formed due to oligomerization [59].

In summary, the solvent wettability of membranes plays a key role in the separation performance of organic solvents at a molecular level, as it strongly influences the solvent-membrane and solute-membrane interactions.

1.3.3 Surface roughness

Next we discuss the surface roughness, as it is an important structural property of OSN membranes. It is typically measured by atomic force microscopy (AFM) and reflected in terms of the average roughness (S_a), the root mean square of the roughness data (S_q) and the mean difference between the highest peaks and the lowest valleys (S_z) [1]. To understand the effects of surface roughness on the wettability of solid surfaces, the well-known Wenzel [60] and Cassie-Baxter [61] models have been proposed. According to these models, there are two regimes of wetting of a rough surface: (I) a homogeneous regime with a two-phase solid–liquid interface and (II) a non-homogeneous or composite regime with a three phase solid–air-liquid interface in which the air pockets are trapped between the solid surface and liquid (Figure 1.2) [62, 63]. In Wenzel's model, the liquid completely fills the rough structure of the solid surface and increasing the surface roughness makes hydrophobic surfaces more hydrophobic and hydrophilic surfaces more hydrophilic. The Cassie-Baxter model describes that the liquid drop sits on the top asperities of a dual scale surface structure and air is trapped in the rough structure underneath the liquid, increasing the water contact angle. Work by Peyravi *et al.* [64] demonstrated that the loading of amine-functionalized TiO_2 nanoparticles into a polyamide (PA) thin layer increased the surface roughness as well as the surface hydrophilicity. Furthermore, they concluded that the effect of incorporated TiO_2 nanoparticles on the membrane surface roughness was more significant than on the surface chemistry. These findings indicate the membrane performance can be controlled by changing the surface roughness. Namvar-Mahboub *et al.* [65] and Jadav *et al.* [66] reported similar results by measuring a lower membrane surface roughness upon loading a lower amounts of nanoparticles into a polymeric matrix, while at higher loadings it increased due to the agglomeration of these nanoparticles.

It is noteworthy to say that the surface roughness scales with the overall surface area and consequently also with the permeation flux. For instance, Sun *et al.* [67] showed that the addition of triethylamine (TEA) and camphor sulfonic acid (CSA) into the m-phenylenediamine (MPD) solution during an interfacial polymerization reaction enhanced the surface roughness of the synthesized PA

membranes as well as the surface area, and consequently increases the permeation flux through the membrane. However, it must be noted that, there is always a trade-off relationship between the surface area and the fouling ability of membranes by increasing the surface roughness.

On the one hand, water flux increases upon increasing roughness as the effective surface area becomes larger; on the other hand, the flux may decreases because of increasing fouling. It is well-known that the more rough the surfaces is, the higher the surface area and therefore a higher fouling can be expected. For example, clogging of valleys on the membrane surface was found to result in a significant loss of permeate flux [68].

In summary, Sections 1.3.1 to 1.3.3 describe the importance of the surface membrane properties on the permeation/separation performance of OSN membranes. The surface charge, roughness and wettability affect the solute-solvent-membrane interactions and will influence the final separation performance.

1.4 Surface modification methods of OSN membranes

1.4.1 Modification of polymeric OSN membranes

Most of the polymeric membranes used in OSN have an asymmetric structure that consists of a porous sublayer which provides the mechanical strength and a dense skin layer that plays the main role in the separation processes [6]. These asymmetric membranes are divided into two major categories, (i) integrally skinned asymmetric (ISA), and (ii) thin film composites (TFC) membranes [69].

ISA membranes are prepared via a phase-inversion method as developed for the first time by Loeb and Sourirajan [70]. This method involves the precipitation of a casting solution by immersion in a coagulation non-solvent bath (in most cases water). Phase-inversion techniques are currently used for the preparation of a wide range of polymeric membranes ranging from microfiltration to gas separation [71-76]. TFC membranes consist of a separating layer on top of a porous substrate. Plasma-induced techniques, thin-film formation via polymerization, polyelectrolyte modifications and grafting are well-established methods for the preparation of ultrathin and dense skin layers on porous supports for OSN applications [22, 24].

Modification methods that have been proposed and also applied for tuning the properties of OSN membranes can be divided into two categories: either only the surface is modified or the surface is modified along with the bulk membrane material (Figure 1.3, top for definitions). An example of the last category is chemical cross-linking as an efficient approach to improve the performance of OSN membranes, which does not only improve the (bulk) stability of the membrane, but also may affect the membrane surface properties. This research topic has been reviewed recently [1, 2, 77].

Incorporation of nanoparticles into the polymer matrix is another method that influences both surface and bulk structures simultaneously. In this technique, the modification step (*i.e.* the loading of nanoparticles) takes place during the membrane preparation (*in-situ* modification). It must be noted, however, that often the main target of the addition of nanoparticles into the polymer matrix is to improve the surface properties of the membranes. Hence, TFN membranes, composed of a very thin film containing nanoparticles on a porous support are fabricated. Examples of methods that address the modification of the surface without changing the bulk membrane structure and properties, include the plasma-induced techniques [78] and the addition of a skin (top) layer by using polyelectrolytes in combination with membranes having relatively small pores sizes [79]. A schematic showing the different approaches in terms of the surface and bulk modification is presented in Figure 1.3.

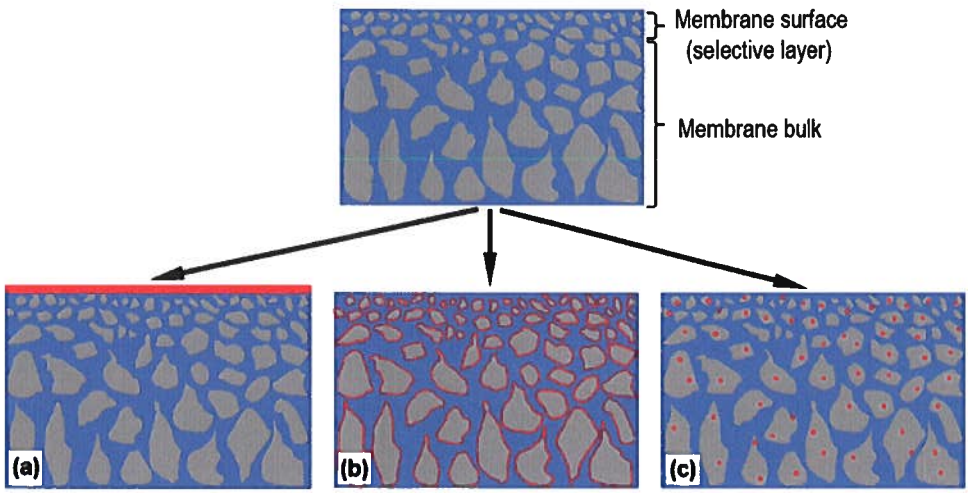

Figure 1.3 Schematic of the modification methods applied for OSN membranes: (a) modification of the skin (top) layer, modification of the top surface and bulk structure and (c) *in-situ* modification of the surface and bulk structure.

Radiation/light-induced modification

Among the modification methods used for tuning the membrane surface properties, light irradiation is an effective method due to its simplicity, low operation cost and mild reaction conditions. This method has been recognized as a well-known technique for the preparation of polymeric membranes from precursors, initiating polymerization and cross-linking reactions [80]. Preparation and modification of polymeric NF membranes with high antifouling properties for aqueous feeds is one of the most relevant applications of irradiation techniques [81-84]. Within the context of the operation conditions of OSN, the main applications of irradiation methods are the fabrication and the

development of a thin polymeric layer with high stability to improve the membrane performance in organic media. As a first example, electron beam radiation was employed to cross-link polydimethylsiloxane (PDMS) NF membranes and the obtained results indicated that the rejection of 9,10-di-phenylanthracene in xylene was enhanced by increasing the irradiation dose [85]. Membranes with the lower irradiation dose showed a higher degree of swelling and a larger transport region within the selective layer and hence diminishing the size-exclusion effect [86]. UV curing was also used to cross-link the methacrylate (MA) functional groups in the preparation of hydrophilic polyethylene oxide-PDMS-polyethylene oxide (PEO-PDMS-PEO) membranes [87].

The Vankelecom group reported a series of studies on the application of irradiation to improve the performance of different types of OSN membranes [88-94]. In more detail, they performed UV irradiation in air at a wavelength of 254 nm to cross-link ordered nanoporous polymer membranes. These membranes were prepared via blending a block copolymer of polystyrene-*b*-poly(ethylene oxide) (PS-*b*-PEO) and poly(acrylic acid) (PAA). Upon application of a simple UV irradiation method the membranes were not only stable to chlorine solutions, but also to a variety of organic solvents [88]. Other work performed by this group, presents the effects of the local heating of cellulose acetate (CA) and gold nanoparticles (GNPs)-filled polyimide (PI) membranes by irradiation with a continues Argon-ion laser beam (514 nm) [89, 90]. This novel method resulted in increased permeabilities, obviously due to a lower energy loss by convection in the membrane pores and/or free volume, while the rejection properties did not change (Figure 5). Incorporated GNPs in the membrane matrix acted as nano heaters and caused localized heating due to the plasmonic heating effect during irradiation.

Li *et al.* [95] attributed this phenomenon to the fact that local heating lowers the friction between the permeating molecules and the surrounding polymer chains which subsequently increases the flux. However, since rejection is mainly governed by the size exclusion, preferential adsorption or electrostatic repulsion at the membrane surface are hardly affected by local heating.

In a similar study by Li *et al.* [91], silver nanoparticles and LED light were used to cause localized heating, rendering the whole procedure to be more energy efficient, cheaper and less complicated compared to what was discussed above. The permeability of the thus-treated membranes increased and returned to the original value measured without LED light irradiation. This improvement in membrane permeability is due to the heating, rather than to changes in the membrane structure.

Struzynska-Piron *et al.* [93] employed UV curing after a phase-inversion process to fabricate solvent-stable polysulfone (PSf) or PI membranes. The cross-linked PSf and PI membranes showed good stabilities and good permeation performances in organic solvents such as ethyl acetate (EA) and IPA. For example, cross-linked PSf membrane showed 91% rejection and permeability of 8.1 L m^{-2} h^{-1} bar^{-1} for RB/EA and 94% rejection and permeability of 0.2 L m^{-2} h^{-1} bar^{-1} for RB/IPA. Also, UV cross-linked PI membranes showed 96% rejection and permeability of 1.4 L m^{-2} h^{-1} bar^{-1} for RB/IPA. Another study performed by this group [94] shows that using a combination of acyl phosphine

oxide-based photo-initiators with a penta-acrylate cross-linker resulted in PSf UV-cross-linked membranes with a high stability in acetone, n-butyl acetate, EA, toluene and xylene.

UV light approaches were also used to modify PSf membranes prepared with di- to hexa-acrylate cross-linkers and 2,4,6-trimethylbenzoyl-diphenyl-phosphine oxide (TPO) as photo-initiator [92]. UV irradiation improved the cross-linking efficiency and consequently increased the viscosity of the casting solution. As a result the phase inversion mechanism changed from instantaneous to delayed demixing, resulted in more spongy like structure without macrovoid formation [96, 97].

Behnke *et al.* [98] employed UV irradiation to cross-link Lenzing P84® TFC membrane containing a substituted photo-active benzophenone group in its repeating unit (Figure 5a). Abstraction of hydrogen from a methyl group of a nearby aromatic unit upon the UV irradiation resulted in the formation of two radicals and consequently a new covalent bond by recombination of these radicals. The membrane stability in polar aprotic solvent such as DMF is enhanced significantly via the introduction of new reactive side groups by using amino ethyl methacrylate (AEMA) in a reaction with the polymer chain via opening of the imide bond.

Plasma-induced techniques

Surface modification of polymeric membranes by lowtemperature plasma is one of the interesting methods to change the surface chemistry of membranes whereas their bulk properties remain mainly unchanged [99-101]. This technique is very fast, effective and meets environmental standards for clean technology. A large variety of (macro) molecules can be used to react with the formed free active radicals on the membrane surface. Plasma parameters such as power, pressure and sample deposition and also polymerization conditions such as monomer concentration and grafting time are the most effective parameters to control the grafting density and the chain length [80].

Zhao *et al.* [102] and Chen *et al.* [103] employed an Ar-based, low-temperature plasma treatment for styrene grafting on the surface of polyacrylonitrile (PAN) UF membranes to prepare OSN membranes used for the recovery of toluene and methyl ethyl ketone (MEK) from dewaxed oil. Increasing the grafting time leads to smaller pore sizes and lower pore densities with a pore size distribution that is significantly more narrow [104]. However, the results revealed that an increase in the membrane hydrophobicity has a larger effect than decreasing the pore size. Hence, the permeation flux increased by increasing the grafting reaction time.

Plasmas based on Ar, Ar-H_2 and Ar-O_2 were employed to treat surfaces of PDMS OSN membranes [105]. The resulting membranes showed higher rejections for dispersed, neutral components compared to charged dyes, while a very high rejection (≥95%) was obtained with a neat PDMS membrane for charged dyes. The authors explained that plasma treatment decreased the surface hydrophobicity of the PDMS membranes and as a consequence the affinity of the treated

membranes toward neutral dyes decreased significantly. The effects of transport asymmetry of the OSN membranes was studied by Volkov *et al.* [101] for the first time for the PTMSP membranes modified with a plasma treatment using atmospheric air. They found that the permeation properties of the modified PTMSP membranes depended on the membrane orientation with respect to the flow direction. For instance, when the modified surface contacted the feed stream such as MeOH, ethanol (EtOH), propanol and acetone, the permeation fluxes of organic solvents through the membranes were two times lower compared to the unmodified surface. In another work from Karan *et al.* [106] a plasma-enhanced chemical vapor deposition (CVD) reactor was used to synthesize ultrathin diamond-like carbon (DLC) nanosheet membranes on porous alumina (Figure 1.4). Permeation experiments with the DLC nanosheet membranes using a wide range of organic solvents showed higher permeation fluxes (values in the range of UF membranes) with high retention times. They concluded that hydrophobic pores (of 1 nm diameter) in the selective carbon layer deposited on a porous alumina support resulted in an ultrafast viscous permeation of organic solvent through the DLC membranes.

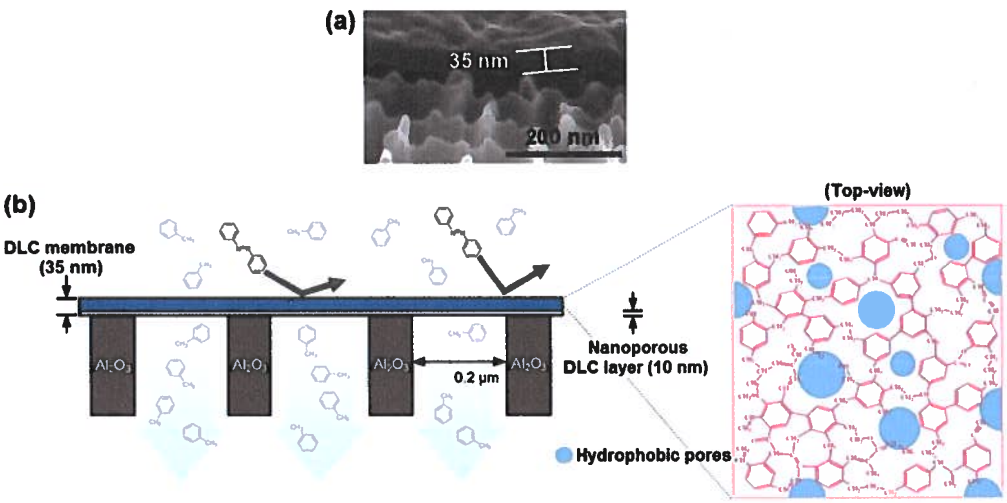

Figure 1.4 (a) Cross-sectional SEM image of 35-nm-thick DLC membrane and (b) Schematic presentation of a free-standing DLC membrane formed on submicron pores of a porous alumina support (reproduced with permission from Science Ltd.) [106].

Thin film formation via polymerization

In the early 1980s, pioneering work on interfacial polymerization was performed by Cadotte *et al.* [107] to prepare TFC aromatic PA membranes. Interfacial polymerization is known as a well-established and useful method to synthesize a dense and active top-layer on a porous support to prepare composite RO and NF membranes [6]. Although interfacial polymerization was mainly

used to prepare TFC membranes used in separation of aqueous feed streams [108], it was developed to synthesize membranes for filtration in organic solvent media as well [2, 6]. Application possibilities of this method for the preparation of composite OSN membranes strongly depend on the specific molecular structure of the top-layer and chemical stability of the porous support in organic solvents [6, 109]. Generally this method entails the application of an ultra-thin film upon an asymmetric, porous support-layer via an *in-situ* polymerization reaction occurring at the interface between two immiscible solvents containing reactive monomers.

Since thin films play the main role in the separation of organic solvents, it is important to obtain a very stable thin films with high separation abilities and permeation properties. Interfacial polymerization of MPD and a blend of trimesoylchloride (TMC) with fluoro-alkyl acyl chloride in the organic phase formed hydrophobic PA membranes with a high stability in DMF [110]. These membranes showed a significantly higher permeation flux without sacrificing rejection for nonpolar solvents.

Controlling the rate of the interfacial polymerization reaction and the wettability of the formed thin film by additives are efficient ways to improve the final performance of the prepared membranes [111]. Sodium dodecyl sulfate (SDS) surfactant and TEA/CSA were added to the MPD solution during the IP, resulting in a significant increase of the permeation of MeOH through the TFC OSN membrane [67]. Wettability enhancement of the membrane surface by the addition of SDS improved adsorption of MPD on the substrate [112]. Also, TEA as an acid acceptor increased the reaction rate and formed organic water-soluble salts between its amine group and the sulfonic group of CSA, which leads to an increase of the surface porosity of TFC membrane after interfacial polymerization [113, 114].

Jimenez Solomon *et al.* [115] reported that solvent activation of the TFC membranes after interfacial polymerization reaction dramatically improved the organic solvent fluxes without compromising rejection. DMF and DMSO have similar Hildebrand solubility parameters to those of the PA top layer (24.8, 26.6 and 23 $(MPa)^{1/2}$, respectively) and can act as a good swelling agents. The swelling and morphology of the thin film PA NF and RO membranes have been studied in great detail by Freger [116], using atomic force microscopy (AFM). The swelling was found to increase along the following series: acidic brine < basic brine < pure water. Enhanced swelling was observed for the (looser) outmost polymer parts. It was concluded that for NF membranes, there was a reasonable correlation between the swelling and permeability properties and the salinity and pH of the feed.

In a closely related method, Li *et al.* [117] applied *in-situ* polymerization to synthesize a polypyrrole (PPy)-modified top layer on different UF support membranes. A solution of pyrrole monomer and EtOH was casted on the porous support and polymerized to form a PPy selective layer. The resulting OSN membrane showed high stability in harsh aprotic solvents such as DMF and

tetrahydrofuran (THF) with desirable permeation behavior. For instance, permeability and rejection of THF/RB mixture were found to be 67.1 L m^{-2} h^{-1} bar^{-1} and 98%, respectively for the membrane prepared on the PAN-H support.

The Livingstone group [118] prepared ultrafast permeable PA nanofilms with outstanding rejections to separate negatively charged solutes from MeOH. They controlled the rate of interfacial reaction between MPD and TMC on a sacrificial layer of cadmium hydroxide nanostrands to prepare a sub-10 nm PA film on P84 and alumina support (Figure 1.5). The formed nanostrand layers were removed after PA formation by acid dissolution. They report that the DMF activated PA nanofilm on alumina support, which was prepared with a 1-min interfacial reaction of 3 wt% of MPD in aqueous solution, resulting in an excellent permeability with high rejection. For instance, for the mixtures of MeOH and 6-hydroxy-2-naphthalenesulfonic acid (HNSA) sodium salt, MO, Naphthalene brown and Acid Fuchsin (AF), permeabilites and rejection performances of 52.2, 52.0, 52.0 and 51.8 L m^{-2} h^{-1} bar^{-1} and 98.5, 98.9, 99.9 and 99.9% were found, respectively.

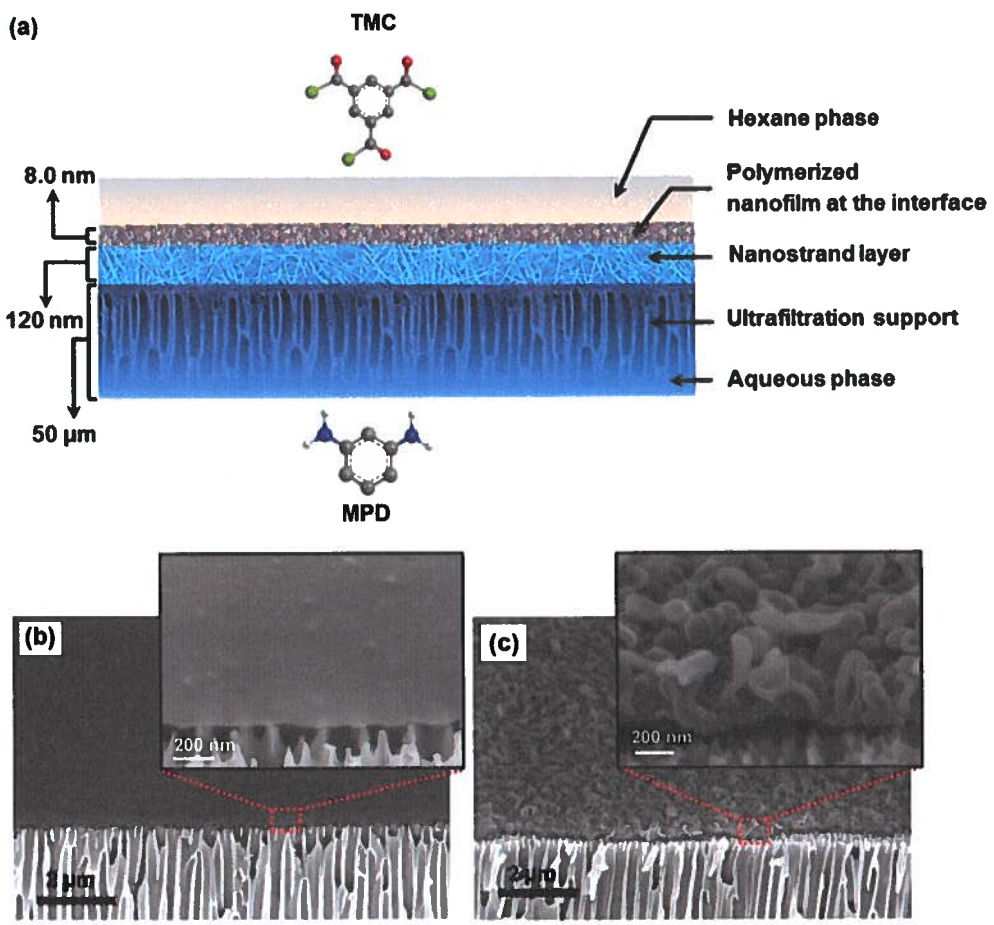

Figure 1.5 PA nanofilm prepared via the controlled interfacial polymerization: (a) schematic of the controlled interfacial polymerization process, (b) smooth PA nanofilm on alumina support (0.1% of MPD in a 10-min interfacial reaction) and (c) crumpled PA nanofilm on alumina support (3% of MPD in a 1-min interfacial reaction) (reproduced with permission from Science Ltd) [118].

In the design of high-performance OSN membranes, the use of segmented polymer networks (SPN) is another approach to prepare a highly-engineered top layer on a porous support. Li *et al.* [119] employed *in-situ* polymerization to synthesize a multifunctional thin SPN selective layer on PAN porous support. They prepared SPN via free radical copolymerization of the hydrophilic *bis*(acrylate)-terminated PEO as macromolecular cross-linker with different hydrophobic acrylate monomers and Perkadox as the radical initiator. These membranes showed an excellent rejection of RB in organic solvents including IPA (rejection of 99% RB with a permeability up to 0.4 L m^{-2} h^{-1} bar^{-1}), THF (rejection of 99.3% RB with a permeability up to 1.3 L m^{-2} h^{-1} bar^{-1}) and DMF (rejection of 96% RB with a permeability up to 2.7 L m^{-2} h^{-1} bar^{-1}).

Polyelectrolyte modification

Polyelectrolytes are a class of macromolecules with functional groups that either are permanently charged or can be charged under specific pH conditions. Decher and his co-worker pioneered [120-122] the so-called layer-by-layer (LbL) technique for the preparation of multilayer thin films onto a charged surface by the alternating deposition of polycations and polyanions. This surface modification approach has been widely used in various applications, including drug delivery [123], sensors [124, 125] and also in membrane separations [79, 126]. Polyelectrolyte multilayer (PEM) thin films are considered to be good candidate for OSN applications as well, since thin selective layers have proven to be highly permeable and to some extend selective for charged molecules, while they have excellent stability in common organic solvents [42, 126, 127].

Li *et al.* [128] used poly(diallyldimethylammonium chloride) (PDDA) and sulfonated poly(ether ether ketone) (SPEEK) to prepare PEM membrane on hydrolyzed PAN (H-PAN). The resulting membranes were used for the separation of charged aromatic dyes such as RB, crystal violet, methyl orange (MO) and AF. The PEM membranes showed a high chemical stability and high separation performances in aprotic solvents like THF and DMF. In addition, solvent stability and permeation flux in the presence of salt improved dramatically without sacrificing selectivity [129]. Addition of NaCl to the PE solution used for the PEM membrane formation results in the screening of charges and consequently the intramolecular repulsion of equally charged PE monomers reduces. This resulted in coil-like PE chains with a more loopy (rather than stretched) configuration. Upon adsorption, the thickness and density of membranes were significantly affected. The change in the PE solution resulted in membranes with thicker and looser selective layers (Figure 1.6). In a similar study

performed by Chen *et al.* [127], PDDA/SPEEK multilayers were successfully deposited on the H-PAN coated with silicon particles and applied for filtration of polar aprotic solvents such as THF and DMF. The highest selectivity was found for those systems that have the same charge for the PEM membrane top layer and the solutes. In more detail, a SPEEK-terminated PEM membrane is negatively charged resulting in a Donnan exclusion of negatively charged solute.

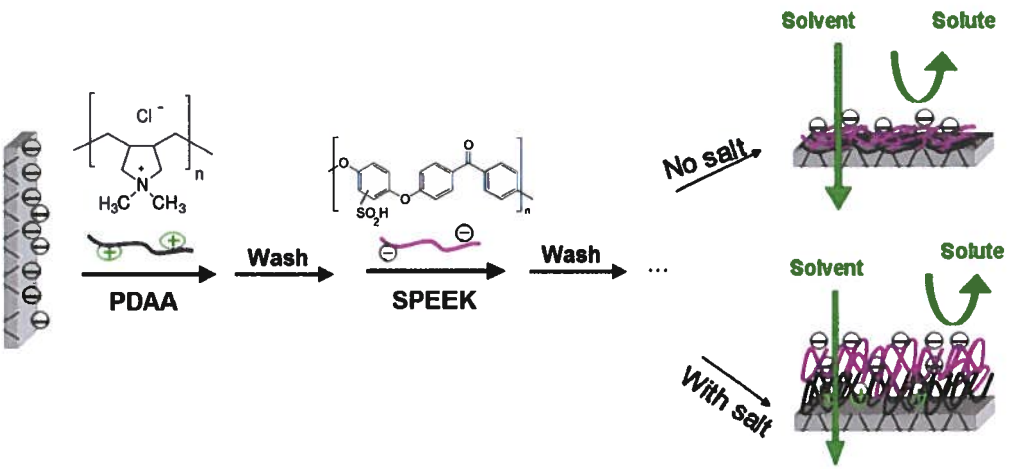

Figure 1.6 PA Schematic of the effects of NaCl salt on PE adsorption (reproduced with permission from Elsevier Science Ltd.) [129].

In addition, Ahmadiannamini *et al.* [130] used PAA as a weak polyanion to prepare of PDDA/PAA PEM membranes in different NaCl concentrations and pH conditions. The thickness of the deposited layers decreased as the pH value of PE solutions increased up to 4. At these pH values, less material was required to compensate all charges present on the previously deposited layers due to the increasing in charge density of PAA chains. By further increasing the pH, the thickness increased again because the resulting higher charge density of the PAA chains. These membranes showed good chemical stability and rejection in filtration processes of aprotic solvents such as THF. In another study performed by this group, the effects of H^+-form and Na^+-form of poly(vinyl sulfate) PVS and poly(sodium styrene sulfonate) PSS as poly anions were investigated on filtration performance of DMF and THF [43]. The membranes prepared with the H^+-form of the polyanions showed higher permeabilities and higher rejections than the ones prepared with the Na^+ salts because of their loopier structures and their higher surface charges.

Incorporation of nanoparticles

The preparation of organic–inorganic composite membranes, called mixed matrix membranes (MMMs), is a promising approach to improve the thermal stability, mechanical strength and solvent resistance of the membranes. The main challenge in preparing MMMs membranes is to make a proper connection between the polymer and inorganic phases via covalent bonds, Van der Waals forces or hydrogen bonds to reduce or ideally avoid leaching of nanoparticles during operation. MMMs for OSN application have been prepared in three different ways: (i) dispersing the inorganic filler in the polymer solution [25, 89, 90, 95, 131-137], (ii) *in-situ* polymerization, *i.e.* dispersion of nanoparticles in solutions before polymerization [64, 65, 138-140], and (iii) self-assembling and pre-assembling of nanoparticles, *i.e.* the synthesis of inorganic nanoparticles using precursors during the membrane formation and nanoparticles functionalization before polymerization [141-143].

The use of inorganic materials to enhance the performance of OSN membranes was first proposed at KU Leuven one decade ago by Gevers *et al.* [131, 132] who tested the incorporation of three types of fillers, namely silica, carbon and zeolites into PDMS membranes. They found that the addition of inorganic fillers in the PDMS improved the performance of the membrane for separation of non-polar solvents by reducing the swelling of the PDMS network. Zeolite-filled (ZSM-5) PDMS showed much stronger anti-swelling properties than those PDMS films filled with silica and carbon. This was attributed to an improved dispersion of zeolite in the polymer solution, stronger cross-linking effects. Dobrak-Van Berlo *et al.* [133] showed that incorporation of 15 wt% silicalite fillers into the PDMS matrix reduced the swelling significantly and improved the retention for dye/n-propanol systems. Vandezande *et al.* [25] also confirmed the positive role of silicalite on the reduction of swelling by making asymmetric silicalite-filled PI membranes using the phase inversion technique. The addition of more nano-zeolite suspension to the casting solution changed the membrane morphology from a finger-like to a sponge-like structure, *i.e.* from elongated macrovoids to spherical microvoids. The latter type of voids were reported to make the membrane more resistant to compaction and swelling.

The incorporation of metal-organic frameworks (MOFs) as a filler for the preparation of OSN membranes was explored by Basu *et al.* [134]. MOFs are a relatively new class of porous crystalline materials that are composed of metal ions joined by organic ligands, often polycarboxylic acids, via strong coordinative bonds. The nanocomposite membranes prepared by incorporating of $Cu_3(BTC)_2$, MIL-47, MIL-53(Al) and ZIF-8 into the PDMS matrix showed enhanced permeability, but decreased solute rejection compared with the pure PDMS/PI membrane due to a poor adhesion of the MOFs to the PDMS network. Campbell *et al.* [135] produced MMMs by dispersing pre-formed particles of the MOF HKUST-1 in PI P84 dope solutions. The synthesized MMMs demonstrated both (i) higher

rejections of styrene oligomers in the treatment of polystyrene solutions in acetone, and (ii) lower flux decline than those observed for the pure membranes.

TiO_2 nanoparticles have been extensively applied for making MMMs with improved antifouling, hydrophilicity, permselectivity, and photo-catalytic properties. Soroko *et al.* [136] prepared the first MMMs for OSN applications by dispersing TiO_2 nanoparticles in a PI solution. The formation of macrovoids, which is common in phase inversion membranes, was suppressed by the addition of TiO_2 nanoparticles and finally disappeared at higher loadings (>3 wt.%). Compaction resistance of the prepared membranes improved without adversely affecting the flux and rejection in treatment of styrene oligomer mixtures in EtOH. Li *et al.* [137] fabricated thermally stable and solvent resistant TiO_2-PAN hybrid hollow fiber membranes. The thermogravimetric analysis (TGA) results showed high thermal stability of the prepared membranes, which could persist up to 400 °C with a slight weight loss. In order to find the solvent resistance of TiO_2-PAN hybrid fiber membranes, they were exposed to various boiling solvents including N,N-dimethylacetamide (DMAc) and the changes in axial length and weight were measured afterwards. The original PAN membrane was found to dissolve rapidly in most of these solvents, whereas the axial length of the hybrid membranes swelled slightly in the range of 0.8–6.7% and their weight increased from 3.3% to 7.4%.

Novel inorganic fillers like multi-walled carbon nanotubes (MWNTs), MOFs and graphene oxide (GO) have been already utilized for the fabrication of thin film hybrid OSN membranes [138-140]. Roy *et al.* [138] fabricated interfacial polymerization-generated PA membranes by the dispersion of MWNTs in either the organic phase or the aqueous phase. Raw MWNTs were functionalized with hydrophilic (–COOH) groups or hydrophobic groups (–CONHR) (via microwave treatment) to disperse in a poly(ethylene imine) (PEI)-containing aqueous solution and also in an *iso*-phthaloyl dichloride (IPD)-containing organic solution. Their permeation results demonstrated that the MeOH flux of the synthesized membranes is enhanced by an order of magnitude due to nano gaps between the external surfaces of functionalized MWNTs and the polymeric matrix, while the Brilliant blue rejection was at higher value of 91%. A similar permeation behavior was observed for the PPy-based OSN membranes embedding GO [140]. In these membranes, pyrrole absorbed onto the GO surface due to the π-π interactions and electrostatic attractions [144, 145]. This resulted in polymerization around GO and the formation of thinner selective layers on the surface of the porous PAN-H. Separation experiments revealed that due to the presence of polymer-coated GO in the active layer of the membranes, permeabilites of MeOH, EtOH and IPA significantly increased without sacrificing the rejection of RB.

Sorribas *et al.* [139] conducted the same interfacial polymerization reaction and synthesized TFN membranes containing 50-150 nm size MOF nanoparticles (ZIF-8, MIL-53(Al), NH_2-MIL-53(Al) and MIL-101(Cr)) on top of cross-linked PI porous supports. They found that organic solvent (MeOH and THF) permeations increased by embedding MOFs into the PA thin layer compared to filler-free

membranes without sacrificing styrene oligomers rejection (>90%). Common nanoparticles and zeolites were also utilized for making thin film OSN membranes. Namvar-Mahboub *et al.* [65] fabricated TFN membranes by the incorporation of amine-functionalized UZM-5 nanoparticles into the PA layer synthesized via an interfacial polymerization of MPD with TMC (Figure 1.7).

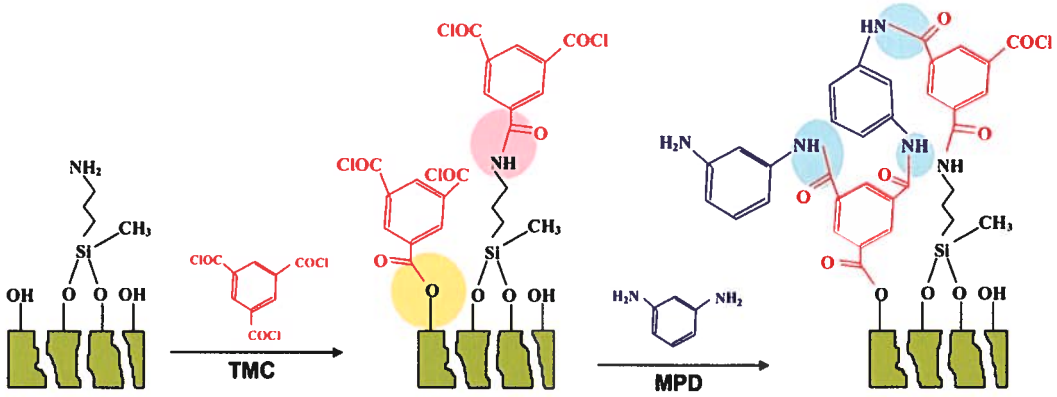

Figure 1.7 Schematic of chemical reactions between amine-functionalized-UZM-5, TMC and MPD during PA synthesis (reproduced with permission from Elsevier Science Ltd.) [65].

These membranes were studied in a dewaxing solvent recovery process (MEK and toluene from lube oil). The work indicates that the presence of UZM-5 in the PA layer improved both oil rejection and permeate flux under an optimal concentration of 0.02% w/v of UZM-5. The increase in permeate flux upon the addition of UZM-5 was attributed to the pore diameter of UZM-5. In other words, modified UZM-5 with an average pore diameter of 16.8 Å which was loaded at 0.02% w/v into the PA thin film provides a pathway for toluene (6.1 Å) and MEK (5.2 Å) whereas the lube oil macromolecules were rejected. In the higher loading contents of UZM-5, the PA thin layer became less cross-linked with more interface defects and consequently the permeability increased, while the oil rejection declined significantly. Peyravi *et al.* [64] synthesized TFN membranes by incorporation of surface-modified TiO_2 nanoparticles into a thin layer of co-PA network fabricated by *in-situ* interfacial polymerization reaction. TFN membranes represented higher MeOH flux than filler-free TFC membranes with a slight sacrifice in dye rejection during the NF of a MeOH/dye solution.

Despite outstanding advantages of MMMs, the preparation of these membranes with defect-free hybrid active layer is still challenging. The main problem to be solved is the severe aggregation of the nanoparticles due to their high surface area and their weak compatibility with polymer materials [141]. As a result, often non-selective voids are formed at the interface of polymer and inorganic nanoparticles, which typically reduces rejection values significantly. Inspired by the mechanism of mineralization, MMMs can be synthesized by using some functional groups of the polymer as catalyst to generate inorganic nanoparticles via hydrolysis and condensation of inorganic precursors.

Applying this technique, inorganic nanoparticles with uniform size distribution can be generated and self-assembled within the polymer matrix. Due to the good compatibility between the polymer and nanoparticles formation of non-selective voids can also be eliminated. For example, Zhang *et al.* [141] assembled SiO_2 and TiO_2 nanoparticles into the polymer by hydrolysis of the inorganic precursors, tetraethoxysilane and tetra-n-butyltitanate, respectively, using -NH_2/-NH-groups of PEI. They evaluated the performance of their self-assembled MMMs for OSN application using n-heptane, toluene, butanone, EA, and IPA as solvents, and polyethylene glycol (PEG) as solute. It was shown that the presence of nanoparticles improved the solvent resistance of the synthesized membranes (*i.e.* swelling was below 6%). Interestingly, these types of MMMs showed an increase in the solute rejection with a slight decline in solvent flux by increasing the nanoparticle loading, which is not common in hybrid membranes. Siddique *et al.* [142] followed the same technique and synthesized self-assembled MMMs by using (3-amino propyl)trimethoxy silane (APTMS) as a cross-linking agent as well as an organo silicone precursor to generate an inorganic network. The SiO_2 network is generated by the hydrolysis and condensation of the methoxysilane moieties in APTMS. The NF of organic solvents such as acetone, DMF and dichloromethane (DCM) showed reduction in flux after treatment with this organic–inorganic based cross-linker. However, MMMs membranes were improved in terms of rigidity and strength as well as resistance to compaction and swelling. In another study, Siddique *et al.* [143] fabricated pre-assembled MMMs membranes by incorporating nano-sized polymer particles with methacrylate moieties onto the surface of cross-linked PI UF support membranes. Multiple layers of these nanoparticles (120 nm and 300 nm in diameter) spin-coated on the PI support and the nanoscale interstitial spaces formed between the particles served as permeation channels. In order to prevent removal of nanoparticles from the surface in the OSN process, they were cross-linked to the support by a photo-initiated, free-radical polymerization using UV light. The NF performance of the synthesized membranes was evaluated in solvents such as acetone and toluene. The molecular weight cut-off (MWCO) of the membranes, measured by a styrene oligomer mixture as solute, was in the range of 200 to 1,000 g mol^{-1} which depended on the nanoparticle diameter and the thickness of the nanoparticle layer. Membranes coated with nanoparticles showed better rejection and more resistance against compaction compared to commercial polymeric membranes because of their more rigid structure.

1.4.2 Modification of ceramic OSN membranes

Ceramic membranes show advantageous properties compared to polymeric membranes under harsh conditions, including high pH, high temperature or using organic solvents. In general, ceramic membranes have an asymmetric structure as well, composed of at least two different porosity levels including a macroporous support, an active microporous top layer and an intermediate layer with a pore size between that of the support and the active layer [6, 146]. The macro porous support

provides the mechanical strength for the ceramic membranes. Normally, the sol-gel synthesis method is used to prepare the active top layer of ceramic membranes. Despite these superior characteristics ceramic membranes contain surface hydroxyl groups (OH), hampering the applications in non-aqueous separations due to their highly hydrophilic nature [147-151]. Pioneering work on using ceramic membranes for OSN has been reported by Tsuru *et al.* [31, 32] While large pore sizes (70 nm in diameter) showed a viscous flow mechanism for MeOH, EtOH, and 1-propanol, the permeation mechanism through porous membranes having pore diameters of 1 to 5 nm was found to be different; small molecules showed higher permeabilities than larger molecules. Later, this research group successfully applied the sol-gel method to prepare porous silica-zirconia RO membranes [152]. According to their filtration experiments, membranes containing pores of 1 nm in diameter showed a high potential for the separation of organic solvents with EtOH fluxes of up to 3 kg m^{-2} h^{-1} at 30 bar and a MWCO as low as 200 Da.

As discussed in Section 1.2, to improve the separation performance of the above-mentioned ceramic OSN membranes, surface chemistry plays an important role. First, the pore sizes can be reduced to nanometer dimensions and, second, the wetting properties can be tuned by the nature of the compounds used in the surface modification. In order to prepare high-performance ceramic membranes for OSN applications, the top layer should be grafted by hydrophobic functional groups, for instance via silylation chemistry [1, 147, 153, 154]. Here we discuss different approaches that cover, silylation, calcination of alkyl-modified colloidal dispersions, a sol-gel based sintering method and Grignard chemistry, showing the diversity of the reported strategies.

To render the ceramic membranes with superior hydrophobicity and filtration performance, Dutczak *et al.* [155] prepared capillary OSN membranes by a combination of the advantages of ceramic supports such as high mechanical, thermal and chemical stability with high separation properties of the PDMS coating layer. It was shown that relatively low PDMS concentrations (<15 w/w % in toluene) are necessary to fabricate very thin (*i.e.* 6-20 μm for 3.75% w/w PDMS) and defect-free PDMS top-layer on the porous support. Composite membranes prepared by coating of PDMS on the inside of a 20 nm pore size α-alumina support showed the best performance. This membrane was stable for over 40 h in toluene with a permeability of 1.6 L m^{-2} h^{-1} bar^{-1} and a MWCO of ~500 Da. In another and novel approach, Pinheiro *et al.* [150] employed PDMS-grafted γ-alumina ceramic membranes in OSN of n-hexane, toluene and IPA. The authors developed a two step-method to graft PDMS on the surface of ceramic membranes. In this approach 3-amino propyl triethoxy silane (APTES) was applied on the surface of a ceramic membrane by either a vapor phase or a solution phase technique in the first step. In the next step, an epoxy-terminated PDMS was grafted onto the APTES layer. PDMS-grafted γ-alumina membranes showed excellent stability in polar and non-polar solvents, whereas the non-polar solvents showed the higher permeabilities. In similar work performed by this group [156], mono vinyl-terminated PDMS was grafted on the surface

of mesoporous γ-alumina membranes using (3-mercaptopropyl)triethoxysilane (MPTES) as a linking agent. The results revealed that silylation of the mesoporous γ-alumina substrate by vapor phase deposition provided a more uniform and homogeneous distribution of the products compared to solution phase deposition. This was explained by just a silane monolayer formation for the vapour phase method and multilayers formed using the solution phase method [153]. The toluene permeability of the membranes was reduced from 5.3 to 2.1 L m^{-2} h^{-1} bar^{-1} upon PDMS grafting. They concluded that the effect of pore size reduction after PDMS grafting was more significant than the effect of the increase of hydrophobicity.

The sol-gel approach is an alternative route to prepare nanometer-sized pores in ceramic membranes. Tsuru *et al.* [157] employed methylated SiO_2 colloidal sol solutions to prepare organic/inorganic hybrid membranes with nano-size pores (2−4 nm in diameter). In their method, methylated SiO_2 dispersions coated on a porous support and subsequently calcined at 400−600 °C in an inert atmosphere. Permeation experiments with poly olefin oligomers in n-hexane solutions showed an n-hexane permeability of 7.2−27 L m^{-2} h^{-1} bar^{-1} and a MWCO between 1000−2000 Da.

Also Zeidlet *et al.* used a sol-gel based approach to prepare low-MWCO ceramic OSN membranes [158]. They developed hydrophobic NF tubular ceramic membranes with an active layer of titanium dioxide/zirconium dioxide with integrated carbon. Diethanol amine (DEA) was added to the sintering sol (titania + zirconia) in order to increase the amount of carbon. DEA acted as a complexation agent preventing the complete hydrolysis of the titanium/zirconium precursors and to support the formation of a polymeric sol. The filtration experiments with a mixture of different molecular weight samples of polystyrene (PS) in THF solution revealed a MWCO ~350 Da, confirming an excellent separation ability of these membranes. Besides the permeation results, permporometry measurements proved the benefits of this new method to change the original pore size of 40 nm diameter to the desired value to retain the molecules, but large enough to enable solvent permeation.

Rezaei Hosseinabadi *et al.* [34] investigated a Grignard grafting method to functionalize tubular TiO_2 membranes with a series of n-alkyl groups and appropriate organometallic Grignard reagents in order to change membrane affinity to specific solvents and/or solutes (Figure 1.8).

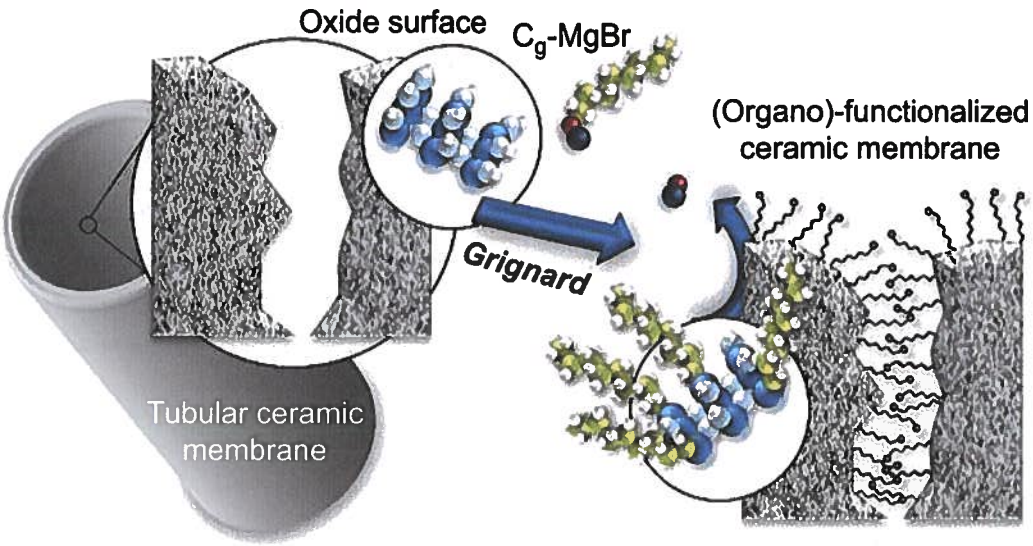

Figure 1.8 Schematic representation of the Grignard grafted ceramic membranes (with permission from Elsevier Science Ltd.) [159].

The 'amphiphilic character', reflected by water contact angles in the range of 60-90° of these alkyl-grafted ceramic membranes, was explained by the presence of both grafted organic groups and remaining OH groups at the membrane surface. The permeation flux of both polar and non-polar solvents through this type of partial hydrophobic ceramic NF membranes was obviously high, while the modification did not change the MWCO.

As discussed in this chapter, both organic (polymeric) and inorganic (ceramic) materials have been widely used for the fabrication of OSN membranes. Combining the ceramic materials with high non-swelling and non-compaction properties with polymeric materials with high selectivity properties can result in high-performance OSN membrane. The resulting hybrid inorganic-organic membranes combine the best of two world: the superior properties of ceramics with tuned surface properties by proper organic/polymer chemistry. Development, characterization and performance tests of the new type of hybrid ceramic membranes for the purification of organic solvents are the main focus of this thesis.

1.4 Thesis outline

This thesis describes the research performed to improve the performance of ceramic membranes for application in organic solvent nanofiltration processes by chemical modification of the membrane surfaces using facile, novel and efficient techniques. A brief overview is given below.

In **Chapter 2** of this thesis, the results are described of the modification of γ-alumina membranes by a directly grafting procedure to covalently attach different poly (maleic anhydride-*alt*-1-alkenes) (1-hexene, 1-decene, 1-hexadecene, and 1-octadecene). The solvent permeability and solute separation performance of these novel polymer-grafted γ-alumina membranes were investigated for the separation of Sudan Black B solutes from toluene and ethyl acetate.

In **Chapter 3** of this thesis, poly (styrene-*co*-maleic anhydride) having different molecular weights, were applied for the covalent and direct grafting onto γ-alumina membranes. We observed that the high molecular weight copolymer mostly grafted on the surface, and not inside the pores, of the γ-alumina membranes and provided a highly packed and thin surface layer. Partly pore modification was found for the applied lower molecular weight copolymers. The OSN performances of these membranes were studied for separation of dyes with different molecular weights, *i.e.* Sudan Black B (*MW* = 456 Da), Sudan Red 7B (*MW* = 379 Da), and Sudan Orange G (*MW* = 214 Da) from toluene and ethyl acetate.

In **Chapter 4** of this thesis, two MOFs, *i.e.* MIL-53(Al) and NH_2-MIL-53(Al), were made on top of α-alumina membranes and formed a continuous thin layer. These MOF modified α-alumina membranes showed excellent dye adsorption properties for Rose Bengal from methanol and isopropanol.

In **Chapter 5** of this thesis, the fabrication of an ultrathin melamine-based microporous polymer networks with a layer thickness of *ca.* 400 nm, supported by α-alumina membranes is reported. They showed an excellent solvent permeation and solute separation for Sudan Red 7B, Solvent Green 3, Sudan Black B and Bromothymol Blue from either toluene or n-heptane. As an example, an n-heptane permeability as high as 9.2 L m^{-2} h^{-1} bar^{-1} was found in combination with a very high rejection of ~ 99% of dye molecules with a molecular weight of ≥ 457 Da.

In **Chapter 6** the obtained knowledge from the previous chapters is summarized, and presented together with some recommendations for the preparation of high-performance hybrid ceramic/polymeric OSN membranes.

It is noted that Chapters 2-5 have been written as individual publications and can be read independently. As a consequence, there is some overlap in the introductions of these chapters.

References

[1] P. Marchetti, M.F. Jimenez Solomon, G. Szekely, A.G. Livingston, Molecular Separation with Organic Solvent Nanofiltration: A Critical Review, Chemical Reviews, 114 (2014) 10735-10806.
[2] X.Q. Cheng, Y.L. Zhang, Z.X. Wang, Z.H. Guo, Y.P. Bai, L. Shao, Recent Advances in Polymeric Solvent-Resistant Nanofiltration Membranes, Advances in Polymer Technology, 33 (2014) 21455.
[3] N. Hilal, H. Al-Zoubi, N.A. Darwish, A.W. Mohamma, M. Abu Arabi, A comprehensive review of nanofiltration membranes:Treatment, pretreatment, modelling, and atomic force microscopy, Desalination, 170 (2004) 281-308.
[4] S. Hermans, H. Mariën, C. Van Goethem, I.F.J. Vankelecom, Recent developments in thin film (nano)composite membranes for solvent resistant nanofiltration, Current Opinion in Chemical Engineering, 8 (2015) 45-54.
[5] A.W. Mohammad, Y.H. Teow, W.L. Ang, Y.T. Chung, D.L. Oatley-Radcliffe, N. Hilal, Nanofiltration membranes review: Recent advances and future prospects, Desalination, 356 (2015) 226-254.
[6] P. Vandezande, L.E.M. Gevers, I.F.J. Vankelecom, Solvent resistant nanofiltration: separating on a molecular level, Chemical Society Reviews, 37 (2008) 365-405.
[7] M. Sadrzadeh, J. Hajinasiri, S. Bhattacharjee, D. Pernitsky, Nanofiltration of oil sands boiler feed water: Effect of pH on water flux and organic and dissolved solid rejection, Separation and Purification Technology, 141 (2015) 339-353.
[8] A.V. Volkov, G.A. Korneeva, G.F. Tereshchenko, Organic solvent nanofiltration: Prospects and application, Russian Chemical Reviews, 77 (2008) 983-993.
[9] A.R.S. Teixeira, J.L.C. Santos, J.G. Crespo, Solvent resistant diananofiltration for production of steryl esters enriched extracts, Separation and Purification Technology, 135 (2014) 243-251.
[10] D. Peshev, L.G. Peeva, G. Peev, I.I.R. Baptista, A.T. Boam, Application of organic solvent nanofiltration for concentration of antioxidant extracts of rosemary (Rosmarinus officiallis L.), Chemical Engineering Research and Design, 89 (2011) 318-327.
[11] R. Valadez-Blanco, F.C. Ferreira, R.F. Jorge, A.G. Livingston, A membrane bioreactor for biotransformations of hydrophobic molecules using organic solvent nanofiltration (OSN) membranes, Journal of Membrane Science, 317 (2008) 50-64.
[12] P.G.N. Mertens, F. Cuypers, P. Vandezande, X. Ye, F. Verpoort, I.F.J. Vankelecom, D.E. De Vos, Ag0 and Co0 nanocolloids as recyclable quasihomogeneous metal catalysts for the hydrogenation of α,β-unsaturated aldehydes to allylic alcohol fragrances, Applied Catalysis A: General, 325 (2007) 130-139.
[13] F.C. Ferreira, H. Macedo, U. Cocchini, A.G. Livingston, Development of a Liquid-Phase Process for Recycling Resolving Agents within Diastereomeric Resolutions, Organic Process Research & Development, 10 (2006) 784-793.
[14] M.G. Buonomenna, J. Bae, Organic Solvent Nanofiltration in Pharmaceutical Industry, Separation & Purification Reviews, 44 (2014) 157-182.
[15] G. Székely, J. Bandarra, W. Heggie, B. Sellergren, F.C. Ferreira, Organic solvent nanofiltration: A platform for removal of genotoxins from active pharmaceutical ingredients, Journal of Membrane Science, 381 (2011) 21-33.
[16] R. Abejón, A. Garea, A. Irabien, Analysis and optimization of continuous organic solvent nanofiltration by membrane cascade for pharmaceutical separation, AIChE Journal, 60 (2014) 931-948.
[17] L.S. White, C.R. Wildemuth, Aromatics Enrichment in Refinery Streams Using Hyperfiltration, Industrial & Engineering Chemistry Research, 45 (2006) 9136-9143.
[18] L.S. White, Development of large-scale applications in organic solvent nanofiltration and pervaporation for chemical and refining processes, Journal of Membrane Science, 286 (2006) 26-35.
[19] R.M. Gould, L.S. White, C.R. Wildemuth, Membrane separation in solvent lube dewaxing, Environmental Progress, 20 (2001) 12-16.
[20] P. Marchetti, A. Butté, A.G. Livingston, An improved phenomenological model for prediction of solvent permeation through ceramic NF and UF membranes, Journal of Membrane Science, 415–416 (2012) 444-458.
[21] P. Marchetti, A. Butté, A.G. Livingston, NF in organic solvent/water mixtures: Role of preferential solvation, Journal of Membrane Science, 444 (2013) 101-115.
[22] G. Szekely, M.F. Jimenez-Solomon, P. Marchetti, J.F. Kim, A.G. Livingston, Sustainability assessment of organic solvent nanofiltration: From fabrication to application, Green Chemistry, 16 (2014) 4440-4473.
[23] M. Mulder, Basic Principles of Membrane Technology, 2nd ed. ed., Kluwer Academic Publisher: Dordrecht, 2004.
[24] L.G. Peeva, S. Malladi, A. Livingston, Nanofiltration operations in nonaqueous systems, in: L.G. Drioli (Ed.) Comprehensive Membrane Science and Engineering, Elsevier, Oxford, 2010.

[25] P. Vandezande, L.E.M. Gevers, P.A. Jacobs, I.F.J. Vankelecom, Preparation parameters influencing the performance of SRNF membranes cast from polyimide solutions via SEPPI, Separation and Purification Technology, 66 (2009) 104-110.
[26] P. Vandezande, X. Li, L.E.M. Gevers, I.F.J. Vankelecom, High throughput study of phase inversion parameters for polyimide-based SRNF membranes, Journal of Membrane Science, 330 (2009) 307-318.
[27] S. Tsarkov, V. Khotimskiy, P.M. Budd, V. Volkov, J. Kukushkina, A. Volkov, Solvent nanofiltration through high permeability glassy polymers: Effect of polymer and solute nature, Journal of Membrane Science, 423-424 (2012) 65-72.
[28] A.V. Volkov, V.V. Parashchuk, D.F. Stamatialis, V.S. Khotimsky, V.V. Volkov, M. Wessling, High permeable PTMSP/PAN composite membranes for solvent nanofiltration, Journal of Membrane Science, 333 (2009) 88-93.
[29] A. Volkov, A. Yushkin, A. Grekhov, A. Shutova, S. Bazhenov, S. Tsarkov, V. Khotimsky, T.J.H. Vlugt, V. Volkov, Liquid permeation through PTMSP: One polymer for two different membrane applications, Journal of Membrane Science, 440 (2013) 98-107.
[30] D. Fritsch, P. Merten, K. Heinrich, M. Lazar, M. Priske, High performance organic solvent nanofiltration membranes: Development and thorough testing of thin film composite membranes made of polymers of intrinsic microporosity (PIMs), Journal of Membrane Science, 401–402 (2012) 222-231.
[31] T. Tsuru, T. Sudou, S.-i. Kawahara, T. Yoshioka, M. Asaeda, Permeation of Liquids through Inorganic Nanofiltration Membranes, Journal of Colloid and Interface Science, 228 (2000) 292-296.
[32] T. Tsuru, T. Sudoh, T. Yoshioka, M. Asaeda, Nanofiltration in non-aqueous solutions by porous silica–zirconia membranes, Journal of Membrane Science, 185 (2001) 253-261.
[33] T. Tsuru, M. Narita, R. Shinagawa, T. Yoshioka, Nanoporous titania membranes for permeation and filtration of organic solutions, Desalination, 233 (2008) 1-9.
[34] S. Rezaei Hosseinabadi, K. Wyns, V. Meynen, R. Carleer, P. Adriaensens, A. Buekenhoudt, B. Van der Bruggen, Organic solvent nanofiltration with Grignard functionalised ceramic nanofiltration membranes, Journal of Membrane Science, 454 (2014) 496-504.
[35] G. Dong, H. Li, V. Chen, Challenges and opportunities for mixed-matrix membranes for gas separation, Journal of Materials Chemistry A, 1 (2013) 4610-4630.
[36] W.J. Lau, S. Gray, T. Matsuura, D. Emadzadeh, J. Paul Chen, A.F. Ismail, A review on polyamide thin film nanocomposite (TFN) membranes: History, applications, challenges and approaches, Water Research, 80 (2015) 306-324.
[37] J. Stawikowska, A.G. Livingston, Assessment of atomic force microscopy for characterisation of nanofiltration membranes, Journal of Membrane Science, 425–426 (2013) 58-70.
[38] Y. Zhao, Q. Yuan, A comparison of nanofiltration with aqueous and organic solvents, Journal of Membrane Science, 279 (2006) 453-458.
[39] P.W. Atkins, Physical Chemistry, Oxford University Press, Oxford, UK, 2006.
[40] W.M. Haynes, CRC Handbook of Chemistry and Physics, 93th ed. ed., CRC Press, 2012.
[41] L.E.M. Gevers, G. Meyen, K. De Smet, P. Van De Velde, F. Du Prez, I.F.J. Vankelecom, P.A. Jacobs, Physico-chemical interpretation of the SRNF transport mechanism for solutes through dense silicone membranes, Journal of Membrane Science, 274 (2006) 173-182.
[42] Q. Zhao, Q.F. An, Y. Ji, J. Qian, C. Gao, Polyelectrolyte complex membranes for pervaporation, nanofiltration and fuel cell applications, Journal of Membrane Science, 379 (2011) 19-45.
[43] P. Ahmadiannamini, X. Li, W. Goyens, B. Meesschaert, W. Vanderlinden, S. De Feyter, I.F.J. Vankelecom, Influence of polyanion type and cationic counter ion on the SRNF performance of polyelectrolyte membranes, Journal of Membrane Science, 403–404 (2012) 216-226.
[44] W.R. Bowen, J.S. Welfoot, Modelling the performance of membrane nanofiltration—critical assessment and model development, Chemical Engineering Science, 57 (2002) 1121-1137.
[45] D. Bhanushali, S. Kloos, D. Bhattacharyya, Solute transport in solvent-resistant nanofiltration membranes for non-aqueous systems: experimental results and the role of solute–solvent coupling, Journal of Membrane Science, 208 (2002) 343-359.
[46] X.J. Yang, A.G. Livingston, L. Freitas dos Santos, Experimental observations of nanofiltration with organic solvents, Journal of Membrane Science, 190 (2001) 45-55.
[47] B. Van der Bruggen, J. Schaep, D. Wilms, C. Vandecasteele, Influence of molecular size, polarity and charge on the retention of organic molecules by nanofiltration, Journal of Membrane Science, 156 (1999) 29-41.
[48] A.N. Zhukov, Integrated investigations of the electrosurface properties of nonaqueous disperse and capillary systems, Advances in Colloid and Interface Science, 134–135 (2007) 330-345.
[49] D. Bhanushali, S. Kloos, C. Kurth, D. Bhattacharyya, Performance of solvent-resistant membranes for non-aqueous systems: solvent permeation results and modeling, Journal of Membrane Science, 189 (2001) 1-21.

[50] J. Geens, K. Boussu, C. Vandecasteele, B. Van der Bruggen, Modelling of solute transport in non-aqueous nanofiltration, Journal of Membrane Science, 281 (2006) 139-148.
[51] B. Van der Bruggen, J. Geens, C. Vandecasteele, Fluxes and rejections for nanofiltration with solvent stable polymeric membranes in water, ethanol and n-hexane, Chemical Engineering Science, 57 (2002) 2511-2518.
[52] J. Geens, K. Peeters, B. Van der Bruggen, C. Vandecasteele, Polymeric nanofiltration of binary water–alcohol mixtures: Influence of feed composition and membrane properties on permeability and rejection, Journal of Membrane Science, 255 (2005) 255-264.
[53] J. Geens, B. Van der Bruggen, C. Vandecasteele, Characterisation of the solvent stability of polymeric nanofiltration membranes by measurement of contact angles and swelling, Chemical Engineering Science, 59 (2004) 1161-1164.
[54] T. Van Gestel, B. Van Der Bruggen, A. Buekenhoudt, C. Dotremont, J. Luyten, C. Vandecasteele, G. Maes, Surface modification of γ-Al2O3/TiO 2 multilayer membranes for applications in non-polar organic solvents, Journal of Membrane Science, 224 (2003) 3-10.
[55] J. Geens, B. Van Der Bruggen, C. Vandecasteele, Transport model for solvent permeation through nanofiltration membranes, Separation and Purification Technology, 48 (2006) 255-263.
[56] D.o.R. Machado, D. Hasson, R. Semiat, Effect of solvent properties on permeate flow through nanofiltration membranes: Part II. Transport model, Journal of Membrane Science, 166 (2000) 63-69.
[57] S.P. Pujari, L. Scheres, A.T.M. Marcelis, H. Zuilhof, Covalent Surface Modification of Oxide Surfaces, Angewandte Chemie International Edition, 53 (2014) 6322-6356.
[58] D.K. Aswal, S. Lenfant, D. Guerin, J.V. Yakhmi, D. Vuillaume, Self assembled monolayers on silicon for molecular electronics, Analytica Chimica Acta, 568 (2006) 84-108.
[59] M. Lessel, O. Bäumchen, M. Klos, H. Hähl, R. Fetzer, M. Paulus, R. Seemann, K. Jacobs, Self-assembled silane monolayers: an efficient step-by-step recipe for high-quality, low energy surfaces, Surface and Interface Analysis, 47 (2015) 557-564.
[60] R.N. Wenzel, Resistance of solid surfaces to wetting by water, Industrial & Engineering Chemistry, 28 (1936) 988-994.
[61] A.B.D. Cassie, S. Baxter, Wettability of porous surfaces, Transactions of the Faraday Society, 40 (1944) 546-551.
[62] S.-H. Hsu, K. Woan, W. Sigmund, Biologically inspired hairy structures for superhydrophobicity, Materials Science and Engineering: R: Reports, 72 (2011) 189-201.
[63] M. Nosonovsky, B. Bhushan, Lotus Versus Rose: Biomimetic Surface Effects, in: M. Nosonovsky, B. Bhushan (Eds.) Green Tribology, Springer Berlin Heidelberg, 2012, pp. 25-40.
[64] M. Peyravi, M. Jahanshahi, A. Rahimpour, A. Javadi, S. Hajavi, Novel thin film nanocomposite membranes incorporated with functionalized TiO2 nanoparticles for organic solvent nanofiltration, Chemical Engineering Journal, 241 (2014) 155-166.
[65] M. Namvar-Mahboub, M. Pakizeh, S. Davari, Preparation and characterization of UZM-5/polyamide thin film nanocomposite membrane for dewaxing solvent recovery, Journal of Membrane Science, 459 (2014) 22-32.
[66] G.L. Jadav, P.S. Singh, Synthesis of novel silica-polyamide nanocomposite membrane with enhanced properties, Journal of Membrane Science, 328 (2009) 257-267.
[67] S.P. Sun, T.S. Chung, K.J. Lu, S.Y. Chan, Enhancement of flux and solvent stability of Matrimid® thin-film composite membranes for organic solvent nanofiltration, AIChE Journal, 60 (2014) 3623-3633.
[68] E.M. Vrijenhoek, S. Hong, M. Elimelech, Influence of membrane surface properties on initial rate of colloidal fouling of reverse osmosis and nanofiltration membranes, Journal of Membrane Science, 188 (2001) 115-128.
[69] R.W. Baker, Membrane Technology and Applications, Second Edition ed., WILEY, 2004.
[70] S. Loeb, S. Sourirajan, Sea water demineralization by means of an osmotic membrane, Adv. Chem. Ser., 38 (1963) 117-132.
[71] Y. Gençal, E.N. Durmaz, P.Z. Çulfaz-Emecen, Preparation of patterned microfiltration membranes and their performance in crossflow yeast filtration, Journal of Membrane Science, 476 (2015) 224-233.
[72] M. Amirilargani, T. Mohammadi, Synthesis and characterization of asymmetric polyethersulfone membranes: effects of concentration and polarity of nonsolvent additives on morphology and performance of the membranes, Polymers for Advanced Technologies, 22 (2011) 962-972.
[73] E. Saljoughi, S.M. Mousavi, Preparation and characterization of novel polysulfone nanofiltration membranes for removal of cadmium from contaminated water, Separation and Purification Technology, 90 (2012) 22-30.
[74] D.M. Stevens, B. Mickols, C. V. Funk, Asymmetric reverse osmosis sulfonated poly(arylene ether sulfone) copolymer membranes, Journal of Membrane Science, 452 (2014) 193-202.

[75] J. Chen, H. Huang, L. Zhang, H. Zhang, A novel high-flux asymmetric p(VDF-HFP) membrane with a dense skin for ethanol pervaporation, RSC Advances, 4 (2014) 24126-24130.
[76] G. Bakeri, S. Naeimifard, T. Matsuura, A.F. Ismail, A porous polyethersulfone hollow fiber membrane in a gas humidification process, RSC Advances, 5 (2015) 14448-14457.
[77] D.Y. Xing, S.Y. Chan, T.S. Chung, The ionic liquid [EMIM]OAc as a solvent to fabricate stable polybenzimidazole membranes for organic solvent nanofiltration, Green Chemistry, 16 (2014) 1383-1392.
[78] A.K. Pabby, S.S.H. Rizvi, A.M.S. Requena, Handbook of Membrane Separations: Chemical, Pharmaceutical, Food, and Biotechnological Applications, Second Edition ed., CRC Press 2015.
[79] L.Y. Ng, A.W. Mohammad, C.Y. Ng, A review on nanofiltration membrane fabrication and modification using polyelectrolytes: Effective ways to develop membrane selective barriers and rejection capability, Advances in Colloid and Interface Science, 197-198 (2013) 85-107.
[80] V. Kochkodan, N. Hilal, A comprehensive review on surface modified polymer membranes for biofouling mitigation, Desalination, 356 (2015) 187-207.
[81] D. He, H. Susanto, M. Ulbricht, Photo-irradiation for preparation, modification and stimulation of polymeric membranes, Progress in Polymer Science, 34 (2009) 62-98.
[82] C. Qiu, Q.T. Nguyen, Z. Ping, Surface modification of cardo polyetherketone ultrafiltration membrane by photo-grafted copolymers to obtain nanofiltration membranes, Journal of Membrane Science, 295 (2007) 88-94.
[83] C. Qiu, F. Xu, Q.T. Nguyen, Z. Ping, Nanofiltration membrane prepared from cardo polyetherketone ultrafiltration membrane by UV-induced grafting method, Journal of Membrane Science, 255 (2005) 107-115.
[84] M.N. Abu Seman, M. Khayet, Z.I. Bin Ali, N. Hilal, Reduction of nanofiltration membrane fouling by UV-initiated graft polymerization technique, Journal of Membrane Science, 355 (2010) 133-141.
[85] J.P. Robinson, E.S. Tarleton, K. Ebert, C.R. Millington, A. Nijmeijer, Influence of cross-linking and process parameters on the separation performance of poly(dimethylsiloxane) nanofiltration membranes, Industrial and Engineering Chemistry Research, 44 (2005) 3238-3248.
[86] J.P. Robinson, E.S. Tarleton, C.R. Millington, A. Nijmeijer, Evidence for swelling-induced pore structure in dense PDMS nanofiltration membranes, Filtration, 4 (2004) 50-56.
[87] D.F. Stamatialis, N. Stafie, K. Buadu, M. Hempenius, M. Wessling, Observations on the permeation performance of solvent resistant nanofiltration membranes, Journal of Membrane Science, 279 (2006) 424-433.
[88] X. Li, C.-A. Fustin, N. Lefevre, J.-F. Gohy, S.D. Feyter, J.D. Baerdemaeker, W. Egger, I.F.J. Vankelecom, Ordered nanoporous membranes based on diblock copolymers with high chemical stability and tunable separation properties, Journal of Materials Chemistry, 20 (2010) 4333-4339.
[89] K. Vanherck, I. Vankelecom, T. Verbiest, Improving fluxes of polyimide membranes containing gold nanoparticles by photothermal heating, Journal of Membrane Science, 373 (2011) 5-13.
[90] K. Vanherck, S. Hermans, T. Verbiest, I. Vankelecom, Using the photothermal effect to improve membrane separations via localized heating, Journal of Materials Chemistry, 21 (2011) 6079-6087.
[91] Y. Li, T. Verbiest, R. Strobbe, I.F.J. Vankelecom, Silver nanoparticles as localized "nano-heaters" under LED light irradiation to improve membrane performance, Journal of Materials Chemistry A, 2 (2014) 3182-3189.
[92] I. Strużyńska-Piron, M.R. Bilad, J. Loccufier, L. Vanmaele, I.F.J. Vankelecom, Influence of UV curing on morphology and performance of polysulfone membranes containing acrylates, Journal of Membrane Science, 462 (2014) 17-27.
[93] I. Struzynska-Piron, J. Loccufier, L. Vanmaele, I.F.J. Vankelecom, Synthesis of solvent stable polymeric membranes via UV depth-curing, Chemical Communications, 49 (2013) 11494-11496.
[94] I. Strużyńska-Piron, J. Loccufier, L. Vanmaele, I.F.J. Vankelecom, Parameter Study on the Preparation of UV Depth-Cured Chemically Resistant Polysulfone-Based Membranes, Macromolecular Chemistry and Physics, 215 (2014) 614-623.
[95] Y. Li, T. Verbiest, I. Vankelecom, Improving the flux of PDMS membranes via localized heating through incorporation of gold nanoparticles, Journal of Membrane Science, 428 (2013) 63-69.
[96] M. Amirilargani, E. Saljoughi, T. Mohammadi, M.R. Moghbeli, Effects of coagulation bath temperature and polyvinylpyrrolidone content on flat sheet asymmetric polyethersulfone membranes, Polymer Engineering & Science, 50 (2010) 885-893.
[97] E. Saljoughi, M. Amirilargani, T. Mohammadi, Effect of PEG additive and coagulation bath temperature on the morphology, permeability and thermal/chemical stability of asymmetric CA membranes, Desalination, 262 (2010) 72-78.
[98] S. Behnke, M. Ulbricht, Thin-film composite membranes for organophilic nanofiltration based on photo-cross-linkable polyimide, Reactive and Functional Polymers, 86 (2015) 233-242.
[99] M. Ulbricht, Advanced functional polymer membranes, Polymer, 47 (2006) 2217-2262.
[100] F.S. Denes, S. Manolache, Macromolecular plasma-chemistry: an emerging field of polymer science, Progress in Polymer Science, 29 (2004) 815-885.

[101] A.V. Volkov, S.E. Tsarkov, A.B. Gilman, V.S. Khotimsky, V.I. Roldughin, V.V. Volkov, Surface modification of PTMSP membranes by plasma treatment: Asymmetry of transport in organic solvent nanofiltration, Advances in Colloid and Interface Science.
[102] Z.P. Zhao, J. Li, J. Chen, C.X. Chen, Nanofiltration membrane prepared from polyacrylonitrile ultrafiltration membrane by low-temperature plasma: 2. Grafting of styrene in vapor phase, Journal of Membrane Science, 251 (2005) 239-245.
[103] J. Chen, J. Li, Z.-P. Zhao, D. Wang, C.-X. Chen, Nanofiltration membrane prepared from polyacrylonitrile ultrafiltration membrane by low-temperature plasma: 5. Grafting of styrene in vapor phase and its application, Surface and Coatings Technology, 201 (2007) 6789-6792.
[104] M.N. Abu Seman, N. Hilal, M. Khayet, UV-photografting modification of NF membrane surface for NOM wfouling reduction, Desalination and Water Treatment, 51 (2013) 4855-4861.
[105] S. Aerts, A. Vanhulsel, A. Buekenhoudt, H. Weyten, S. Kuypers, H. Chen, M. Bryjak, L.E.M. Gevers, I.F.J. Vankelecom, P.A. Jacobs, Plasma-treated PDMS-membranes in solvent resistant nanofiltration: Characterization and study of transport mechanism, Journal of Membrane Science, 275 (2006) 212-219.
[106] S. Karan, S. Samitsu, X. Peng, K. Kurashima, I. Ichinose, Ultrafast Viscous Permeation of Organic Solvents Through Diamond-Like Carbon Nanosheets, Science, 335 (2012) 444-447.
[107] J.E. Cadotte, R.J. Petersen, R.E. Larson, E.E. Erickson, A new thin-film composite seawater reverse osmosis membrane, Desalination, 32 (1980) 25-31.
[108] K.P. Lee, T.C. Arnot, D. Mattia, A review of reverse osmosis membrane materials for desalination—Development to date and future potential, Journal of Membrane Science, 370 (2011) 1-22.
[109] S.-P. Sun, S.-Y. Chan, T.-S. Chung, A slow–fast phase separation (SFPS) process to fabricate dual-layer hollow fiber substrates for thin-film composite (TFC) organic solvent nanofiltration (OSN) membranes, Chemical Engineering Science, 129 (2015) 232-242.
[110] M.F. Jimenez Solomon, Y. Bhole, A.G. Livingston, High flux hydrophobic membranes for organic solvent nanofiltration (OSN)-Interfacial polymerization, surface modification and solvent activation, Journal of Membrane Science, 434 (2013) 193-203.
[111] B. Khorshidi, T. Thundat, B.A. Fleck, M. Sadrzadeh, Thin film composite polyamide membranes: parametric study on the influence of synthesis conditions, RSC Advances, 5 (2015) 54985-54997.
[112] D. Li, H. Wang, Recent developments in reverse osmosis desalination membranes, Journal of Materials Chemistry, 20 (2010) 4551-4566.
[113] M.A. Kuehne, R.Q. Song, N.N. Li, R.J. Petersen, Flux enhancement in TFC RO membranes, Environmental Progress, 20 (2001) 23-26.
[114] I.-C. Kim, B.-R. Jeong, S.-J. Kim, K.-H. Lee, Preparation of high flux thin film composite polyamide membrane: The effect of alkyl phosphate additives during interfacial polymerization, Desalination, 308 (2013) 111-114.
[115] M.F. Jimenez Solomon, Y. Bhole, A.G. Livingston, High flux membranes for organic solvent nanofiltration (OSN)-Interfacial polymerization with solvent activation, Journal of Membrane Science, 423-424 (2012) 371-382.
[116] V. Freger, Swelling and Morphology of the Skin Layer of Polyamide Composite Membranes: An Atomic Force Microscopy Study, Environmental Science & Technology, 38 (2004) 3168-3175.
[117] X. Li, P. Vandezande, I.F.J. Vankelecom, Polypyrrole modified solvent resistant nanofiltration membranes, Journal of Membrane Science, 320 (2008) 143-150.
[118] S. Karan, Z. Jiang, A.G. Livingston, Sub–10 nm polyamide nanofilms with ultrafast solvent transport for molecular separation, Science, 348 (2015) 1347-1351.
[119] X. Li, M. Basko, F.D. Prez, I.F.J. Vankelecom, Multifunctional membranes for solvent resistant nanofiltration and pervaporation applicarions bases on segmented polymer network, Journal of Physical Chemistry B, 112 (2008) 16539-16545.
[120] G. Decher, J.D. Hong, J. Schmitt, Buildup of ultrathin multilayer films by a self-assembly process: III. Consecutively alternating adsorption of anionic and cationic polyelectrolytes on charged surfaces, Thin Solid Films, 210–211, Part 2 (1992) 831-835.
[121] G. Decher, Fuzzy Nanoassemblies: Toward Layered Polymeric Multicomposites, Science, 277 (1997) 1232-1237.
[122] G. Decher, M. Eckle, J. Schmitt, B. Struth, Layer-by-layer assembled multicomposite films, Current Opinion in Colloid & Interface Science, 3 (1998) 32-39.
[123] W. Feng, X. Zhou, C. He, K. Qiu, W. Nie, L. Chen, H. Wang, X. Mo, Y. Zhang, Polyelectrolyte multilayer functionalized mesoporous silica nanoparticles for pH-responsive drug delivery: layer thickness-dependent release profiles and biocompatibility, Journal of Materials Chemistry B, 1 (2013) 5886-5898.
[124] D. Ullien, P.J. Harmsma, S.M.C. Abdulla, B.M. de Boer, D. Bosma, E.J.R. Sudhölter, L.C.P.M. de Smet, W.F. Jager, Protein detection on biotin-derivatized polyallylamine by optical microring resonators, Optics Express, 22 (2014) 16585-16594.

[125] G.Z. Garyfallou, L.C.P.M. de Smet, E.J.R. Sudhölter, The effect of the type of doping on the electrical characteristics of electrolyte–oxide–silicon sensors: pH sensing and polyelectrolyte adsorption, Sensors and Actuators B: Chemical, 168 (2012) 207-213.
[126] N. Joseph, P. Ahmadiannamini, R. Hoogenboom, I.F.J. Vankelecom, Layer-by-layer preparation of polyelectrolyte multilayer membranes for separation, Polymer Chemistry, 5 (2014) 1817-1831.
[127] D. Chen, Solvent-resistant nanofiltration membranes based on multilayered polyelectrolytes deposited on silicon composite, Journal of Applied Polymer Science, 129 (2013) 3156-3161.
[128] X. Li, S. De Feyter, D. Chen, S. Aldea, P. Vandezande, F.D. Prez, I.F.J. Vankelecom, Solvent-resistant nanofiltration membranes based on multilayered polyelectrolyte complexes, Chemistry of Materials, 20 (2008) 3876-3883.
[129] X. Li, W. Goyens, P. Ahmadiannamini, W. Vanderlinden, S. De Feyter, I. Vankelecom, Morphology and performance of solvent-resistant nanofiltration membranes based on multilayered polyelectrolytes: Study of preparation conditions, Journal of Membrane Science, 358 (2010) 150-157.
[130] P. Ahmadiannamini, X. Li, W. Goyens, N. Joseph, B. Meesschaert, I.F.J. Vankelecom, Multilayered polyelectrolyte complex based solvent resistant nanofiltration membranes prepared from weak polyacids, Journal of Membrane Science, 394–395 (2012) 98-106.
[131] L.E.M. Gevers, I.F.J. Vankelecom, P.A. Jacobs, Zeolite filled polydimethylsiloxane (PDMS) as an improved membrane for solvent-resistant nanofiltration (SRNF), Chemical Communications, (2005) 2500-2502.
[132] L.E.M. Gevers, I.F.J. Vankelecom, P.A. Jacobs, Solvent-resistant nanofiltration with filled polydimethylsiloxane (PDMS) membranes, Journal of Membrane Science, 278 (2006) 199-204.
[133] A. Dobrak-Van Berlo, I.F.J. Vankelecom, B. Van der Bruggen, Parameters determining transport mechanisms through unfilled and silicalite filled PDMS-based membranes and dense PI membranes in solvent resistant nanofiltration: Comparison with pervaporation, Journal of Membrane Science, 374 (2011) 138-149.
[134] S. Basu, M. Maes, A. Cano-Odena, L. Alaerts, D.E. De Vos, I.F.J. Vankelecom, Solvent resistant nanofiltration (SRNF) membranes based on metal-organic frameworks, Journal of Membrane Science, 344 (2009) 190-198.
[135] J. Campbell, G. Szekely, R.P. Davies, D.C. Braddock, A.G. Livingston, Fabrication of hybrid polymer/metal organic framework membranes: mixed matrix membranes versus in situ growth, Journal of Materials Chemistry A, 2 (2014) 9260-9271.
[136] I. Soroko, A. Livingston, Impact of TiO2 nanoparticles on morphology and performance of crosslinked polyimide organic solvent nanofiltration (OSN) membranes, Journal of Membrane Science, 343 (2009) 189-198.
[137] W. Li, Z. Yang, Q. Meng, C. Shen, G. Zhang, Thermally stable and solvent resistant self-crosslinked TiO2/PAN hybrid hollow fiber membrane fabricated by mutual supporting method, Journal of Membrane Science, 467 (2014) 253-261.
[138] S. Roy, S.A. Ntim, S. Mitra, K.K. Sirkar, Facile fabrication of superior nanofiltration membranes from interfacially polymerized CNT-polymer composites, Journal of Membrane Science, 375 (2011) 81-87.
[139] S. Sorribas, P. Gorgojo, C. Téllez, J. Coronas, A.G. Livingston, High flux thin film nanocomposite membranes based on metal-organic frameworks for organic solvent nanofiltration, Journal of the American Chemical Society, 135 (2013) 15201-15208.
[140] L. Shao, X. Cheng, Z. Wang, J. Ma, Z. Guo, Tuning the performance of polypyrrole-based solvent-resistant composite nanofiltration membranes by optimizing polymerization conditions and incorporating graphene oxide, Journal of Membrane Science, 452 (2014) 82-89.
[141] H. Zhang, H. Mao, J. Wang, R. Ding, Z. Du, J. Liu, S. Cao, Mineralization-inspired preparation of composite membranes with polyethyleneimine-nanoparticle hybrid active layer for solvent resistant nanofiltration, Journal of Membrane Science, 470 (2014) 70-79.
[142] H. Siddique, E. Rundquist, Y. Bhole, L.G. Peeva, A.G. Livingston, Mixed matrix membranes for organic solvent nanofiltration, Journal of Membrane Science, 452 (2014) 354-366.
[143] H. Siddique, L.G. Peeva, K. Stoikos, G. Pasparakis, M. Vamvakaki, A.G. Livingston, Membranes for organic solvent nanofiltration based on preassembled nanoparticles, Industrial and Engineering Chemistry Research, 52 (2013) 1109-1121.
[144] C. Zhu, J. Zhai, D. Wen, S. Dong, Graphene oxide/polypyrrole nanocomposites: one-step electrochemical doping, coating and synergistic effect for energy storage, Journal of Materials Chemistry, 22 (2012) 6300-6306.
[145] S. Konwer, R. Boruah, S. Dolui, Studies on Conducting Polypyrrole/Graphene Oxide Composites as Supercapacitor Electrode, Journal of Electronic Materials, 40 (2011) 2248-2255.
[146] S. Smith, Oil recovery process including treating permeate from a ceramic membrane to enhance oil recovery, in: US Patent, US 20140262254 A1, 2014.
[147] B. Verrecht, R. Leysen, A. Buekenhoudt, C. Vandecasteele, B. Van der Bruggen, Chemical surface modification of γ-Al2O3 and TiO2 toplayer membranes for increased hydrophobicity, Desalination, 200 (2006) 385-386.

[148] A. Sah, H.L. Castricum, A. Bliek, D.H.A. Blank, J.E. ten Elshof, Hydrophobic modification of γ-alumina membranes with organochlorosilanes, Journal of Membrane Science, 243 (2004) 125-132.
[149] T. Van Gestel, B. Van der Bruggen, A. Buekenhoudt, C. Dotremont, J. Luyten, C. Vandecasteele, G. Maes, Surface modification of γ-Al2O3/TiO2 multilayer membranes for applications in non-polar organic solvents, Journal of Membrane Science, 224 (2003) 3-10.
[150] A.F.M. Pinheiro, D. Hoogendoorn, A. Nijmeijer, L. Winnubst, Development of a PDMS-grafted alumina membrane and its evaluation as solvent resistant nanofiltration membrane, Journal of Membrane Science, 463 (2014) 24-32.
[151] T. Tsuru, M. Miyawaki, H. Kondo, T. Yoshioka, M. Asaeda, Inorganic porous membranes for nanofiltration of nonaqueous solutions, Separation and Purification Technology, 32 (2003) 105-109.
[152] T. Tsuru, M. Miyawaki, T. Yoshioka, M. Asaeda, Reverse osmosis of nonaqueous solutions through porous silica-zirconia membranes, AIChE Journal, 52 (2006) 522-531.
[153] A.F.M. Pinheiro, Development and characterization of polymer-grafted ceramic membranes for solvent nanofiltration (Ph.D. thesis), in, University of Twente, The Netherlands, 2013.
[154] V. Ingolf, P. Petra, N. Andreas, H. Thomas, D. Gregor, Ceramic nanofiltration membrane for use in organic solvents and method for the production thereof, in: Eur. Pat., 2004.
[155] S.M. Dutczak, M.W.J. Luiten-Olieman, H.J. Zwijnenberg, L.A.M. Bolhuis-Versteeg, L. Winnubst, M.A. Hempenius, N.E. Benes, M. Wessling, D. Stamatialis, Composite capillary membrane for solvent resistant nanofiltration, Journal of Membrane Science, 372 (2011) 182-190.
[156] C.R. Tanardi, A.F.M. Pinheiro, A. Nijmeijer, L. Winnubst, PDMS grafting of mesoporous γ-alumina membranes for nanofiltration of organic solvents, Journal of Membrane Science, 469 (2014) 471-477.
[157] T. Tsuru, T. Nakasuji, M. Oka, M. Kanezashi, T. Yoshioka, Preparation of hydrophobic nanoporous methylated SiO2 membranes and application to nanofiltration of hexane solutions, Journal of Membrane Science, 384 (2011) 149-156.
[158] S. Zeidler, P. Puhlfürß, U. Kätzel, I. Voigt, Preparation and characterization of new low MWCO ceramic nanofiltration membranes for organic solvents, Journal of Membrane Science, 470 (2014) 421-430.
[159] A. Basile, A. Figoli, M. Khayet, Pervaporation, Vapour Permeation and Membrane Distillation: Principles and Applications, 1st Edition ed., ELSEVIER, 2015.

Chapter

2

Poly (maleic anhydride-alt-alkenes) directly grafted to γ-alumina for high-performance organic solvent nanofiltration membranes

This chapter contains parts of the following publication:

M. Amirilargani, R. B. Merlet, A. Nijmeijer, L. Winnubst, L. C. P. M. de Smet, E. J. R. Sudhölter, , *J. Membr. Sci*, **(2018)**, 456, 259-266.

In this chapter a novel and simple method is described to couple covalently poly (maleic anhydride-*alt*-1-alkenes) to γ-alumina nanofiltration membranes for the first time. The 1-alkenes varied from 1-hexene, 1-decene, 1-hexadecene to 1-octadecene. The grafting reaction was between the reactive anhydride moieties of the polymer and surface hydroxyl groups, resulting in highly stable bonds. The modified membranes were investigated for their permeation and rejection performance of Sudan Black (SB, *MW*=457 Da) in either toluene and ethyl acetate (EA) solution, and very high rejections (>90%) and high permeation fluxes were observed compared to unmodified membranes. Initially, the SB in toluene solution was found to bind strongly to the surface hydroxyl groups of the unmodified membranes, an effect that was not observed in EA solution.

2.1 Introduction

Nanofiltration is a pressure-driven, membrane-based separation technique with performance properties between those of ultrafiltration (UF) and reverse osmosis (RO) membranes [1, 2]. Organic solvent nanofiltration (OSN) is a young separation technique with applications ranging from the recovery of homogeneous catalysts to the purification of organic solvents [3-7]. For such applications a high chemical, mechanical and thermal membrane stability, an excellent long-time performance, and a limited pre-treatment and maintenance are often desired [8].

As polymer-based membranes have a tendency to swell or even dissolve in organic solvents, the use of ceramic membranes for OSN has therefore been growing rapidly in recent years [9-12]. Ceramic membranes show the desired high mechanical strength, are resistant to compaction and do not swell. Despite these superior properties the presence of surface hydroxyl groups makes them hydrophilic which limits their use in non-aqueous media.

A challenging strategy to overcome this limitation is by masking the surface hydroxyl groups by chemical modification with organic monolayers or polymers [3, 13, 14]. The resulting hybrid organic-ceramic membranes combine the best of two worlds: the superior properties of ceramics with tuned surface properties by proper organic/polymer chemistry. While the fabrication of hybrid organic-inorganic membranes with incorporated nanoparticles has been widely studied [15-20], hybrid polymeric-ceramic membranes in the area of OSN are much less explored. Such hybrid membranes can be obtained by two different methods. Firstly, by in-situ modification of ceramic membranes via sol-gel techniques, where the modification takes place during the selective layer preparation step. Secondly, by post modification of the ceramic membranes with polymers [11, 21-26]. The grafting of organic/polymeric moieties to alumina membranes has proven to be a convenient post-modification technique to adjust and control the membrane properties [13]. The surface OH groups are first treated with a primer acting as a linker/coupling agent between the surface OH and the organic/polymer moiety [27, 28]. In order to obtain this first step, various silane coupling agents have been investigated [29, 30]. For instance, 3-amino propyl triethoxy silane (APTES) and 3-mercapto propyl triethoxy silane (MPTES) were used as linker for the covalent grafting of polydimethylsilane (PDMS) to γ-alumina membranes [13, 31-33].

We have now explored the application of maleic anhydride-*alt*-1-alkenes alternating copolymers in the modification of inorganic membranes for the first time. The maleic anhydride unit is highly reactive towards surface OH-groups, enabling direct covalent polymer coupling, thus without the use of a linker unit. In addition, the 1-alkene unit can be varied from short chain to long chain alkenes, enabling tuning of the affinity of the functionalized membranes with various organic solvents. Here, we have investigated a series of four copolymers: three tailor-made alternating copolymers using 1-hexene to 1-hexadecene and one commercially available copolymer containing a hydrophobic

block based on 1-octadecene. The (physico-) chemical properties of these compounds are studied in detail, before providing a comprehensive investigation on the performance of γ-alumina membranes grafted with these copolymers.

2.2 Experimental section

2.2.1 Materials

All chemicals were purchased from Sigma-Aldrich, unless otherwise indicated. 1-Hexene (≥99%), 1-octene (98%), 1-decene (purum, ≥97%, Fluka) and 1-hexadecene (>99%, TCI Europe N.V.) were used for the alternating copolymerization reaction. 2,2′-Azo-bis-iso-butyronitrile (AIBN) (purum, ≥98%) was recrystallized twice from methanol. Maleic anhydride (MA) (puriss, ≥99%) was purified before use by recrystallization from anhydrous benzene and followed by sublimation. Poly(maleic anhydride-*alt*-1-octadecene) (number-average molecular weight Mn: 30-50 kDa). Flat disc-shaped α-alumina membranes (having a diameter of 39 mm, a thickness of 2 mm, and a pore diameter of 80 nm) supporting a thin (3 μm) γ-alumina layer (mean pore diameter of 5 nm), and mesoporous γ-alumina flakes with a pore diameter of ca. 5 nm, were all purchased from Pervatech B.V., The Netherlands.

2.2.2 Copolymerization procedure

MA (50 mmol), AIBN (0.5 mmol) and the respective 1-alkene (C_6, C_{10} and C_{16}) (50 mmol) were dissolved in anhydrous 1,4-dioxane (10 ml). The reaction mixture was then deaerated by a freeze-thaw method (3×) and sealed under argon atmosphere. Typically, the reaction proceeded for 4 h at 70 °C after which the reaction solution was added dropwise to methanol (100 ml, 5 °C). The precipitated polymers were collected by filtration, and reprecipitated from a tetrahydrofuran (THF) solution by pouring into methanol (5 °C). The solid material was dried for 24 h at 30 °C under vacuum. The obtained alternating copolymers of MA and 1-alkenes are further referred as P(MA-*alt*-C_X) where X indicates the number of carbon atoms of the used alkene.

2.2.3 Grafting to γ-alumina flakes and supported γ-alumina membrane

The unmodified γ-alumina membranes were washed with water and soaked in ethanol/water (2:1, vol) mixture for 24 h at room temperature to clean the surface. Then, the membranes were dried at 100 °C for 12 h under vacuum and subsequently dipped into a stirred 0.2 wt% solution of the different alternating copolymers in acetone for 12 h. Any contact between the membrane and the magnet stirrer bar was prevented. The samples were washed with pure acetone (3 times). Each membrane

sample was subsequently treated at a temperature of 10 °C above their respective glass transition temperature (T_g; see Figure A2.6) for 3 h. To remove any non-grafted alternating copolymers, the membranes were washed with acetone for 12 h in a Soxhlet apparatus. The same grafting procedure of the P(MA-*alt*-C_X) copolymers was performed for grafting to the unmodified γ-alumina flakes. A schematic diagram of the whole modification procedure is shown in Figure 2.1. As shown, nucleophilic attack by the surface hydroxyl groups promotes ring opening of maleic anhydride and esterification reaction, resulting in carboxyl group formation. The membranes grafted with different copolymers are further referred to as γ-alumina-*g*-C_X, where X has the meaning as indicated before.

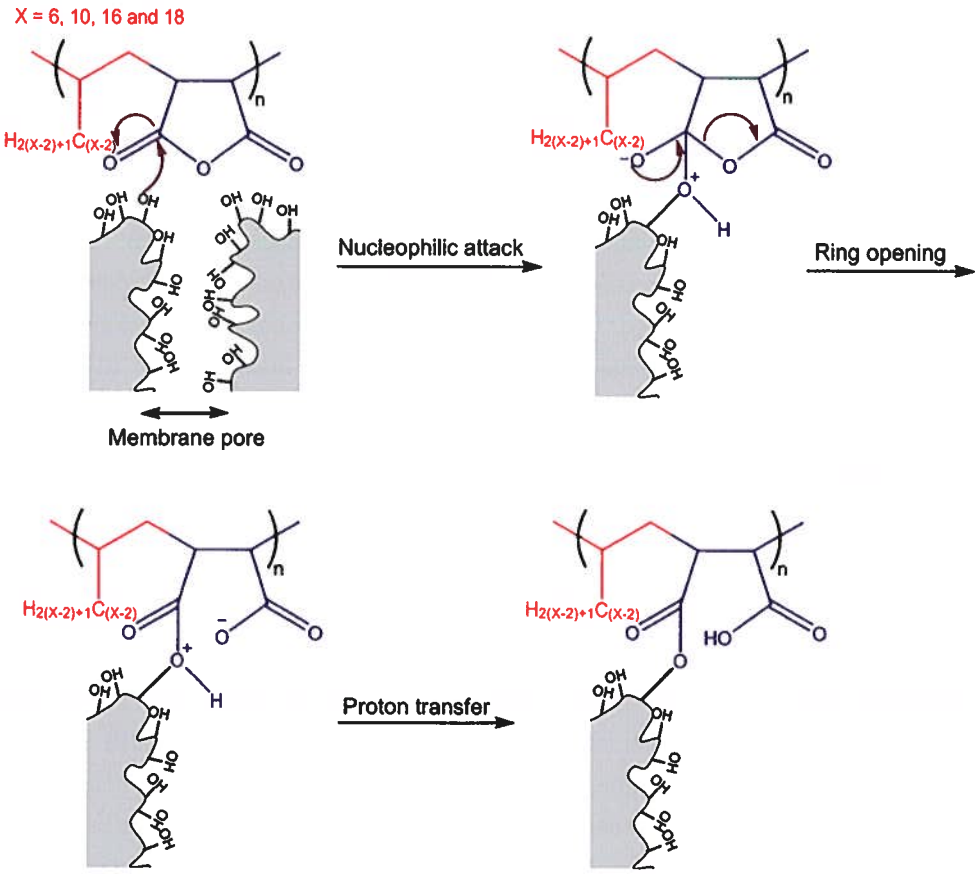

Figure 2.1 Schematic diagram showing the grafting process of the alternating copolymers to γ-alumina membranes.

2.2.4 Characterizations

Materials characterization

The number average molecular weight (Mn) of the different synthesized alternating copolymers was determined by gel permeation chromatography (GPC) in a mixture of THF:acetic acid (9:1, vol.) as eluent (flow rate: 1 ml min^{-1}, at 40 °C). The molecular weight and polydispersity index (PDI = *Mw*/*Mn*) were calibrated with polystyrene (PS) standards. Proton nuclear magnetic resonance (^{1}H-NMR) spectra of the different alternating copolymers in $CDCl_3$ were recorded at room temperature using a 400 MHz pulsed Fourier Transform NMR spectrometer (Agilent 400-MR DD2). Fourier transform infrared (FTIR) spectra of the different alternating copolymers in KBr tablets were measured using a Nicolet iS50 FTIR (Thermo Fisher Scientific Co., Madison, USA) spectrophotometer in the range of 4000-500 cm^{-1}. Each spectrum was captured by 128 scans at a resolution of 4 cm^{-1}. The thermogravimetric properties of the modified γ-alumina flakes were determined by a thermogravimetric analyzer (TGA; Mettler Toledo, TGA/SDTA 851e). The samples were heated under a N_2 atmosphere from 25 to 850 °C at a heating rate of 10 °C min^{-1}. The T_g of the different alternating copolymers were determined under an N_2 atmosphere using a Perkin Elmer 6000 differential scanning calorimeter (DSC). The samples were first heated to 250 °C and then cooled to 25 °C, before the DSC recordings started by heating to 250 °C at a heating rate of 10 °C min^{-1}. N_2 adsorption-desorption experiments were performed at -196 °C for both the unmodified and copolymers grafted γ-alumina flakes, using a Quantachrome Autosorb 1MP apparatus. The surface areas were determined by using the Brunauer-Emmet-Teller (BET) method, while the pore size distributions were determined from the desorption branch of the isotherm by the Barret-Joyner-Halenda (BJH) method. The effects of surface modification on the morphology and surface roughness was studied by analyzing the membrane surface topology using an atomic force microscope (AFM, NT-MDT, Ntegra). The roughness average (Sa) in a 500 nm × 500 nm area of the membrane surface was determined from three-dimensional AFM images. Energy dispersive X-ray (EDX) analysis was conducted in the low-vacuum mode at 10 kV using JEOL 6010 LA scanning electron microscopy (SEM). The surface wetting properties (hydrophilicity/hydrophobicity) of the differently modified membranes were determined by their static water contact angle using a Krüss FM40 Easy Drop Standard instrument. According to the standard sessile drop method, a drop of water was put on the top surface of the membrane and the contact angle was measured optically using a camera from the initial contact of the water drop. At least two measurements per membrane and three different samples of each membrane were analysed and the average values are reported.

OSN experiment procedure

Freshly grafted membranes were used for our permeation experiments. These experiments were carried out at a transmembrane pressure (TMP) of 8 bar at room temperature using a dead-end pressure cell made from stainless steel (purchased from Pervatech B.V.). The system is pressurised using inert argon. Prior to each experiment, the membranes were preconditioned with the organic solvent for 12 h. The effective area of each membrane was 8.9 cm^2 and at least three different samples of each membrane type were tested to study the reproducibility. The model solution to be separated was composed of 20 mg L^{-1} of Sudan Black (SB) in either ethyl acetate (EA) or toluene. During the permeation, the feed solution was stirred at 400 rpm to minimize concentration polarization. The membrane cell was filled with 50 ml of feed solution per membrane and 20 ml (*i.e.*, 40% recovery) of the permeate was collected for each membrane at the permeate side. In between the separation experiments, the membrane cell was thoroughly cleaned and the membranes were rinsed with the solvent used before, dipped in absolute ethanol for 8 h and then cleaned in an ultrasonic bath of absolute ethanol for 5 min. Finally, the cleaned membranes were dried in a vacuum oven at 60 °C for 24 h before the next experiment started. The membrane flux was calculated according to Equation 2.1 [15],

$$\text{Flux} = J = \frac{V}{At} = [\text{L m}^{-2}\,\text{h}^{-1}] \qquad (2.1)$$

where J is the solvent flux [L m^{-2} h^{-1}], V is the permeate volume [L], A is the effective membrane surface area [m^2] and t is the collecting permeate sample time [h]. The rejections (R) of the SB dye were calculated from the SB concentration in the permeate (C_p) and initial concentration in the feed (C_f), using Equation 2.2 [15]:

$$R = \left(1 - \frac{C_p}{C_f}\right) \times 100\% \qquad (2.2)$$

The SB concentrations were determined spectrophotometrically using a double beam UV-Vis spectrophotometer (Shimadzu, UV-1800).

2.3 Results and discussions

Before discussing the OSN performances of the modified membranes in Section 3.3, we first present and discuss the molecular characterization of the synthesized alternating copolymers and physio-chemical characterization of the copolymer-grafted flakes and membranes in Sections 3.1 and 3.2, respectively.

2.3.1 Characterization of the synthesized alternating copolymers

In Table 2.1 the number average molecular weight (*Mn*), weight average molecular weight (*Mw*) and PDI of the alternating copolymers as measured by GPC are shown. The *Mw* ranges between

~27 and ~36 Da, and Mn ranges between ~17 and ~23 kDa. The average number of repeating units is calculated from Mn divided by the molecular weight of the repeating unit. From the used molar ratios of MA and 1-alkene to AIBN initiator in our synthesis procedure, the number of repeating units in the copolymer is expected to be 100. Indeed, for alkene lengths X = 6 and 10 this is observed. For X = 16, the number of repeating units is found to be 55. It is speculated that solubility limitations of the growing polymer chain is accountable for this observation. In addition, the molecular weight was found to be independent of the alkene length used in the polymerization reaction. The same observation was reported before for the alternating copolymers made of MA and different monomers [34-36]. The PDI ranges from 1.49 to 1.56, which is characteristic for free radical polymerizations.

Table 2.1 Molecular weights and PDI values of the MA/α-olefins (C_6–C_{18}) copolymers.

Copolymer	*Mw* (Da)	*Mn* (Da)	PDI	N
Poly(MA-*alt*-C_6)	27281	18272	1.49	100
Poly(MA-*alt*-C_{10})	36562	23520	1.55	99
Poly(MA-*alt*-C_{16})	27644	17732	1.56	55
Poly(MA-*alt*-C_{18})	28246	18230	1.55	81

N = average number of repeating units

The ^{1}H-NMR spectra of the different copolymers are shown in Figures A2.1-2.4. The obtained results are similar to those reported for copolymers of MA and 1-alkenes [37]. The FTIR spectra of all copolymers used are shown in Figure A2.5, including a detailed assignment of the most characteristic bands. Finally, the thermal properties of the copolymers synthesized with different 1-alkenes are presented in the Figure A2.6. The obtained T_g values of the copolymers are in excellent agreement with literature [38].

2.3.2 Characterization of copolymer-grafted flakes and membranes

The FTIR spectra of the copolymer-grafted γ-alumina are shown in Figure 2.2. As shown, some characteristic peaks of the copolymers appeared for the grafted flakes. Small peak observed at 1730 cm^{-1} can be assigned to the C=O bond of esters and carboxylic acids indicating successful grafting. Two peaks observed at 1225 and 1467 cm^{-1} of can be related to the C-O stretching vibration of the anhydride group of copolymers during the grafting to γ-alumina flakes. They also may attributed to the partially hydrolization of copolymers. The peak observed at 1781 cm^{-1} is attributed to the stretching vibrations of the carbonyl group and is indicative for anhydride functionality. The peaks at 2925 and 2853 cm^{-1} can be attributed to the 1-alkene moiety in the copolymers and are clearly presented in the γ-alumina-*g*-copolymers. The observed higher intensity of the peaks for the γ-Al_2O_3-*g*-C_{18} are attributed to the higher grafting density of C_{18}.

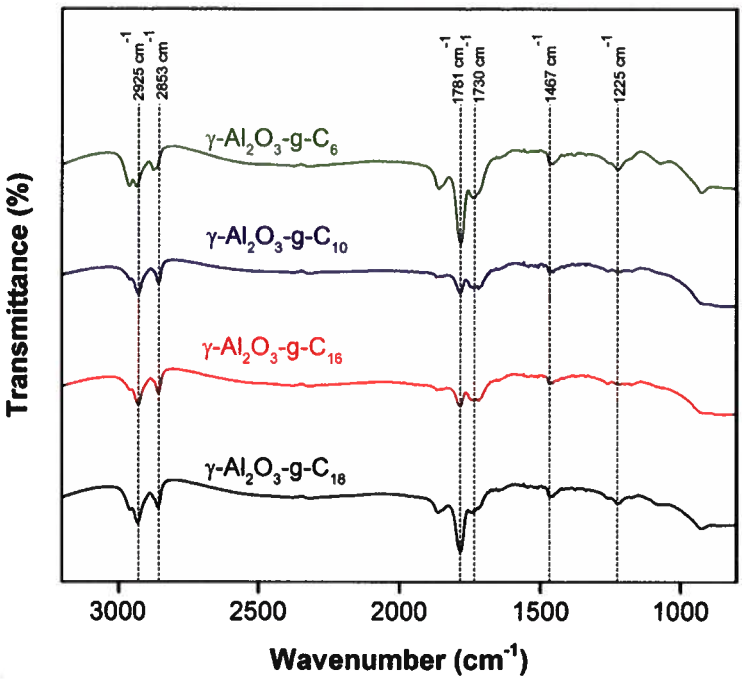

Figure 2.2 FTIR spectra of the γ-alumina flakes grafted with different copolymers. The spectra were obtained by subtracting the spectrum of unmodified γ-alumina from each measurement.

The TGA results of the pure γ-alumina flakes and copolymer-grafted flakes are presented in Figure A2.7. The total weight loss of the unmodified γ-alumina flake was just over 9 wt% at 850 °C, which is attributed to the removal of water molecules trapped inside the nanopores and to the dehydration of surface OH groups. The additional weight loss of the modified γ-alumina flakes is about 1-1.5 wt%, which can be related the loss of copolymers. The weight loss increased by grafting and the loss reached a maximum value of ~10.5 wt% for the γ-alumina-*g*-C_{18}. In addition, γ-alumina-*g*-C_{10} flakes showed the lowest weight loss of ~10 wt%, indicating the lowest coverage of grafted copolymer of this series.

N_2 adsorption-desorption isotherm showed that the pore size of the grafted flakes are almost the same as those of the unmodified flakes (Figure A2.8 and Figure A2.9). This strongly suggests that only the top surface of the flakes was modified.

TGA results of the unmodified γ-alumina membrane and copolymer-grafted membranes are presented in the Figure A2.10. The total weight loss of the unmodified membrane was ~0.15% and increased to 0.4 - 0.5% for the copolymer-grafted membranes. Although, there is no significant difference between the total weight loss of copolymer-grafted membrane, γ-alumina-*g*-C_{18}

membranes showed the highest total weight loss of ~0.5% indicating highest grafting density of poly(MA-*alt*-C_{18}).

AFM analysis was carried out to quantitatively study the roughness and roughness changes at the nanoscale of the unmodified and copolymer-grafted membranes at the nanoscale (Figure A2.11). In Figure A2.11 a, the image of the unmodified γ-alumina membrane shows a peak-valley structure, while the images of the grafted membranes become smoother as reflected by the reduced Sa values, i.e. the arithmetic average of the 3D roughness. The values of Sa for X=10 and 16 are less pronounced compared to X=6 and 18 (Figures A2.11 b-e). Small differences in grafting density may be the reason for that observation, i.e. a lower grafting densities lead to a lower reduction of Sa. Indeed for X=10, it was found that the weight loss in the TGA experiments was lower compared to others, indicating the lower grafting density (Figure A2.7 and A2.10).

Low-vacuum mode EDX was performed in this study to analyze the elemental composition of the surface of both unmodified and γ-alumina-*g*-C_{10} membranes and the results are presented in Figure 3. The integrity of membrane surface morphology will be preserved in low-vacuum mode EDX as no additional conductive coating is needed. As presented in Figures 2.3 a and 2.3 b, carbon (C), oxygen (O), aluminium (Al) and phosphorus (P) were found in both unmodified and γ-alumina-*g*-C_{10}. However, the C atom content of the γ-alumina-*g*-C_{10} is significantly higher than observed for the unmodified membrane. This proves that the membrane surface is covered with copolymer.

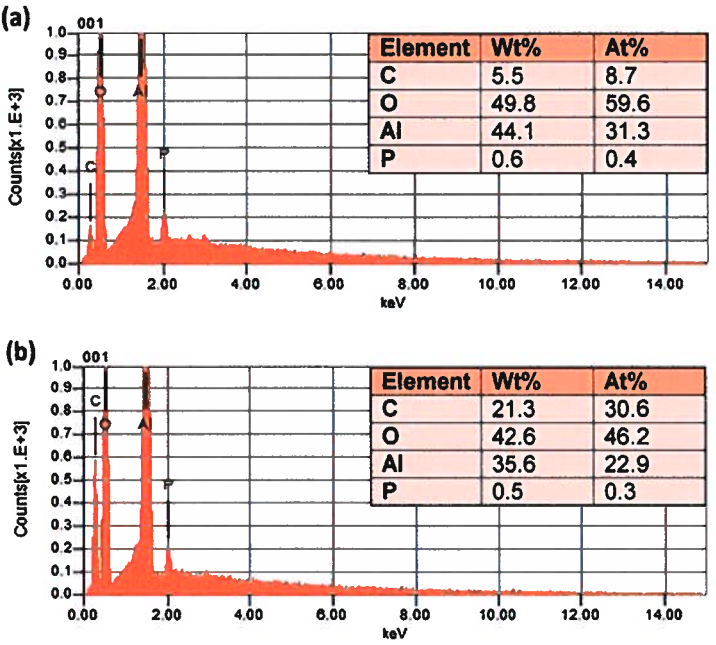

Figure 2.3 Elemental analysis of the (a) unmodified and (b) γ-alumina-*g*-C_{10} membrane by EDX.

The effect of grafting the alternating copolymers to the γ-alumina membranes on the hydrophilic/hydrophobic surface properties was investigated by static water contact angle measurements. Upon grafting, the static water contact angle increases, and this increase is larger for increasing alkyl chain length (X from 6 to 18, see Figure 2.4), reflecting an increase of hydrophobicity of the grafted surface. The highest static water contact angle of ~87 degrees was observed for the copolymer carrying the longest alkyl chain unit (X=18). This water contact angle indicates that the surface is not completely occupied by the alkyl chains. That part of the non-grafted surface OH groups and also the formed carboxylic acid group (COOH) by the anhydride ring opening reaction, contribute to the final surface polarity.

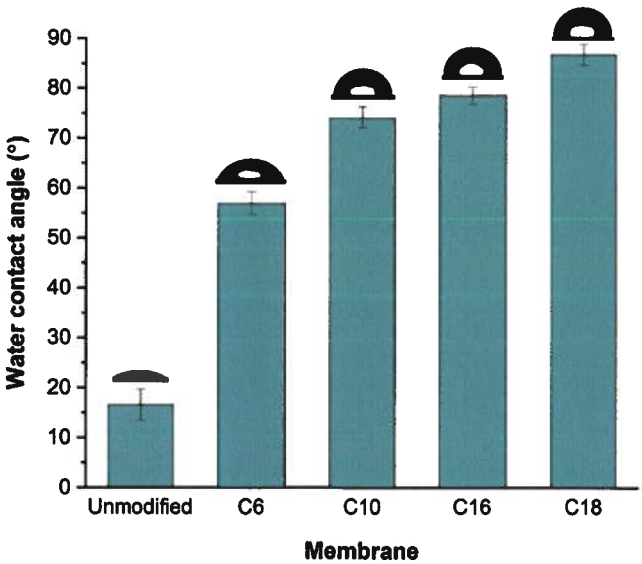

Figure 2.4 Water contact angle of unmodified and grafted membranes.

In conclusion, the grafted ceramic membranes show a strongly reduced surface hydrophilicity in comparison to the unmodified membranes.

2.3.3 OSN performance

The performance of the alternating copolymer-grafted membranes was investigated by permeation of the organic solvents and the rejection of SB solubilised in both EA and toluene. The solvent flux are found to be higher or similar for EA compared to toluene, for both the unmodified and grafted membranes (Figure 2.5).

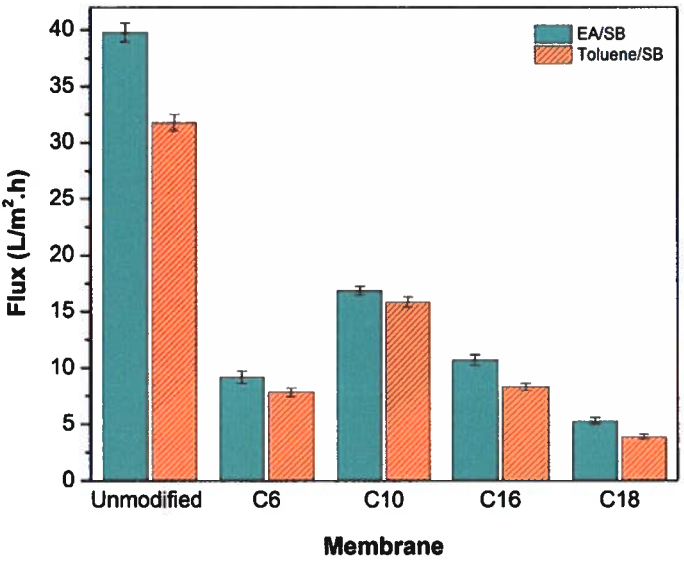

Figure 2.5 Solvent flux of the unmodified and alternating copolymer-*g*-γ-alumina membranes at TMP of 8 bar.

The difference is most pronounced for unmodified membranes. This result indicates a favourable interaction between the hydrophilic alumina pores and the more polar EA compared to the less polar toluene. Grafting reduces the solvent permeation in all cases. The highest flux were observed for C_{10} and C_{16}, while the solvent flux for C_6 and C_{18} were somewhat lower. This correlates nicely with our observed differences in the roughness of the grafted surfaces, obtained by AFM and observed total weight loss by the TGA experiments. The C_{10} and C_{16}-grafted surfaces were less smooth compared to the surfaces grafted by C_6 and C_{18}, explained by a reduced grafting density. This reduced grafting density contributes to the somewhat higher solvent flux.

To quantify the separation performance, UV-vis absorbance spectra of SB in EA and toluene from unmodified and γ-alumina-*g*-C_{10} membranes were obtained as well as optical images of the feed, permeate, and retentate (see Figure A2.12). The rejection was calculated via Equation 2.2 (Section 2.4.2) and the results are presented in Table 2.2. By using this equation, it is assumed that the amount of SB adsorbed to the membrane is negligible compared to the amounts present in retentate and permeate. The validity of this assumption was checked by making a mass balance of the situation after 40% of recovery. In Table 2.2 the SB rejection is calculated based on Equation 2.2 and the adsorbed amount of SB to the membrane are presented. The adsorbed amount of SB to the membrane was calculated from the mass balance of SB in the initial feed, permeate and retentate, and expressed as percent of the initial SB concentration in the feed phase.

Table 2.2 Separation performance of unmodified and copolymer-grafted membranes (40% recovery of the feed)*.

Membrane	SB/EA		SB/Toluene	
	Rejection (%)†	Membrane adsorption (%)	Rejection (%)†	Membrane adsorption (%)
Unmodified	18 ± 2	2	87 ± 1	36
γ-alumina-*g*-C_6	94 ± 1	5	99 ± 1	3
γ-alumina-*g*-C_{10}	90 ± 1	3	98 ± 1	6
γ-alumina-*g*-C_{16}	91 ± 1	2	99 ± 1	4
γ-alumina-*g*-C_{18}	92 ± 1	4	99 ± 1	1

*The model feed solution was a 50 ml mixture of SB (20 mg L^{-1}) in EA and toluene.

†The rejection value are calculated based on the Eq. (2.2), expressing the effects of retention and adsorption of solute by membranes.

It turns out that for most membranes (unmodified and grafted), 1-6% of the initial SB in the feed solution found to be bound to the membrane. The binding sites are most likely the surface OH groups of the alumina membranes and, for the grafted membranes, the formed carboxylic acid groups (COOH) may also play a role. A remarkably high SB adsorption of 36% is found for the unmodified membrane in toluene solution compared to an adsorption of only 2% in EA solution. This has a serious disturbing effect on the calculated (apparent) rejection of 87%. The reason for this large difference in adsorption might be that the more polar EA binds to the pore surface in competition with SB (thus less SB is bound), while the apolar toluene does not bind strongly to the pore surface, making binding of SB favourable. Also, the earlier mentioned lower grafting coverage by copolymers with X=10 and 16 (from solvent permeation flux and AFM measurements), is reflected by the higher adsorption of SB in toluene compared to EA. The amount of bound SB of 1-6% is assumed to be an equilibrium value. For these situations the rejections can be calculated reliably, based on permeate concentrations and initial feed concentrations (Table 2.2). The SB rejection of the copolymer-grafted membranes significantly improved compared to the unmodified membranes. In addition, it was shown that the copolymer-grafted membranes showed slightly higher SB rejection in the presence of toluene compared to EA. The favourable interaction between the polymer grafted surface and toluene compared to EA might be the reason for the higher SB rejection in the presence of toluene than in the presence of EA. Changing the alkene chain length does not show any significant effect on the SB rejection. Our obtained results show that the membrane surface layer properties and the specific solvent/solute interaction with the membrane surface affect the overall performance of OSN membranes [3, 39, 40].

In order to investigate the adsorption equilibrium, the separation performance of unmodified and γ-alumina-*g*-C_{10} membranes with a higher feed volume (200 mL containing 20 mg L^{-1} SB in toluene)

at a TMP of 8 bar was studied. The higher feed volume allows one to investigate whether the adsorption equilibrium is obtained. Different 20 ml batches of permeate were collected separately and analysed by UV-Vis to determine the SB concentration (see Figure A2.13). The variation of SB concentration for each collected sample of permeate is shown in Figure 2.6.

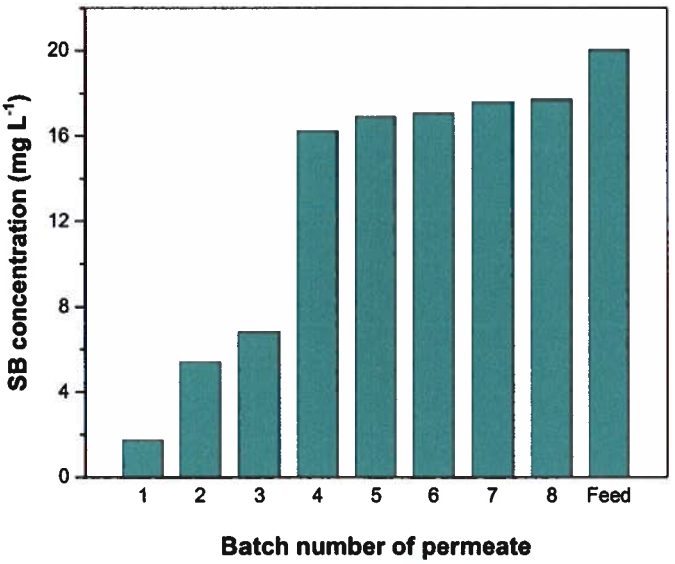

Figure 2.6. SB concentrations from sample to sample for consecutive 20 ml batches of permeate for the unmodified membrane tested with 200 ml of SB/toluene.

Initially the SB concentration was low (~6.8 mg L^{-1} for the batch number 3), while after 60 ml of permeation (30% recovery), the SB concentration significantly increased to ~16.2 mg L^{-1} in the 4th batch. Clearly, after permeating 60 ml, the SB binding sites in the membrane get saturated, and no significant additional loss of SB by binding to the membrane occurred. However the SB concentration in the retentate also might have resulted in a (slight) increase of SB bound to the membrane, as long as the binding sites were not all occupied.

To study the rejection of unmodified and γ-alumina-*g*-C_{10} membranes at different cumulative recoveries, collected batches (20 ml) of permeate were mixed and analysed with UV-Vis (Figure A2.14). For instance, 20% recovery permeate sample were prepared by mixing of 1st and 2nd batch while for the 30% recovery the 3rd batch was also added.

The UV-Vis absorption spectra of the different cumulative recoveries (from 10 up to 80%) for unmodified membrane reveal that the SB concentration increases with recovery (Figure A2.13 a). This was not observed for the γ-alumina-*g*-C_{10} membrane as the SB concentration was found to be almost constant at the full range of recoveries (Figure A2.13 b). The strong affinity of SB in toluene to the unmodified membrane at the first recoveries results in an initially low SB concentration in the

permeate. This affinity is clearly visible by the naked eye (insets in the Figure A2.13 b). As during permeation saturation of the adsorption sites on the γ-alumina is approximated, the SB concentration in the permeate increases, and rejection (as a logical consequence) decreases from ~87 to ~30% (Figure 2.7).

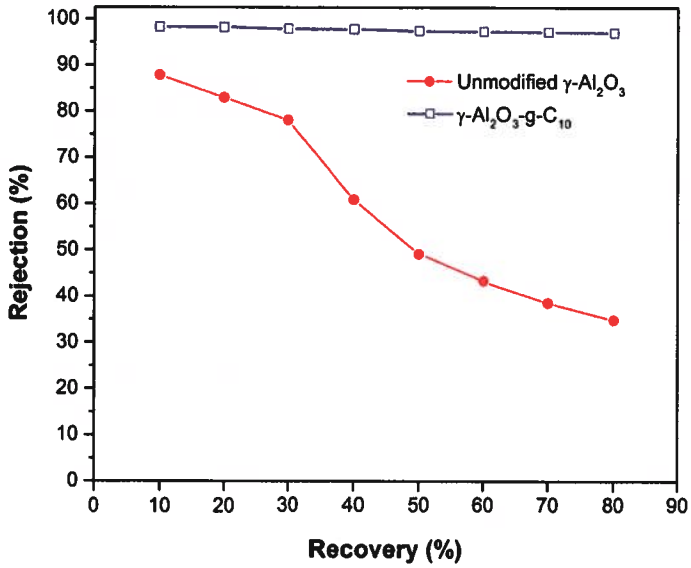

Figure 7. SB rejection from toluene solution as function of recovery observed for unmodified and γ-alumina-*g*-C_{10} membranes.

The photographs taken from the feed, retentate and permeate with different recoveries are presented in Figure A2.15.

To gain more insight into the overall OSN performance of the γ-alumina-*g*-copolymer membranes, the performance of a γ-alumina-*g*-C_{10} membrane for purification of EA and toluene was compared with previously reported functionalized ceramic membranes [21, 29, 41] and commercially polymeric STARMEM 122 membrane [42, 43]. These results are summarized in Figure 2.8. It is observed that the γ-alumina-*g*-C_{10} has the highest rejection values with comparable EA and toluene flux compared with commercially and previously reported ceramic membranes. Only commercial polydimethylsiloxane (PDMS) with different chain lengths was used in previous work on functionalization of γ-alumina membranes [29]. Generally, PDMS grafted γ-alumina membranes showed higher flux of EA and toluene while their rejection values are significantly lower than observed for the γ-alumina-*g*-C_{10} membrane. It is assumed that PDMS with a short chain length (Mw: ~1000 - 1900 Da) is grafted into the internal surface of the pores and narrows the pore diameter. In contrast, in our study the copolymers with higher molecular weight did not graft into the pores. However, the copolymers grafted on the surface of γ-alumina membranes, covered the pores and

resulted in lower flux and significantly higher rejection compared with small-chain PDMS grafted γ-alumina.

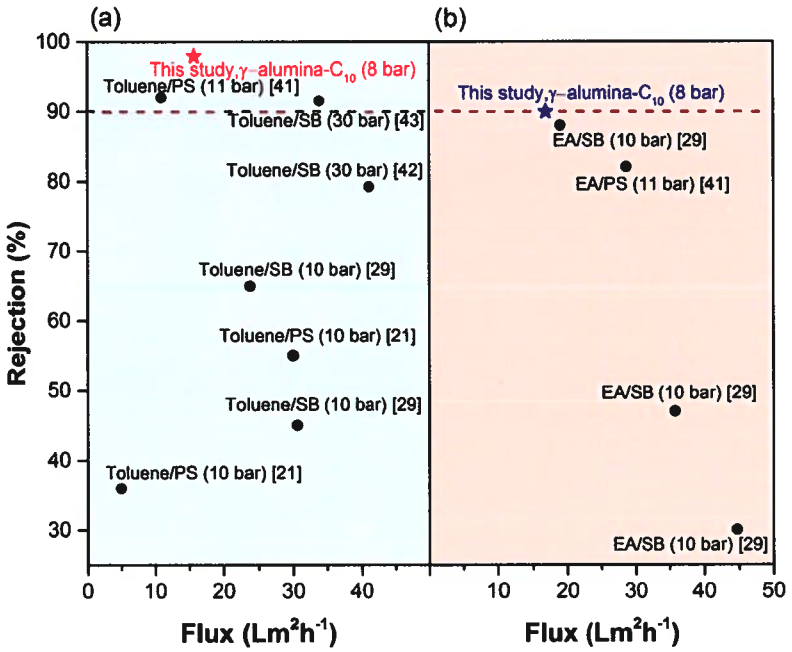

Figure 2.8 Comparison of the OSN performance of γ-alumina-*g*-C_{10} membrane with previously reported functionalized ceramic membranes [21, 29, 41] and commercially polymeric STARMEM 122 membrane [42, 43]: (a) SB or polystyrene (PS, M_w 580 Da) /toluene and (b) SB/EA were used as model feed. The dotted line represented 90% solute rejection.

2.5 Conclusions

Hybrid organic solvent nanofiltration (OSN) membranes were successfully made by covalent modification of ceramic γ-alumina membranes with alternating copolymers from maleic anhydride and 1-alkenes (1-hexene, 1-decene, 1-hexadecene, and 1-octadecene). The maleic anhydride unit in the polymer reacts with the surface OH groups of the ceramic membrane and reduces the surface polarity by masking the surface OH groups. The permeation is sensitive to the grafting density as shown by the higher permeation observed for X=10 and 16 compared to the other, as a result of a somewhat lower grafting density. The modification has a large effect on the increased rejection of Sudan Black (SB) from EA and toluene solution, up to values of 90 and 99%, respectively. For SB in toluene solution it was found that the SB molecules bind more strongly to the surface OH groups present in the unmodified ceramic membrane compared to SB in EA solution. The weaker binding of SB for the EA situation is attributed to a favourable competitive binding of EA with respect to SB for

binding to surface OH groups. For SB in toluene the SB binding is more favourable than the toluene binding. By increasing the permeation volume, a situation is obtained where the bound SB to surface OH groups is close to saturation, and for that situation a SB rejection of ~35% was achieved. Covalent modification of the polar γ-alumina membranes by grafting with alternating copolymers of maleic anhydride and 1-alkenes, increases their hydrophobicity and selectivity, rendering such membranes suitable for OSN.

References

[1] J. Zhang, Y. Hai, Y. Zuo, Q. Jiang, C. Shi, W. Li, Novel diamine-modified composite nanofiltration membranes with chlorine resistance using monomers of 1,2,4,5-benzene tetracarbonyl chloride and m-phenylenediamine, Journal of Materials Chemistry A, 3 (2015) 8816-8824.
[2] J. Zhu, M. Tian, J. Hou, J. Wang, J. Lin, Y. Zhang, J. Liu, B. Van der Bruggen, Surface zwitterionic functionalized graphene oxide for a novel loose nanofiltration membrane, Journal of Materials Chemistry A, 4 (2016) 1980-1990.
[3] M. Amirilargani, M. Sadrzadeh, E.J.R. Sudhölter, L.C.P.M. de Smet, Surface modification methods of organic solvent nanofiltration membranes, Chemical Engineering Journal, 289 (2016) 562-582.
[4] G. Szekely, M.F. Jimenez-Solomon, P. Marchetti, J.F. Kim, A.G. Livingston, Sustainability assessment of organic solvent nanofiltration: From fabrication to application, Green Chemistry, 16 (2014) 4440-4473.
[5] A.V. Volkov, G.A. Korneeva, G.F. Tereshchenko, Organic solvent nanofiltration: Prospects and application, Russian Chemical Reviews, 77 (2008) 983-993.
[6] F.C. Ferreira, H. Macedo, U. Cocchini, A.G. Livingston, Development of a Liquid-Phase Process for Recycling Resolving Agents within Diastereomeric Resolutions, Organic Process Research & Development, 10 (2006) 784-793.
[7] M.G. Buonomenna, J. Bae, Organic Solvent Nanofiltration in Pharmaceutical Industry, Separation & Purification Reviews, 44 (2014) 157-182.
[8] S. Rezaei Hosseinabadi, K. Wyns, V. Meynen, R. Carleer, P. Adriaensens, A. Buekenhoudt, B. Van der Bruggen, Organic solvent nanofiltration with Grignard functionalised ceramic nanofiltration membranes, Journal of Membrane Science, 454 (2014) 496-504.
[9] X.Q. Cheng, Y.L. Zhang, Z.X. Wang, Z.H. Guo, Y.P. Bai, L. Shao, Recent Advances in Polymeric Solvent-Resistant Nanofiltration Membranes, Advances in Polymer Technology, 33 (2014) 21455.
[10] L.G. Peeva, S. Malladi, A. Livingston, Nanofiltration operations in nonaqueous systems, in: L.G. Drioli (Ed.) Comprehensive Membrane Science and Engineering, Elsevier, Oxford, 2010.
[11] A. Dobrak, B. Verrecht, H. Van den Dungen, A. Buekenhoudt, I.F.J. Vankelecom, B. Van der Bruggen, Solvent flux behavior and rejection characteristics of hydrophilic and hydrophobic mesoporous and microporous TiO2 and ZrO2 membranes, Journal of Membrane Science, 346 (2010) 344-352.
[12] N.F.D. Aba, J.Y. Chong, B. Wang, C. Mattevi, K. Li, Graphene oxide membranes on ceramic hollow fibers – Microstructural stability and nanofiltration performance, Journal of Membrane Science, 484 (2015) 87-94.
[13] C.R. Tanardi, I.F.J. Vankelecom, A.F.M. Pinheiro, K.K.R. Tetala, A. Nijmeijer, L. Winnubst, Solvent permeation behavior of PDMS grafted γ-alumina membranes, Journal of Membrane Science, 495 (2015) 216-225.
[14] C.R. Tanardi, R. Catana, M. Barboiu, A. Ayral, I.F.J. Vankelecom, A. Nijmeijer, L. Winnubst, Polyethyleneglycol grafting of γ-alumina membranes for solvent resistant nanofiltration, Microporous and Mesoporous Materials, 229 (2016) 106-116.
[15] J. Campbell, R.P. Davies, D.C. Braddock, A.G. Livingston, Improving the permeance of hybrid polymer/metal-organic framework (MOF) membranes for organic solvent nanofiltration (OSN) - development of MOF thin films via interfacial synthesis, Journal of Materials Chemistry A, 3 (2015) 9668-9674.
[16] J. Campbell, G. Szekely, R.P. Davies, D.C. Braddock, A.G. Livingston, Fabrication of hybrid polymer/metal organic framework membranes: mixed matrix membranes versus in situ growth, Journal of Materials Chemistry A, 2 (2014) 9260-9271.
[17] S. Sorribas, P. Gorgojo, C. Téllez, J. Coronas, A.G. Livingston, High flux thin film nanocomposite membranes based on metal-organic frameworks for organic solvent nanofiltration, Journal of the American Chemical Society, 135 (2013) 15201-15208.
[18] H. Siddique, E. Rundquist, Y. Bhole, L.G. Peeva, A.G. Livingston, Mixed matrix membranes for organic solvent nanofiltration, Journal of Membrane Science, 452 (2014) 354-366.
[19] Y. Li, T. Verbiest, I. Vankelecom, Improving the flux of PDMS membranes via localized heating through incorporation of gold nanoparticles, Journal of Membrane Science, 428 (2013) 63-69.
[20] K. Vanherck, A. Aerts, J. Martens, I. Vankelecom, Hollow filler based mixed matrix membranes, Chemical Communications, 46 (2010) 2492-2494.
[21] S.R. Hosseinabadi, K. Wyns, A. Buekenhoudt, B. Van der Bruggen, D. Ormerod, Performance of Grignard functionalized ceramic nanofiltration membranes, Separation and Purification Technology, 147 (2015) 320-328.
[22] T. Tsuru, T. Sudou, S.-i. Kawahara, T. Yoshioka, M. Asaeda, Permeation of Liquids through Inorganic Nanofiltration Membranes, Journal of Colloid and Interface Science, 228 (2000) 292-296.
[23] T. Tsuru, M. Narita, R. Shinagawa, T. Yoshioka, Nanoporous titania membranes for permeation and filtration of organic solutions, Desalination, 233 (2008) 1-9.
[24] T. Tsuru, M. Miyawaki, T. Yoshioka, M. Asaeda, Reverse osmosis of nonaqueous solutions through porous silica-zirconia membranes, AIChE Journal, 52 (2006) 522-531.

[25] S.M. Dutczak, M.W.J. Luiten-Olieman, H.J. Zwijnenberg, L.A.M. Bolhuis-Versteeg, L. Winnubst, M.A. Hempenius, N.E. Benes, M. Wessling, D. Stamatialis, Composite capillary membrane for solvent resistant nanofiltration, Journal of Membrane Science, 372 (2011) 182-190.
[26] X. Li, C.-A. Fustin, N. Lefevre, J.-F. Gohy, S.D. Feyter, J.D. Baerdemaeker, W. Egger, I.F.J. Vankelecom, Ordered nanoporous membranes based on diblock copolymers with high chemical stability and tunable separation properties, Journal of Materials Chemistry, 20 (2010) 4333-4339.
[27] A.N. A. F. M. Pinheiro, V. G. P. Sripathi and L. Winnubst, Chemical modification/grafting of mesoporous alumina with polydimethylsiloxane (PDMS), European Journal of Chemistry, 6 (2015) 287-295.
[28] A. Amelio, M. Sangermano, R. Kasher, R. Bernstein, A. Tiraferri, Fabrication of nanofiltration membranes via stepwise assembly of oligoamide on alumina supports: Effect of number of reaction cycles on membrane properties, Journal of Membrane Science, 543 (2017) 269-276.
[29] C.R. Tanardi, A. Nijmeijer, L. Winnubst, Coupled-PDMS grafted mesoporous γ-alumina membranes for solvent nanofiltration, Separation and Purification Technology, 169 (2016) 223-229.
[30] X. Qiu, X.-Y. Xu, Y. Liang, H. Guo, The molecularly imprinted polymer supported by anodic alumina oxide nanotubes membrane for efficient recognition of chloropropanols in vegetable oils, Food Chemistry, 258 (2018) 295-300.
[31] A.F.M. Pinheiro, D. Hoogendoorn, A. Nijmeijer, L. Winnubst, Development of a PDMS-grafted alumina membrane and its evaluation as solvent resistant nanofiltration membrane, Journal of Membrane Science, 463 (2014) 24-32.
[32] C.R. Tanardi, A.F.M. Pinheiro, A. Nijmeijer, L. Winnubst, PDMS grafting of mesoporous γ-alumina membranes for nanofiltration of organic solvents, Journal of Membrane Science, 469 (2014) 471-477.
[33] R.B. Merlet, C.R. Tanardi, I.F.J. Vankelecom, A. Nijmeijer, L. Winnubst, Interpreting rejection in SRNF across grafted ceramic membranes through the Spiegler-Kedem model, Journal of Membrane Science, 525 (2017) 359-367.
[34] F. Martínez, E. Uribe, A.F. Olea, Copolymerization of Maleic Anhydride with Styrene and α-Olefins. Molecular and Thermal Characterization, Journal of Macromolecular Science, Part A, 42 (2005) 1063-1072.
[35] M.H. Nasirtabrizi, Z.M. Ziaei, A.P. Jadid, L.Z. Fatin, Synthesis and chemical modification of maleic anhydride copolymers with phthalimide groups, International Journal of Industrial Chemistry, 4 (2013) 11.
[36] O. Kudina, O. Budishevska, A. Voronov, A. Kohut, O. Khomenko, S. Voronov, Synthesis of New Amphiphilic Comb-Like Copolymers Based on Maleic Anhydride and α-Olefins, Macromolecular Symposia, 298 (2010) 79-84.
[37] M.C. Davies, Controlled alternating copolymerisation of maleic anhydride and electron donating monomers, in, Loughborough University, 2002.
[38] I.D. Gunbas, Water-borne, functional coatings from maleic anhydridecontaining copolymers : chemistry and phase behavior, in, Eindhoven University of Technology, 2012.
[39] P. Marchetti, M.F. Jimenez Solomon, G. Szekely, A.G. Livingston, Molecular Separation with Organic Solvent Nanofiltration: A Critical Review, Chemical Reviews, 114 (2014) 10735-10806.
[40] X. Li, W. Goyens, P. Ahmadiannamini, W. Vanderlinden, S. De Feyter, I. Vankelecom, Morphology and performance of solvent-resistant nanofiltration membranes based on multilayered polyelectrolytes: Study of preparation conditions, Journal of Membrane Science, 358 (2010) 150-157.
[41] S.R. Hosseinabadi, K. Wyns, V. Meynen, A. Buekenhoudt, B. Van der Bruggen, Solvent-membrane-solute interactions in organic solvent nanofiltration (OSN) for Grignard functionalised ceramic membranes: Explanation via Spiegler-Kedem theory, Journal of Membrane Science, 513 (2016) 177-185.
[42] S. Darvishmanesh, J. Degrève, B. Van Der Bruggen, Mechanisms of solute rejection in solvent resistant nanofiltration: The effect of solvent on solute rejection, Physical Chemistry Chemical Physics, 12 (2010) 13333-13342.
[43] S. Darvishmanesh, J. Degrè, B.V.D. Bruggen, Performance of solvent-pretreated polyimide nanofiltration membranes for separation of dissolved dyes from toluene, Industrial and Engineering Chemistry Research, 49 (2010) 9330-9338.

Annex

2

Poly (maleic anhydride-alt-alkenes) directly grafted to γ-alumina for high-performance organic solvent nanofiltration membranes

A2.1 Results

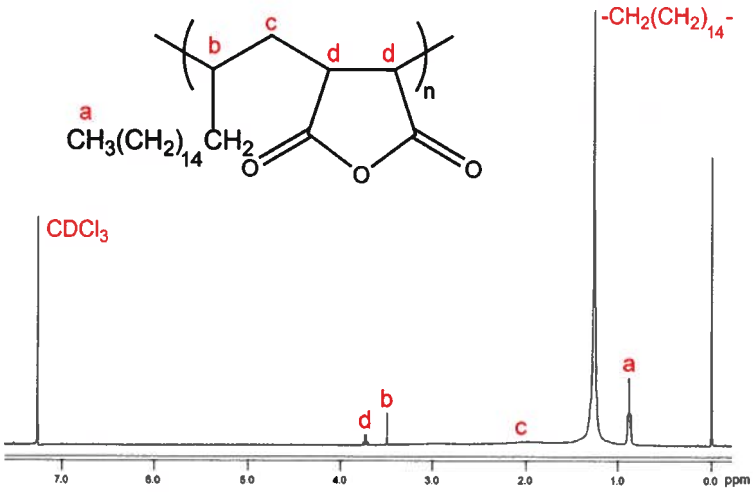

Figure A2.1 ^{1}H-NMR spectrum of P(MA-*alt*-C_{18}).

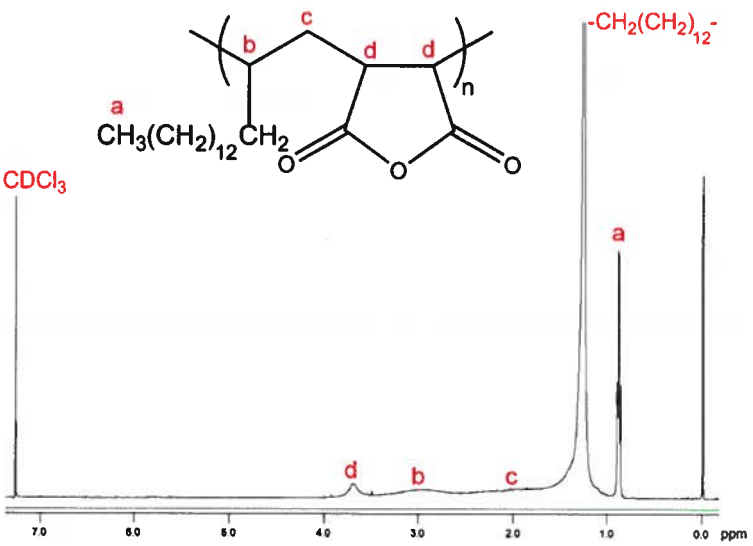

Figure A2.2 ^{1}H-NMR spectrum of P(MA-*alt*-C_{16}).

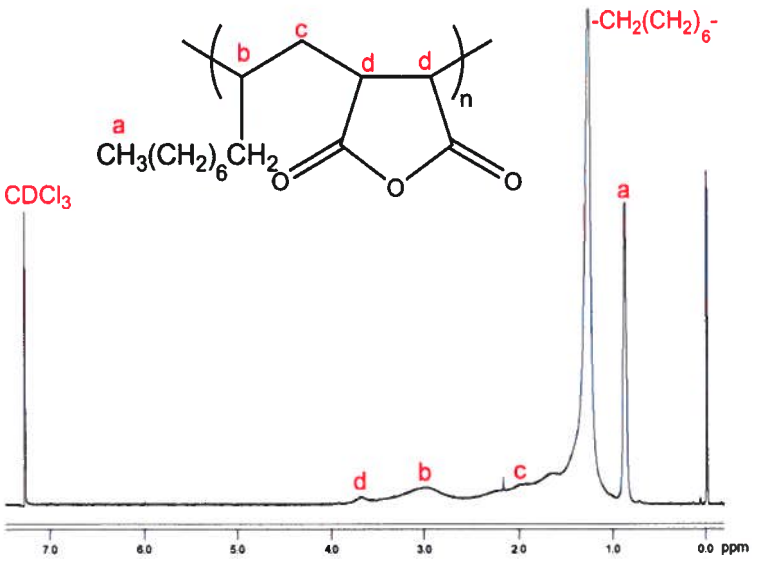

Figure A2.3 ^{1}H-NMR spectrum of P(MA-*alt*-C_{10}).

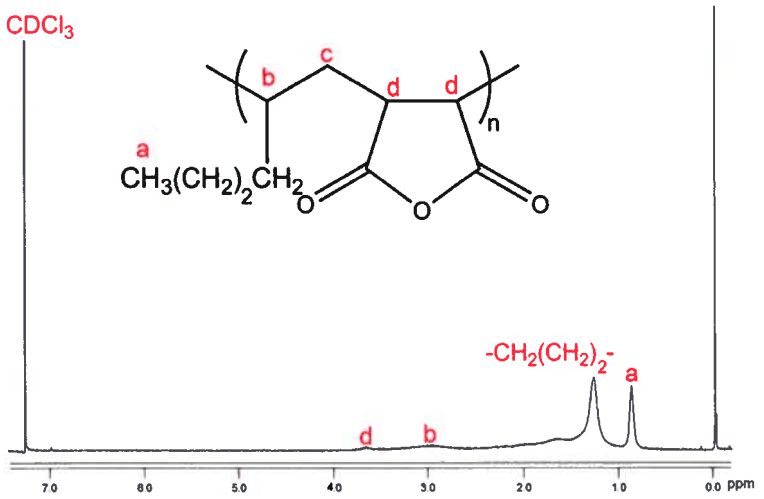

Figure A2.4 ^{1}H-NMR spectrum of P(MA-*alt*-C_6).

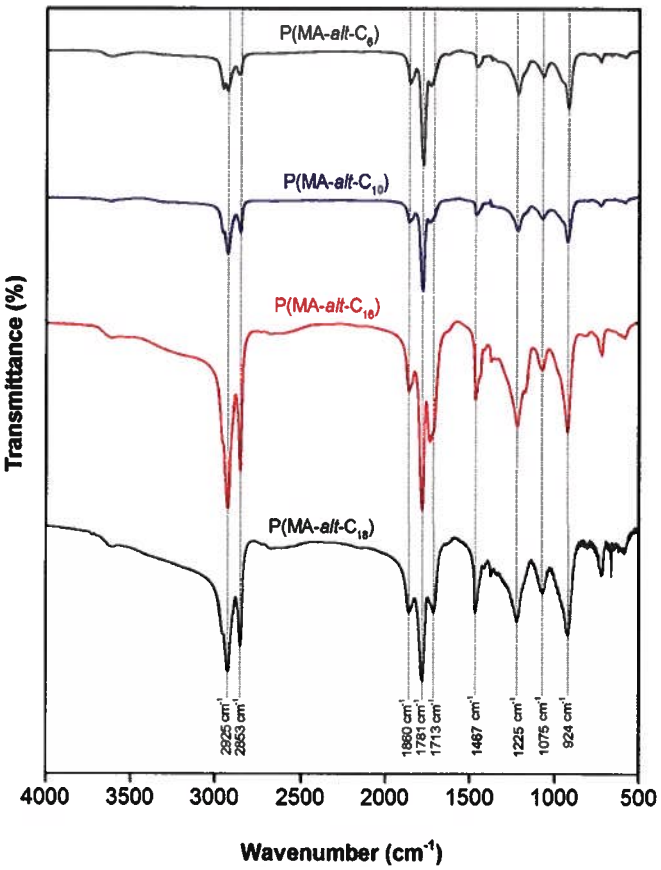

Figure A2.5 FTIR spectra of the different alternating copolymers.

Figure A2.5 shows the FTIR spectra of the copolymers under study. Compared with the spectrum of the commercially available copolymer, all the major characteristic peaks were observed. In more detail, the peaks observed at 2925 and 2853 cm^{-1} are attributed to the alkene residue in the copolymers. The peaks at 1860, 1781 and 1713 cm^{-1} are attributed to the stretching vibrations of the carbonyl group and are indicative for an anhydride functionality[1]. The peak observed at 1713 cm^{-1} is indicative for a carbonyl of an ester (formed upon the reaction with methanol during the purification step); its weakness may be explained by the low amounts of ester compared to the anhydride. The strong peaks observed at 1467, 1225 and 1075 cm^{-1} can be related to the C-O stretching. They also may attributed to the partially hydrolysis of the copolymers. The strong peak at 924 cm^{-1}, which is a characteristic feature of carboxylic acid formation, supports both these arguments. The intensity of the characteristic C-O and C=O related peaks (relative to those in the ~2850 – 2950 region) decreased for increasing alkene chain length.

The thermal stability of different copolymers is presented in Figure A2.6. As shown, up to C_{10} the T_g values decreased for increasing the alkene chain length This is most likely due to the decrease in packing density of the copolymer. However, there is no change in the observed T_g for alkene chains longer than 10. As shown in Table 1, the molecular weight and the average number of repeating units of the copolymer decreased by increasing the number of carbons from 10 to 16. On the one hand, the packing density of P(MA-*alt*-C_{16}) decreased compared with the P(MA-*alt*-C_{10}) due to the longer alkyl chain [2] while on the other hand, P(MA-*alt*-C_{16}) with 55 repeating units is almost 50% shorter than the P(MA-*alt*-C_{10}). This leads to an increase the T_g of P(MA-*alt*-C_{16}). The combination of these two opposite effects resulted in the same T_g for the copolymers synthesized with C_{10} and C_{16}. By further increasing the carbon number of the alkene chain from 16 to 18 the T_g decreased to about 90 ^{0}C, which is in good agreement with the literature [3].

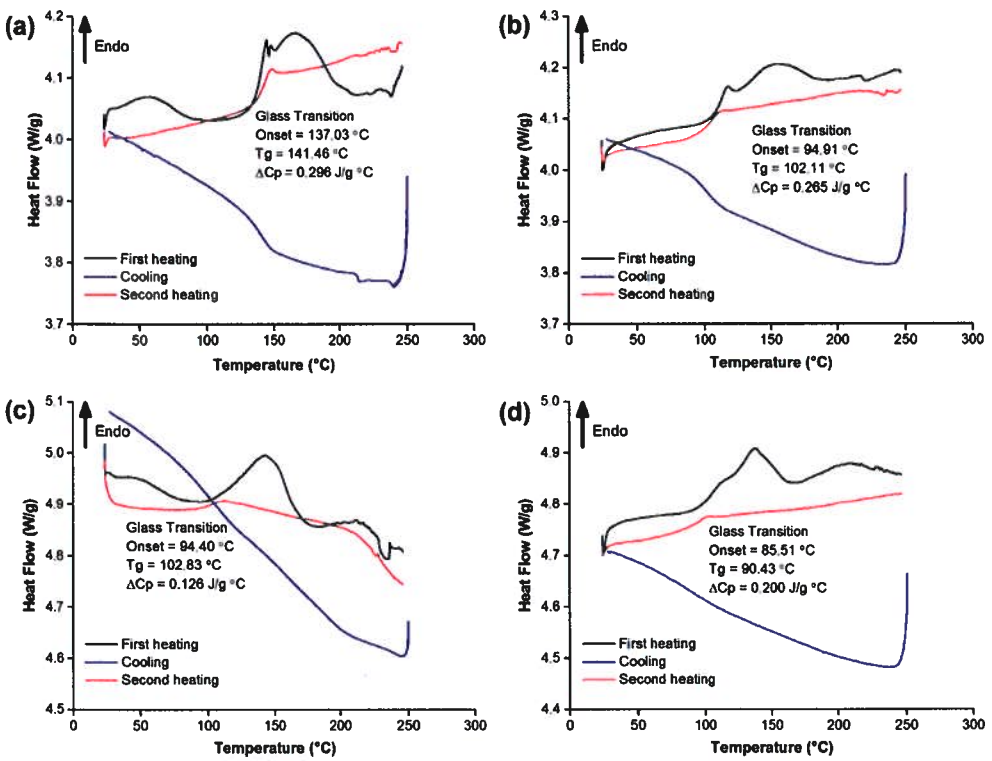

Figure A2.6 DSC thermograms of different copolymers: (a) Poly(MA-*alt*-C_6), (b) Poly(MA-*alt*-C_{10}), (c) Poly(MA-*alt*-C_{16}) and (d) Poly(MA-*alt*-C_{18}).

Successful grafting of copolymers to γ-alumina flakes was confirmed using TGA analysis. Representative TGA curves show that γ-alumina-*g*-C_{10} flakes has a lower weight loss indicates lower grafting density of P(MA-*alt*-C_{10}) compared to other copolymers (Figure A2.7).

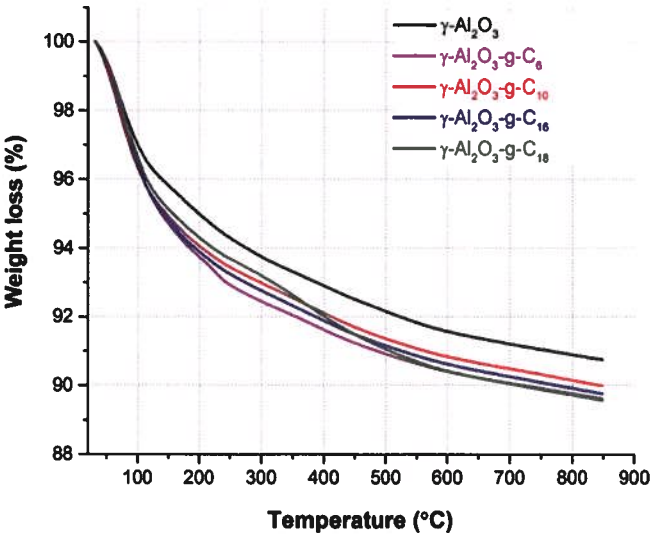

Figure A2.7 TGA curves of the γ-alumina flakes grafted with different copolymers.

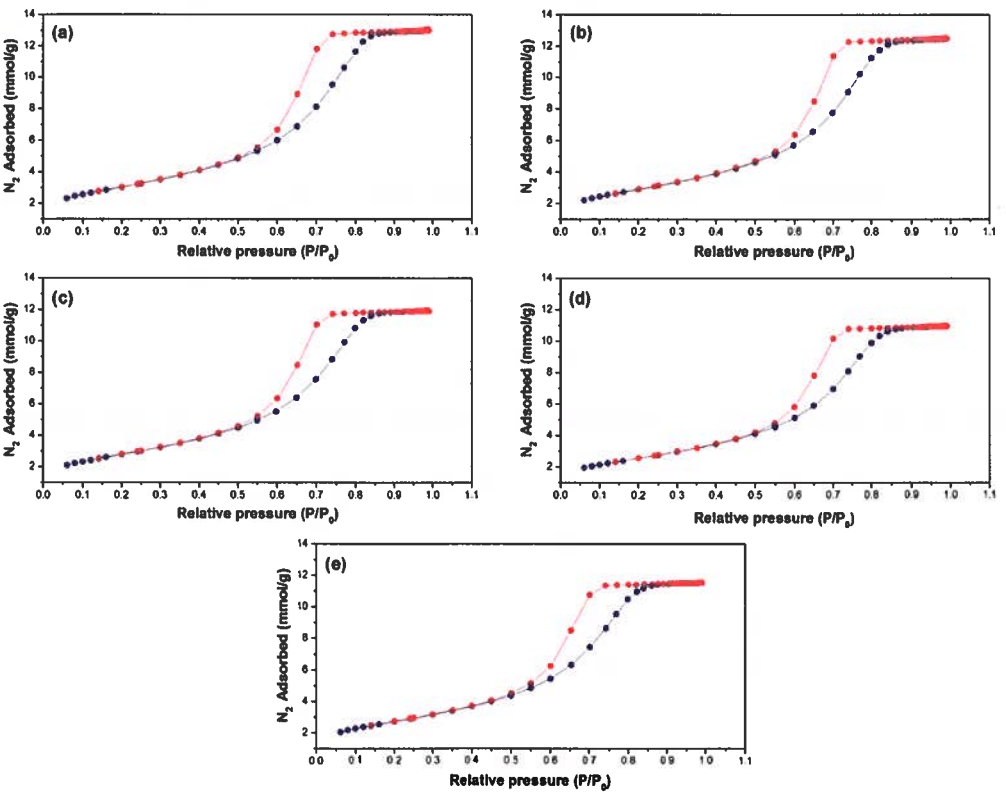

Figure A2.8 N_2 adsorption-desorption isotherm for (a) unmodified flakes, (b) γ-Al_2O_3-*g*-C_6, (c) γ-Al_2O_3-*g*-C_{10}, (d) γ-Al_2O_3-*g*-C_{16} and (e) γ-Al_2O_3-*g*-C_{18}.

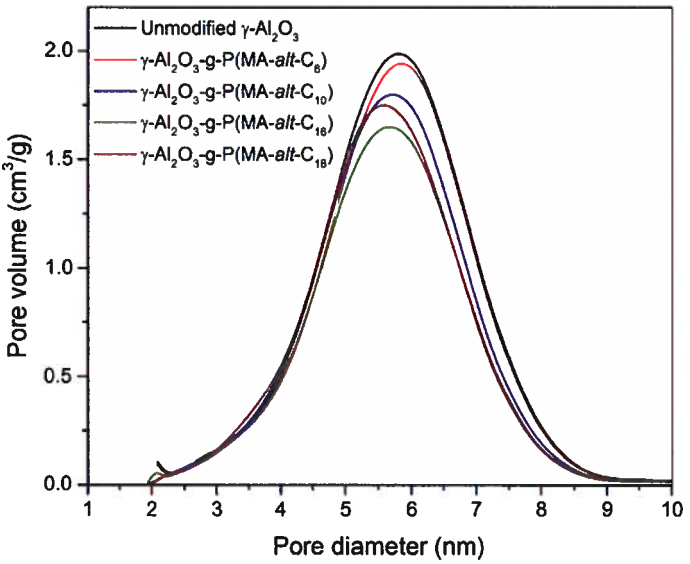

Figure A2.9 Pore size distribution of unmodified and grafted γ-alumina flakes.

Table A2.1 BET surface area and mean pore diameter of unmodified and grafted mesoporous γ-alumina flakes.

Sample	BET surface area (m^2/g)	Mean pore diameter (nm)
Unmodified γ-Al_2O_3	241.5	5.2
γ-Al_2O_3-*g*-C_6	231.0	5.2
γ-Al_2O_3-*g*-C_{10}	222.7	5.1
γ-Al_2O_3-*g*-C_{16}	204.8	5.0
γ-Al_2O_3-*g*-C_{18}	216.2	5.0

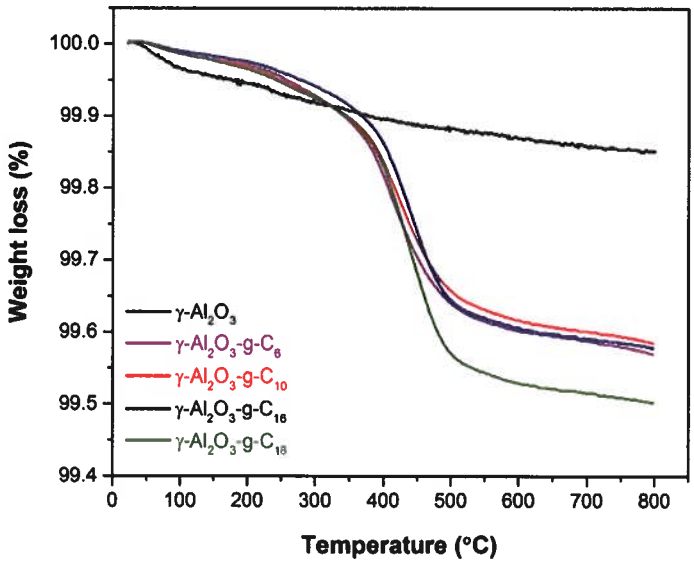

Figure A2.10 TGA curves of the γ-alumina membranes grafted with different copolymers.

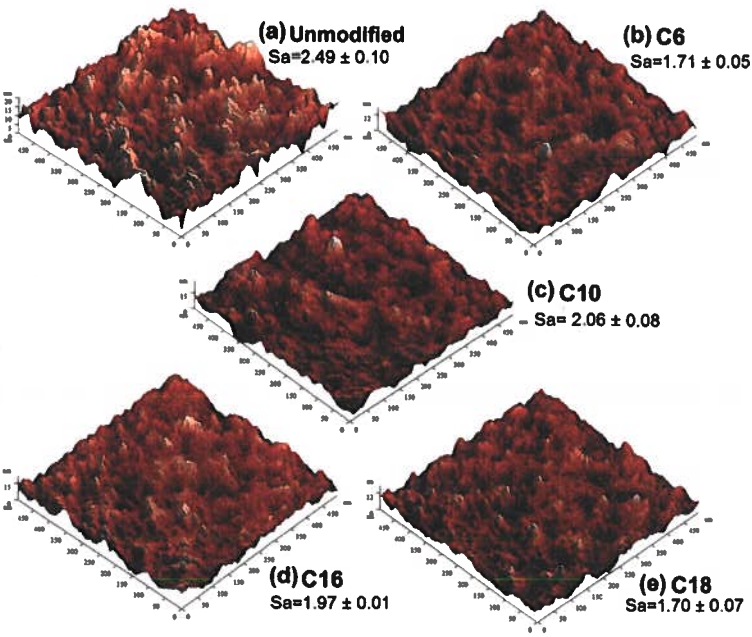

Figure A2.11 Three-dimensional AFM images of (a) unmodified γ-Al_2O_3, (b) γ-Al_2O_3-*g*-C_6, (c) γ-Al_2O_3-*g*-C_{10}, (d) γ-Al_2O_3-*g*-C_{16} and (e) γ-Al_2O_3-*g*-C_{18} membranes.

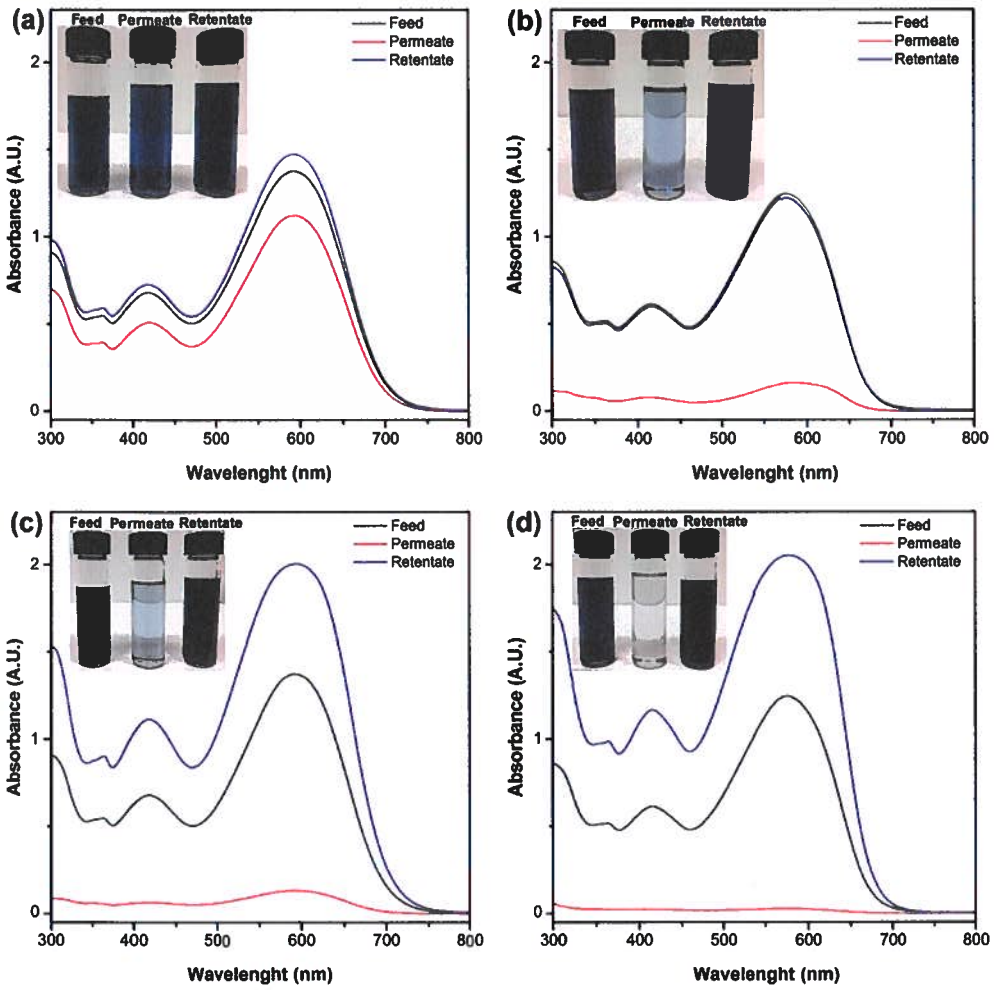

Figure A2.12 UV-vis absorption spectra of SB in (a) EA and (b) toluene for the unmodified γ-alumina membrane and in (c) EA and (d) toluene for the γ-alumina-*g*-C_{10} membrane. The insets show pictures of the feed, permeate and retentate samples.

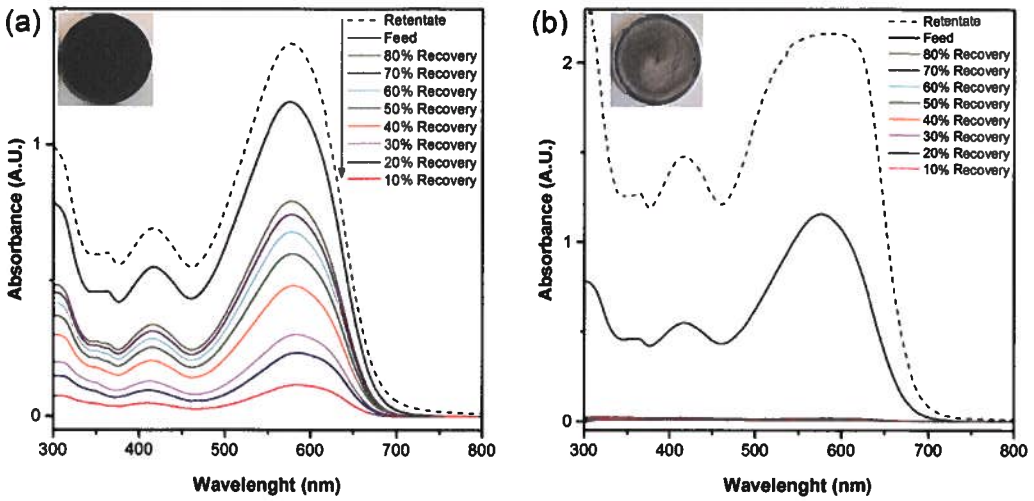

Figure A2.13 UV-vis absorption spectra of SB in toluene at different cumulative permeate recoveries for: (a) unmodified and (b) γ-alumina-*g*-C_{10} membranes. The insets give the photographs taken from an unmodified and a γ-alumina-*g*-C_{10} membrane after testing with SB/toluene. The model feed solution was a 200 ml solution of SB (20 mg L^{-1}) in toluene.

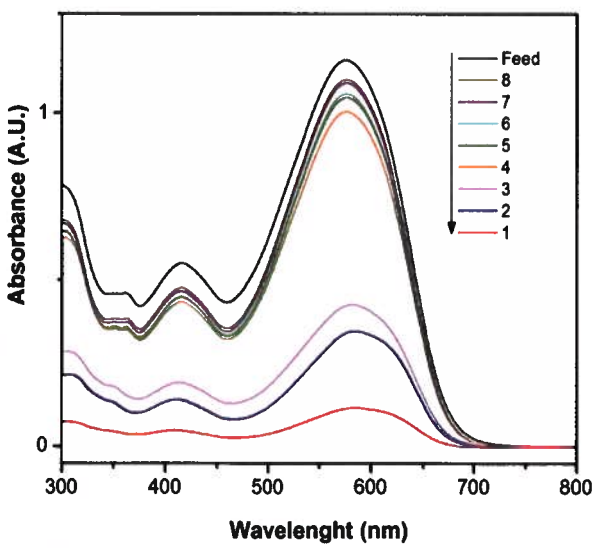

Figure A2.14 UV-vis absorption spectra of SB in toluene of different 20 ml batches of permeate collected for unmodified membrane. The model feed solution was a 200 ml mixture of SB (20 mg L^{-1}) in toluene.

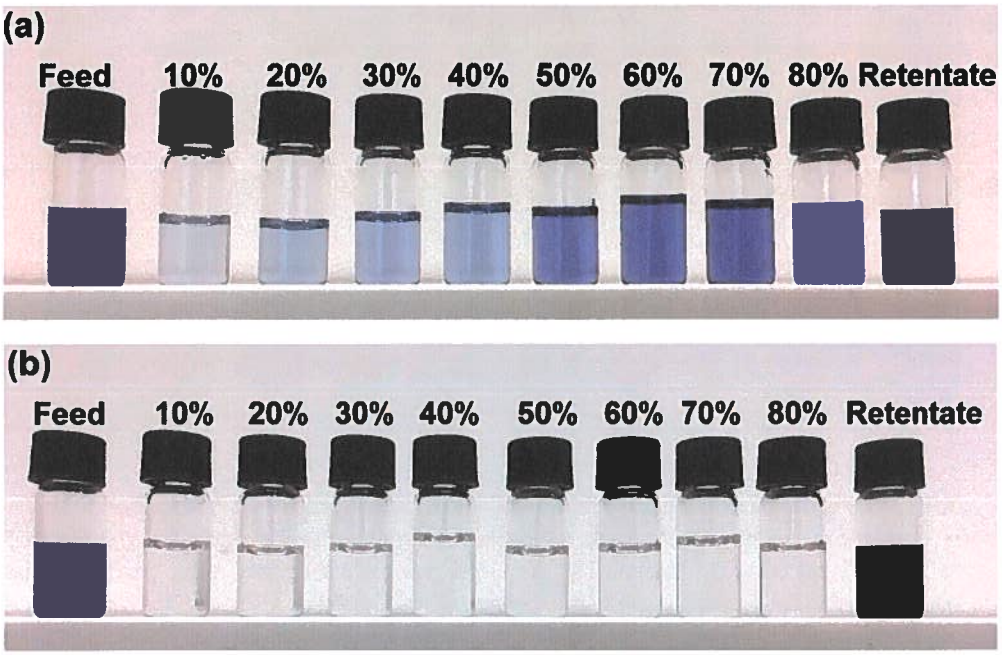

Figure A2.15 Photographs of the feed, retentate and permeate for different recoveries for (a) unmodified and (b) γ-alumina-*g*-C_{10} membranes tested with 200 ml SB/toluene solution.

References

[1] M.C. Davies, Controlled alternating copolymerisation of maleic anhydride and electron donating monomers, in, Loughborough University, 2002.
[2] R.P. Nieuwhof, Alternating side-chain liquid-crystalline copolymers with polar moieties in the backbone in, Wageningen University and Research Centre, 1999.
[3] I.D. Gunbas, Water-borne, functional coatings from maleic anhydridecontaining copolymers : chemistry and phase behavior, in, Eindhoven University of Technology, 2012.

Chapter

3

Molecular separation using poly (styrene-co-maleic anhydride) grafted to γ-alumina: surface versus pore modification

This chapter contains parts of the following publication:

M. Amirilargani, R. B. Merlet, L. Chu, A. Nijmeijer, L. Winnubst, L. C. P. M. de Smet, E. J. R. Sudhölter, , *J. Membr. Sci*, **(2019)**, 582, 298-306.

In this Chapter is reportedthe covalent coupling of poly (styrene-*co*-maleic anhydride) onto γ-alumina in order to develop high-performance organic solvent nanofiltration (OSN) membranes. A high molecular weight (M_w) alternating copolymer of maleic anhydride (MA) and styrene (St) was synthesized and directly grafted to the γ-alumina membrane, while commercially available low M_w random copolymers of styrene (St) and MA were also investigated. It is shown that solute rejection and membrane permeability strongly depend on the nature of the applied copolymer. In particular, the M_w of the copolymer applied is potentially the key for improving the membrane performance. When a high M_w copolymer was applied, the grafted layer covered the surface of the membrane. This results in membranes with a significantly improved rejection, while maintaining a high permeability. In contrast, we observed pore grafting by applying low M_w copolymers, which resulted in membranes with a slightly higher rejection and a dramatically lower permeability compared to unmodified membrane. The best results were obtained by grafting γ-alumina with a high M_w alternating copolymer. These membranes showed a solute rejection of 98% for Sudan Black B (457 g mol^{-1}) in toluene solution, while the permeability remained high at 2.9 L m^{-2} h^{-1} bar^{-1}.

3.1 Introduction

Organic solvent nanofiltration (OSN) is an energy-efficient and sustainable, pressure-driven separation process that ideally can selectively distinguish between solutes in a wide molecular weight range between 50 and 2000 g mol^{-1} [1-3]. Recently, the use of ceramic membranes for OSN applications has generated considerable interest. Ceramic membranes exhibit much better thermal stability, non-swelling behaviour, thermal, chemical and mechanical resistance, excellent long-time performance and uncomplicated cleaning procedures compared to polymeric membranes [4-10]. However, achieving molecularly selective ceramic membranes with desirable solvent permeation is still challenging. Due to the presence of surface hydroxyl groups, pristine ceramics are extremely hydrophilic and thus ill-suited to be used in non-aqueous media [6, 11-15]. Therefore, surface functionalization strategies, the design and making of selective surfaces with precise and controllable separation properties, are needed to remedy this. Tuning the surface wettability and forming a selective thin layer on ceramic oxide surfaces are usually performed via a condensation reaction between the –OH groups present at the native surface and functional group(s) of the grafting agents. For instance, different silane coupling agents such as 3-amino propyl tri-ethoxy silane (APTES) and 3-mercapto propyl tri-ethoxy silane (MPTES) were used for the covalent grafting of polydimethylsiloxane (PDMS) to γ-alumina membranes [11, 16-18].

Recently, we explored the use of maleic anhydride-*alt*-1-alkenes copolymers in the modification of γ-alumina membranes for OSN applications [19]. We showed how changing the functional groups of the copolymer grafted onto the γ-alumina membranes, influenced the membrane performance. The maleic anhydride (MA) unit is highly reactive towards surface hydroxyl groups, enabling direct covalent polymer coupling, thus without the need to use a separate linker unit. However, the research to date tends to focus on improving the OSN performance of neat ceramic membranes rather than exploring the ideal structure of the grafted membranes. Two different approaches can be applied for covalently grafting porous membranes, (i) grafting of the internal surface of the membrane pores to obtain smaller pore size [12, 20-23] and (ii) covering the membrane surface without shrinkage of the ceramic pore [24-26].

The present study aims to reveal the effects of selective layer formation on γ-alumina surfaces versus pore modification. We functionalize the γ-alumina membranes with copolymers of MA and styrene (St) with varying molecular weight and randomness of the two building blocks. We hypothesized that the relatively non-polar aromatic St moieties would introduce more hydrophobicity into the functionalized membranes compared to the previously investigated aliphatic 1-alkenes and consequently would result in membranes with higher organic solvent permeabilities. We have investigated four different MA-St copolymers: one tailor-made copolymer of MA and St with an extremely high molecular weight (M_w) and three commercially available copolymers of low M_w. We demonstrate that the high M_w copolymer was grafted only on top of the ceramic membrane surface

and not in the pores, resulting in the absence of pore shrinkage, while the low molecular weight polymers showed narrowing of the pores as a result that the surface grafting occurs in this situation also inside the pores. Furthermore, we show how these two different hybrid systems of polymer-modified alumina behave as OSN membranes for the separation of solubilized dye molecules. The performances of the unmodified and grafted membranes are investigated by measuring the permeabilities of ethyl acetate and toluene solvents and the retention of Sudan Black B (SB), Sudan Red 7B (SR7B) and Sudan Orange G (SO) organic dye solutes having M_w of 456, 379 and 214 g mol^{-1} respectively.

3.2 Experimental section

3.2.1 Materials

All chemicals were purchased from Sigma-Aldrich, unless indicated otherwise. Styrene (reagent plus, 99.9%) was passed over a column of activated basic alumina to remove the radical inhibitor. 2,2´-Azo-*bis*-*iso*-butyronitrile (AIBN) (purum, ≥98%) was recrystallized twice from methanol. Maleic anhydride (MA) (puriss, ≥99%) was purified before use by recrystallization from anhydrous benzene and followed by sublimation. Besides the synthesized styrene-*co*-maleic anhydride (SMA) copolymer, we used also three commercially available random copolymers of MA and St with different M_w and MA : St molar ratios. Xiran SZ 25010 and Xiran SZ 40005 were a kind gift from Polyscope Polymers (Geleen, The Netherlands). We also used SMA copolymer supplied by ABCR. The three commercially available SMA copolymers assessed in this work are detailed in Table 3.1.

Table 3.1 Properties of commercially available SMA used in this work*.

MA (mol%)	St (mol%)	M_w (kDa)	M_n (kDa)	Commercial name	Supplier
25	75	10	25	Xiran SZ 25010	Polyscope
40	60	5	_____	Xiran SZ 40005	Polyscope
50	50	1.7	_____	_____	ABCR

* Provided by the indicated companies.

Flat disc-shaped α-alumina membranes (having a diameter of 39 mm, a thickness of 2 mm, and a pore diameter of 80 nm) supporting a thin (3 μm) γ-alumina layer (mean pore diameter of 5 nm), and mesoporous γ-alumina flakes with a pore diameter of ca. 5 nm, were all purchased from Pervatech B.V., The Netherlands.

3.2.2 Copolymerization procedure

All synthesis and related material manipulation of the air- and moisture sensitive compounds were performed in oven-dried Schlenk-type glassware on a dual manifold Schlenk line. MA (10 mmol), St (10 mmol) and AIBN (0.2 mmol) were dissolved in anhydrous 1,4-dioxane (20 ml). The reaction mixture was then deaerated by a freeze-thaw method (3×) and sealed under an argon atmosphere. Typically, the reaction proceeded for 3 h at 60 °C after which the reaction solution was added dropwise to methanol. The precipitated polymer was collected by filtration, and reprecipitated from a tetrahydrofuran (THF) solution by pouring into methanol. The solid material was dried for 24 h at 40 °C under vacuum. The obtained copolymer of MA and St is further referred to as synthesized SMA (S-SMA).

3.2.3 Grafting to γ-alumina flakes and supported γ-alumina membrane

SMA copolymers were directly grafted to the γ-alumina membranes according to previously reported procedures[19]. Briefly, nucleophilic attack of the surface hydroxyl groups of the γ-alumina membranes on the carbonyl of the anhydride promotes the ring opening of the MA units of SMA copolymers to form an ester bond with the surface and a remaining carboxylic acid group on the copolymer chain. Prior to copolymer grafting, the alumina membranes were submerged in ethanol/water (2:1, vol) mixture for 24 h at room temperature to clean the surface and then dried at 100 °C for 12 h under vacuum [17]. Subsequently, the dried membranes were dipped into a stirred 0.15 wt% solution of the SMA copolymers in acetone for 12 h and were then washed with pure acetone (3 times). Grafted samples were subsequently treated at 100 °C for 3 h under vacuum. To remove the unreacted and physically adsorbed copolymers, the membranes were washed with acetone for 12 h in a Soxhlet apparatus at 85 °C. The same grafting procedure of the SMA copolymers was performed for modification of the γ-alumina flakes.

3.2.4 Characterizations

Materials characterization

Gel permeation chromatography (GPC) was conducted using a mixture of THF : acetic acid (9:1, vol/vol) as eluent. The number average molecular weight (M_n), weight average molecular weight (M_w) and polydispersity index (PDI = M_w/M_n) were obtained after calibration of the column with polystyrene (PS) standards. Proton nuclear magnetic resonance (^{1}H-NMR) spectrum of the S-SMA in $CDCl_3$ was recorded using a 400 MHz pulsed Fourier Transform NMR spectrometer (Agilent 400-MR DD2). Fourier transform infrared (FTIR) spectra were recorded using a Nicolet iS50 FTIR (Thermo Fisher Scientific Co., Madison, USA) by making samples via the KBr pellet method. Thermogravimetric analysis was done on a TGA/SDTA 851e Mettler Toledo. The samples were heated from 25 to 800

°C at a heating rate of 10 °C min^{-1} under a N_2 atmosphere. Differential scanning calorimetry (DSC) thermal analysis was performed using a Perkin Elmer 6000 analyzer to determine the glass transition temperatures (T_g) of the copolymers. N_2 adsorption-desorption isotherms were collected at -196 °C for both the unmodified and copolymers grafted to γ-alumina flakes, using a Gemini System VII from Micromeritics Instruments Corp. (USA). Specific surface areas were calculated by using the Brunauer-Emmett-Teller (BET) method, while the pore size distributions were evaluated from the desorption data of the N_2 isotherm by the Barret-Joyner-Halenda (BJH) method. Surface grafting densities of copolymers, reflected by values for δ (number of chains nm^{-2}) and ε (mg nm^{-2}) were calculated according to Equations 3.1 and 3.2:

$$\delta = \frac{\left(\frac{M_{Org}}{M_n}\right)N_a}{M_{Inorg}S_{Particle}} \quad (3.1)$$

$$\varepsilon = \frac{M_{Org}}{M_{Inorg}S_{Particle}} \quad (3.2)$$

Here, M_{Org} is the weight of copolymer grafted to the flakes assessed by TGA, M_n is the average molecular weight number of copolymer, N_a is Avogadro's number, M_{Inorg} is the mass of the flakes used for TGA (*i.e.* $M_{Inorg}$is the initial mass, so before TGA analysis minus the weight of grafted copolymer) and $S_{particle}$ is the BET surface area of unmodified γ-Al_2O_3 flakes. X-ray photoelectron spectroscopy (XPS) spectra and XPS depth profiles were recorded on a K-Alpha Thermo Fisher Scientific spectrometer using monochromatic Al Kα radiation at room temperature and at a pressure inside the analysis chamber of about 10^{-8} mbar. To calibrate the obtained XPS spectra the main peak of carbon (C 1s) line was adjusted to the reference value of E_b = 284.8 eV. Sputtering was carried out by an argon ion gun. During the sputtering, the chamber pressure was ~ 4 × 10^{-7} Torr and the ion gun was operated at 1 kV and 1 mA. Further analysis and processing was performed using the Thermo Avantage software package. Atomic force microscopy (AFM) imaging was done in intermittent-contact mode in air with an AFM instrument (NT-MDT, NTEGRA). The arithmetic mean roughness (R_a) and root-mean-square roughness (R_q) of the membranes were determined by imaging 1 μm^2 of each sample. Static water contact angle measurements were performed using a Krüss FM40 Easy Drop Standard instrument. At least two measurements per membrane and three different samples of each membrane were analysed and number-averaged values are reported.

OSN experiment procedure

Membrane performance was tested in a typical stainless steel dead-end pressure cell at a transmembrane pressure (TMP) of 8 bar at room temperature. The system is pressurized using inert argon. Prior to each experiment, the membranes were preconditioned with the organic solvent for 12 h. The effective area of each membrane was 8.9 cm^2 and at least three independently prepared membranes of each type were investigated for each solvent/solute system. The reported results are

the mean values of these measurements. The model solutions for the rejection measurement had a concentration of 20 mg L^{-1} Sudan Black (SB), Sudan Red 7 B (SR7B) or Sudan Orange G (SO) in either ethyl acetate (EA) or toluene. During the filtration, the feed solution was stirred at 400 rpm using a magnet stirrer to minimize concentration polarization near the membrane surface. The membrane cell was filled with 200 ml of feed solution per membrane and 120 ml of the permeate was collected for each membrane at the permeate side (*i.e.*, 60% recovery). The membrane permeability was calculated according to Equation 3.3 [27],

$$\text{Permeability} = \frac{J}{\Delta P} = \frac{V}{\Delta P A t} = [\text{L m}^{-2}\,\text{h}^{-1}\text{bar}^{-1}] \qquad (3.3)$$

where J is the solvent flux [L m^{-2} h^{-1}], ΔP is the applied pressure across the membrane [bar], V is the permeate volume [L], A is the effective membrane surface area [m^2] and t is the collecting permeate sample time [h]. The dye solute rejections (R) were calculated from the solutes concentration in the permeate (C_p) and initial concentration in the feed (C_f), using Equation 4 [27]:

$$R = \left(1 - \frac{C_p}{C_f}\right) \times 100\% \qquad (3.4)$$

Dye concentrations were determined spectrophotometrically using a double beam UV-Vis spectrophotometer (Shimadzu, UV-1800).

3.3 Results and discussions

3.3.1 Characterization of the copolymers

The M_n, M_w and PDI of the S-SMA and commercially purchased random copolymers were determined by GPC are tabulated in Table 3.2. The M_w of the S-SMA is significantly higher than other random copolymers. As shown in the Table 3.2, M_w ranges between ~5 and ~180 kDa, and M_n ranges between ~2 and ~100 kDa.

Table 3.2 Molecular weights and PDI values of the MA/St copolymers.

Copolymer	M_w (Da)		Mn (Da)		PDI*	T_g (°C)
	Measured by GPC	Reported by company	Measured by GPC	Reported by company		
S-SMA	179000	_____	105000	_____	1.70	208.0
Xiran SZ 25010	11339	10000	4911	4000	2.30	124.1
Xiran SZ 40005	4900	5000	2430	_____	2.01	149.0
SMA ABCR	6270	1700	3090	_____	2.02	153.7

* PDI values were calculated using GPC results.

The M_w of the Xiran SZ 25010 and Xiran SZ 40005 copolymer as determined by GPC are close to the values reported by the company (Table 3.1), while the SMA ABCR copolymer shows a higher M_w. For simplicity, Xiran SZ 25010, SMA ABCR and Xiran SZ 40005 random copolymers are further referred to R-SMA 11000, R-SMA 6000 and R-SMA 5000 where 11000, 6000 and 5000 indicate the respective M_w. With a value 1.70 the PDI of the S-SMA copolymer is smaller than those of all commercial copolymers (PDI ≥ 2.0), which is characteristic for random copolymers. The PDI value of the S-SMA copolymer resembles a St-*alternating*-MA rather than St-*random*-MA structure, as was also expected.

The ^{1}H-NMR spectrum of the S-SMA copolymer is shown in Figures A3.1. The FTIR spectra of all copolymers used are shown in Figure A3.2, along with a detailed assignment of the most characteristic peaks.

Thermal stability of the copolymers is shown in Figure A3.3 and recorded T_g values from the second heating cycle are presented in Table 3.2. A significantly higher T_g of the S-SMA is attributed to its lower PDI and alternating sequence of St and MA monomer units, which is in good agreement with the data reported in literature [28].

3.3.2 Grafted flakes and membranes

The FTIR spectra, TGA curves and pore size distribution of the copolymer-grafted γ-alumina flakes are shown in Figure 3.1. FTIR spectra were obtained by subtracting the spectrum of unmodified γ-alumina from each measurement.

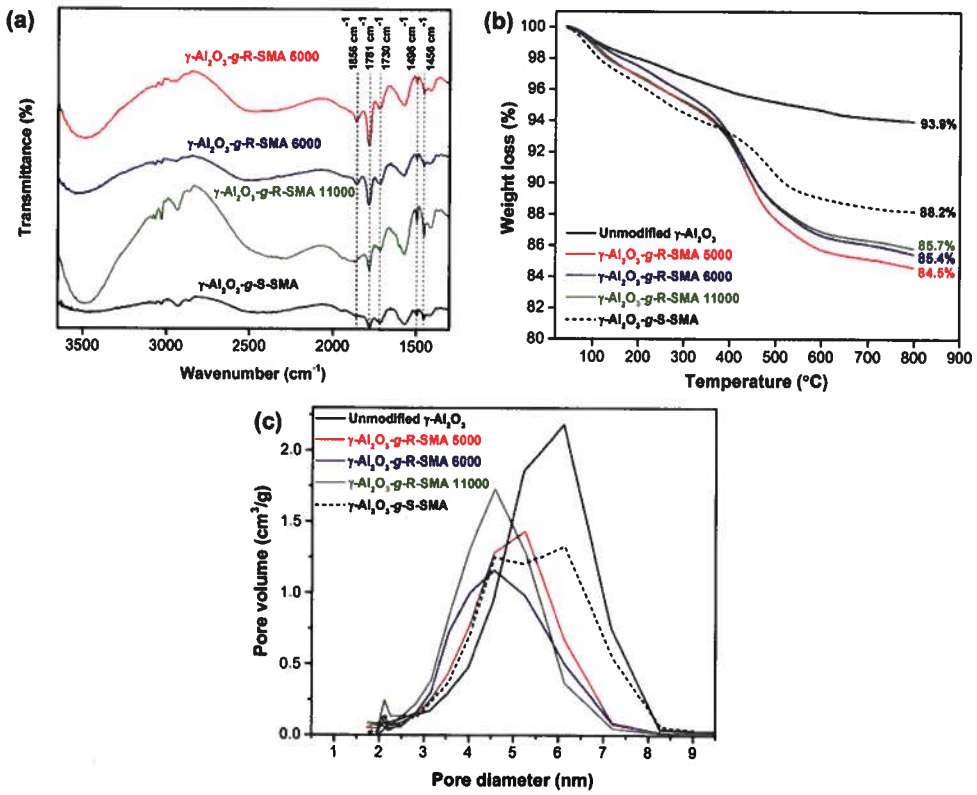

Figure 3.1 (a) FTIR spectra, (b) TGA curves and (c) pore size distribution of unmodified and grafted γ-alumina flakes.

The covalent grafting via ester bond formation becomes clear from the IR adsorption band at 1730 cm^{-1}, which can be assigned to the carbonyl stretching of the ester bond. In addition, some characteristic peaks of the copolymers were observed for the grafted flakes: the peak observed at 1496 cm^{-1} can be attributed to the C=C stretching of styrene and two peaks observed at 1781 and 1856 cm^{-1} are assigned to some unreacted maleic anhydride (C=O stretching vibration) [29]. Bands of the aromatic C-C stretching vibration feature appear at 1456 cm^{-1}.

The TGA results of the unmodified and copolymer-grafted flakes are presented in Figure 3.1 b. The total weight loss of the unmodified γ-alumina flake was just over 6 wt% at 800 °C, which is due to the removal of water molecules trapped within the pores and dehydration of surface hydroxyl groups. Additional weight loss of copolymer grafted flakes which is about 5.7-9.4 wt% indicates successful grafting. In addition, γ-Al_2O_3-*g*-S-SMA showed the lowest weight loss of 11.8 wt%, indicating the lowest coverage of this copolymer. This was expected as the S-SMA with significantly higher M_w mainly covered the surface while random copolymers with lower M_w can graft at the flake surface as well as into the pores.

The N_2 adsorption-desorption isotherms showed a slightly pore diameter shrinkage of 0.3 nm for the γ-Al_2O_3-*g*-S-SMA, while a pore diameter shrinkage of ~ 1 nm was obtained for the flakes grafted with random copolymers (Figure 3.1 c and Figure A3.4). Although the M_w of the applied S-SMA is quite high for possible grafting inside nanopores, still a pore diameter shrinkage of 0.3 nm and a reduction of ~11 m^2 g^{-1} for the BET surface area was observed for the flakes grafted with this copolymer. Contrary to the expectation, this observation could be attributed to a certain level of penetration of the styrene blocks of the copolymers into the pore entrance. In addition, upon grafting with lower M_w random copolymers the BET surface area values of the flakes were found to decrease, confirming pore grafting for this series of flakes (Table 3.3).

The surface grafting density of the copolymers was calculated according to Equations 3.1 and 3.2 and the results are tabulated in Table 3.3. The surface grafting density of S-SMA copolymer was found to be about 0.25 mg m^{-2}. Comparing to grafting density of S-SMA copolymer, significantly higher density is obtained for the series of R-SMA copolymers where R-SMA 5000 showed the highest grafting density of 0.42 mg m^{-2}. This observation is in line with FTIR spectra (Figure 3.1 a) where the higher intensity of the peaks for the γ-Al_2O_3 flakes grafted with random copolymers is due to their higher grafting density.

Table 3.3 BET surface area, mean pore diameter and surface grafting density of unmodified and grafted mesoporous γ-alumina flakes.

Sample	BET surface area (m^2/g)	Pore diameter (nm)	Surface grafting density of applied copolymer	
			δ (chains nm^{-2})	ε (mg m^{-2})
Unmodified γ-Al_2O_3	241.5	5.2	———	———
γ-Al_2O_3-*g*-S-SMA	229.3	4.9	1.4	0.25
γ-Al_2O_3-*g*-R-SMA 11000	207.4	4.2	44.9	0.36
γ-Al_2O_3-*g*-R-SMA 6000	206.2	4.4	74.8	0.38
γ-Al_2O_3-*g*-R-SMA 5000	209.2	4.2	106.2	0.42

The AFM images given in Figure 3.2 show the alumina membranes before and after copolymer grafting with S-SMA and R-SMA 11000. In Figure 3.2 a it is clearly seen that the γ-alumina nanoparticles are closely packed at the membrane surfaces with an R_q of 4.1 nm, while the images obtained from the grafted membranes show a much smoother surface as reflected by reduced R_q values of 3.9 and 1.5 nm, for the membranes grafted with S-SMA and R-SMA 11000 respectively (Figures 3.2 c-f). The value of R_q for S-SMA-grafted membrane is less pronounced compared to R-SMA 11000, which may indicate a lower grafting density [19]. This observation is in line with FTIR,

TGA, N_2 adsorption-desorption and calculated grafting density results of the copolymers grafted flakes (Figure 3.1). The same qualitative trend was observed by Zhao *et al.* [30] who studied the effects of PS M_w on the surface roughness of a spin-coated film on SiO_2. They used a wide M_w range of PS (3700 to 393400 Da) and reported an increase in the surface roughness up to 114200 Da, while the roughness decreased upon the use of high M_w PS.

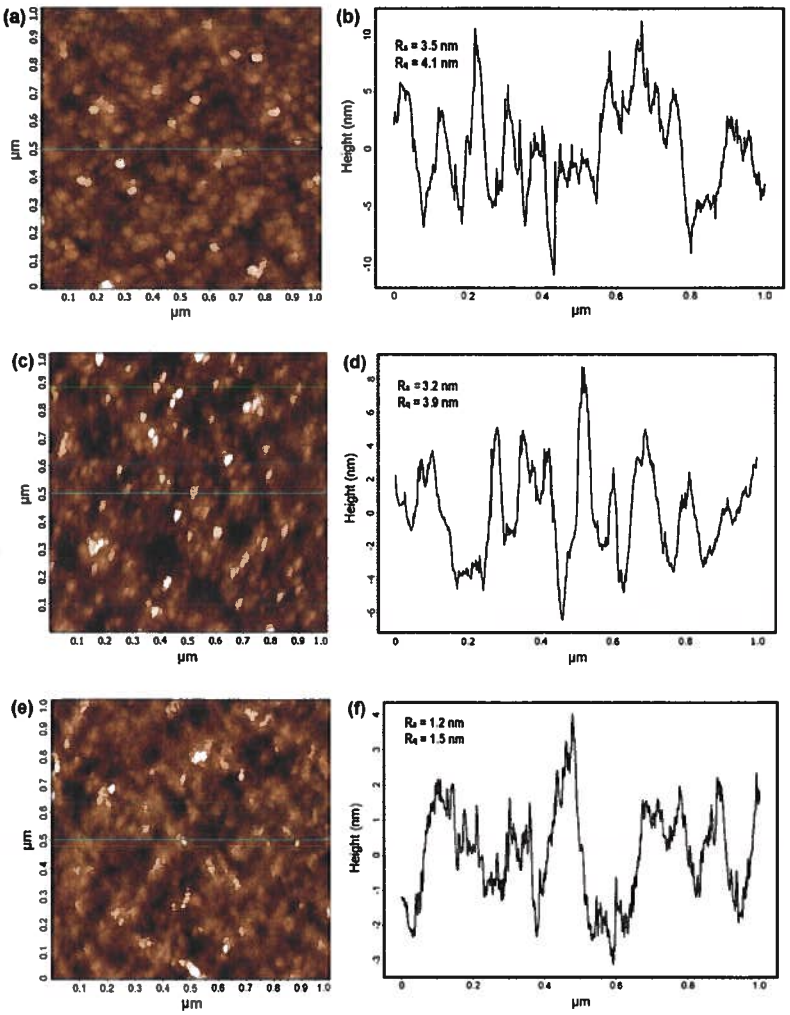

Figure 3.2 AFM images and height profiles of (a,b) unmodified γ-Al_2O_3, (c,d) γ-Al_2O_3-*g*-S-SMA and (e,f) γ-Al_2O_3-*g*-R-SMA 11000 membranes.

To assess the chemical composition of the polymer layer, we employed XPS depth profile analysis on unmodified and copolymer-grafted membranes. After each cycle of sputtering (during 60 sec), the surface chemical composition was assessed by XPS and the obtained results are shown in

Figures 3.3 a, c and e. In addition, Figures 3.3 b, d and f show the XPS C1S spectra depth profiles. The initial atomic percentages of Al, C and O and C/Al ratio before sputtering started, *i.e.* cycle # 0 and last cycle of sputtering, *i.e.* cycle # 59 are summarized in Table A 3.1.

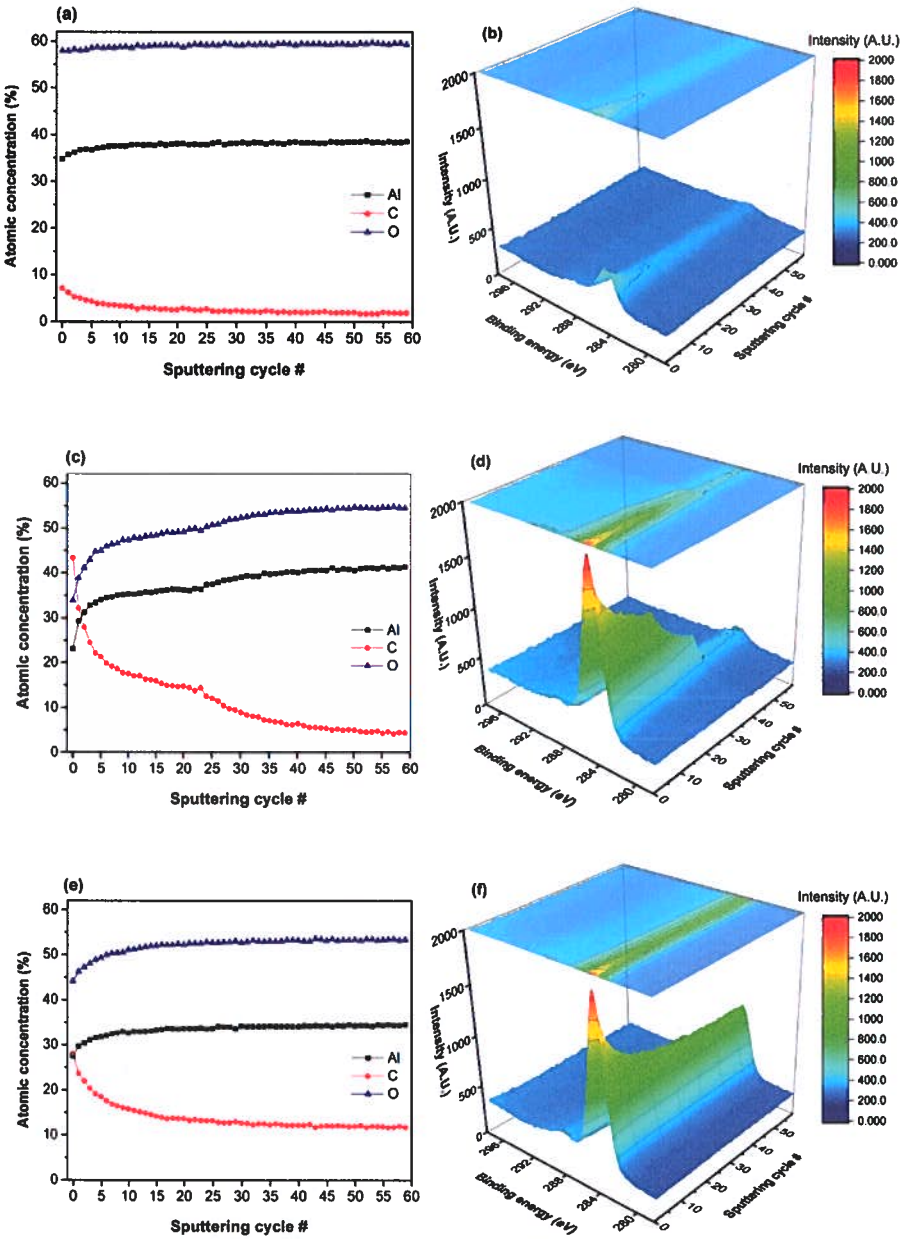

Figure 3.3 XPS atomic concentration depth profile and XPS C1S depth profile analysis of (a,b) unmodified γ-Al_2O_3, (c,d) γ-Al_2O_3-*g*-S-SMA and (e,f) γ-Al_2O_3-*g*-R-SMA 11000 membranes.

The surface atomic concentration of C had increased from ~7 to ~43 and ~28% after grafting of the unmodified membranes with S-SMA and R-SMA 11000 respectively, indicating that the copolymer grafting was successful (Figure 3.3 and Table A3.1). Although the C atomic concentration of γ-Al_2O_3-*g*-S-SMA is ~1.5× higher than the one of γ-Al_2O_3-*g*-R-SMA 11000 at sputtering cycle of 0, it reaches to ~15% after about 15 sputtering cycles for both membranes. In addition, the C concentration appears to reach a plateau value after ~20 sputtering cycles for γAl_2O_3-*g*-R-SMA 11000 (Figure 3.3 e), which was not constant until ~45 cycles of sputtering for γ-Al_2O_3-*g*-S-SMA membrane (Figure 3.3 c). The same behavior was observed for the C1S depth profile analysis of the γ-Al_2O_3-*g*-S-SMA (Figure 3.3 d), which gradually decreased from sputtering cycle of 0 to 59 while it appears to reach a plateau value for R-SMA 11000 grafted membranes after about 20 cycles of sputtering (Figure 3.3 f). These observations clearly suggest that S-SMA is mainly covering the surface, while R-SMA 11000 could penetrate through the nanopores and are grafted inside the pores. Comparable trends were observed for the γ-Al_2O_3-*g*-R-SMA 6000 and γ-Al_2O_3-*g*-R-SMA 5000 membranes (Figure A3.5 and Table A3.1).

The static water contact angles of the grafted membranes have been determined and are tabulated in Figure A3.6. For R-SMA 5000 the lowest value of 53 ± 3° was found, showing the increased hydrophobic nature. (Figure A3.6). In addition, we see that the water contact angle increases upon increasing the M_w of the copolymer and this increase is more pronounced for the S-SMA-grafted membrane, reflecting the higher hydrophobicity of that grafted surface. The membrane grafted with S-SMA showed the highest water contact angle of 105 ± 2°. As observed from the AFM and XPS studies, γ-Al_2O_3-*g*-S-SMA membrane shows the highest surface roughness and significantly more carbon present at the grafted surfaces. This is in line with the observed increased hydrophobicity.

We come overall to the conclusion that the higher M_w S-SMA is mainly grafted on the membrane surface, while the lower M_w random copolymers are also able to enter the nanopores, resulting in grafting both inside the pores and on the outer surface. The next section shows the OSN performances of unmodified and copolymer-grafted membranes.

2.3.3 OSN performance

Ethyl acetate (EA) and toluene are polar and non-polar solvents with tremendous applications and are therefore ideal choices for OSN performance tests using different dyes [31-34]. SB, SR7B and SO were chosen as different solutes and were solubilised in both EA and toluene (Figures 3.4 a-c).

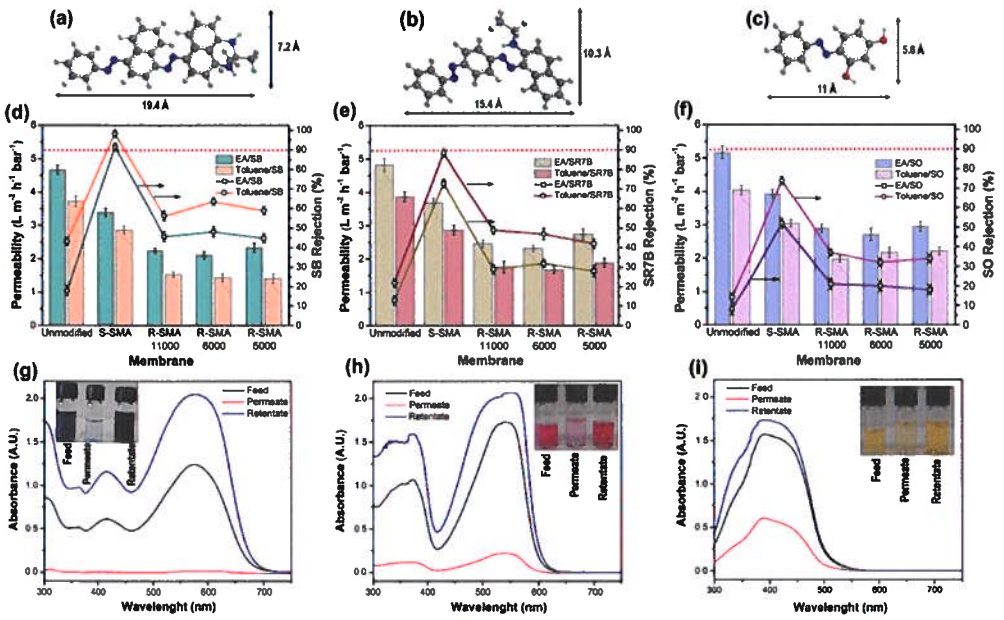

Figure 3.4 Molecular structure of (a) Sudan Black B (SB), (b) Sudan Red 7B (SR7B) and (c) Sudan Orange G (SO). Permeability and dye solute rejection performance of the unmodified and copolymers grafted γ-alumina membranes using (d) SB, (e) SR7B and (f) SO dissolved in ethyl acetate (EA) and toluene solutions. The red dashed line indicates 90% rejection of dye solutes. UV-vis absorption spectra of (g) SB, (h) SR7B and (i) SO in toluene for the γ-Al_2O_3-*g*-S-SMA membrane. The insets show pictures of the feed, permeate and retentate samples.

Grafting of γ-Al_2O_3 membrane with S-SMA dramatically enhanced dye rejection, while it only slightly decreased the solvent permeability. For instance, the grafting of a γ-Al_2O_3 membrane with S-SMA increased the SB rejection from toluene and EA by 125% and 434%, respectively compared to unmodified membranes (Figure 3.4 d). Solute rejection is found to be always lower for lower M_w of the solute. As shown in the Figures 3.4 d-f, γ-Al_2O_3-*g*-S-SMA showed 97, 89 and 75% of rejection for SB, SR7B and SO removal from toluene, respectively. Interestingly, the γ-Al_2O_3 membrane grafted with S-SMA showed the highest solvent permeability and solute rejection among the investigated and modified membranes. It can be seen that both solvent permeability and solute rejection decreased by the grafting of a copolymer with lower M_w on the γ-Al_2O_3 membrane. However, γ-Al_2O_3 membranes grafted with R-SMA 11000, R-SMA 6000 and R-SMA 5000 showed almost identical properties. These observations indicate that the structure of the grafted layer changed from the membrane grafted with S-SMA with significantly higher M_w to other membranes grafted with lower M_w of SMA. This correlates nicely with our earlier observed differences in the structure of the grafted membranes and flakes, obtained by depth profile using XPS, recorded mean pore size by N_2 adsorption-desorption, and observed total weight loss by the TGA experiments. Figure 3.5,

schematically depicts the difference in the modification of the membrane surface for SMA copolymers with different length.

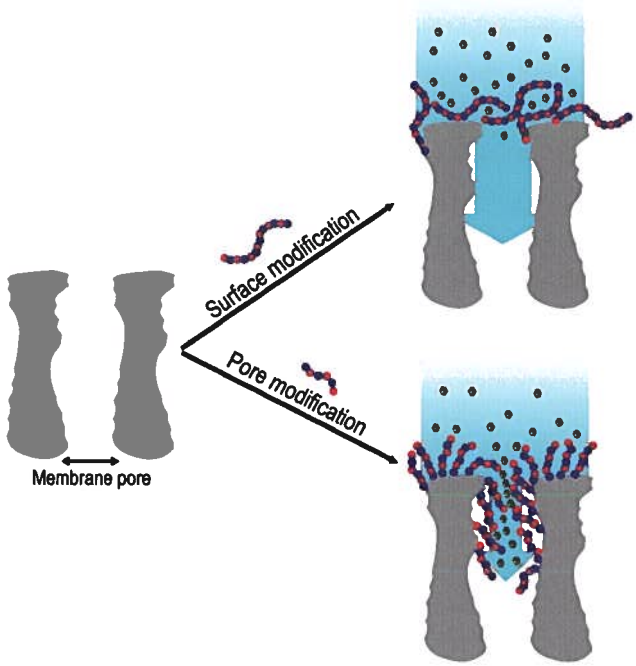

Figure 3.5 Schematic view of surface versus pore modification of γ-Al_2O_3 membrane by the grafting of high M_w (top route) and lower M_w (bottom route) SMA copolymers. For matters of simplicity only one pore is given.

In more detail, the (high M_w) S-SMA copolymers are mostly grafted on the surface of the γ-Al_2O_3 membrane, therefore providing a highly-packed and thin surface layer. This surface layer plays a role as selective layer formed on top of the 5 nm pores of the γ-alumina support. By contrast, the (lower M_w) R-SMA copolymers can penetrate deeper into the gamma alumina layer than the higher M_w S-SMA copolymers. This larger penetration depth is observed by XPS (compare Fig 3d with Fig 3f). Therefore the pores of the γ-alumina membranes grafted with R-SMA work as a selective layer and consequently show a higher resistance to solvent fluxes. In addition, the pores of γ-Al_2O_3-*g*-R-SMA are still too large to separate small solutes from toluene and ethyl acetate and therefore the solute rejections are lower compared to a membrane grafted with the higher M_w S-SMA copolymers.

2.5 Conclusions

In summary, we have utilized styrene-*co*-maleic anhydride (SMA) polymers for the covalent functionalization of γ-Al_2O_3 membranes. We showed that the SMA copolymers are successfully

grafted onto γ-alumina via ester bond formation. This covalent grafting mechanism is independent from the randomness sequence or structure of the copolymer, *i.e.* covalently bonding will take place by existence of the MA part in the copolymer structure. The significant finding emerging from this work is that, this combination of SMA grafted γ-Al_2O_3 produces two distinct structures, (i) mainly a surface-grafted membrane with negligible pore shrinkage and (ii) pore-grafted membranes with more narrow pores. The membrane grafted with the highest M_w of copolymer shows higher permeability and higher solute rejection. This observation is due to the fact that highest coverage of surface pores obtained by using this copolymer while internal pores are not grafted. In this study the grafted γ-Al_2O_3-*g*-S-SMA membrane shows the highest solute rejection with comparable toluene and EA permeabilities compared to other state-of-the-art ceramic and commercially STARMEM 122 membrane [7, 35-38] (Figure 3.6). It is worth mentioning that the SB rejection of the γ-Al_2O_3-*g*-S-SMA membrane is almost similar with the SB rejection reported in our previous study where alternating copolymers of MA and different 1-alkenes were used for membrane modification [19]. This is mainly due to the fact that in both cases the grafted copolymer modified the surface of membrane without pore grafting. However, grafting γ-Al_2O_3 membranes with S-SMA resulted in higher organic solvent permeability. As expected, this observation is due to the St moieties of the applied copolymer which introduce more hydrophobicity compared to the previously investigated aliphatic 1-alkenes and consequently resulted in membranes with higher organic solvent permeabilities.

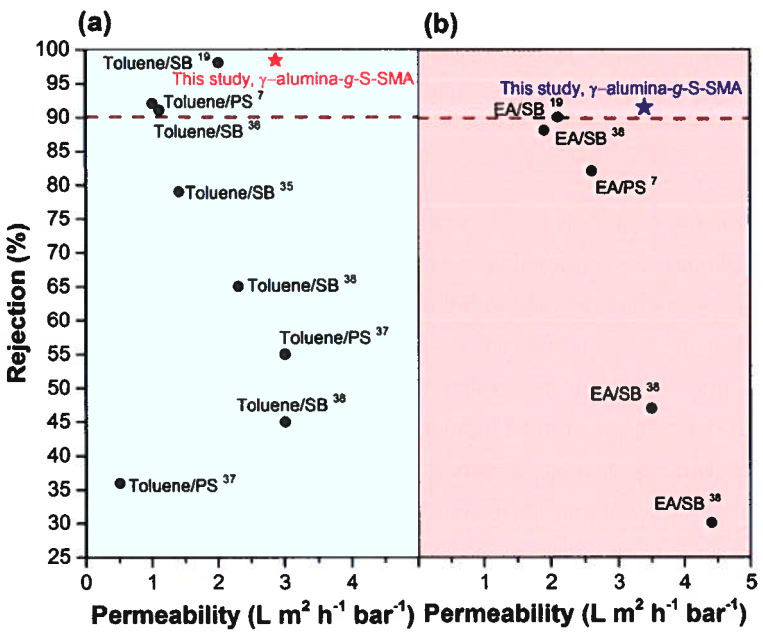

Figure 3.6 Comparison of the OSN performance of γ-Al_2O_3-*g*-S-SMA membrane with state-of-the-art ceramics and commercially polymeric STARMEM 122 membrane: (a) SB or polystyrene (PS, M_w=580

Da)/toluene and (b) SB/EA were used as model feed. The dotted line represents a solute rejection of 90%.

The unique structure of the selective layer of the γ-Al_2O_3 membrane grafted with S-SMA was found to underpin this remarkable OSN performance. Taken together, these findings opens new windows toward tailor-made, molecular-selective OSN membranes and enable further use of these hybrid OSN membranes that retain most of the solute, while maintaining the permeability.

References

[1] M. Navarro, J. Benito, L. Paseta, I. Gascón, J. Coronas, C. Téllez, Thin-Film Nanocomposite Membrane with the Minimum Amount of MOF by the Langmuir–Schaefer Technique for Nanofiltration, ACS Applied Materials & Interfaces, 10 (2018) 1278-1287.
[2] F. Fei, L. Cseri, G. Szekely, C.F. Blanford, Robust Covalently Cross-linked Polybenzimidazole/Graphene Oxide Membranes for High-Flux Organic Solvent Nanofiltration, ACS Applied Materials & Interfaces, 10 (2018) 16140-16147.
[3] C.M. Gilmer, N.B. Bowden, Highly Cross-Linked Epoxy Nanofiltration Membranes for the Separation of Organic Chemicals and Fish Oil Ethyl Esters, ACS Applied Materials & Interfaces, 8 (2016) 24104-24111.
[4] L. Xia, J. Ren, M. Weyd, J.R. McCutcheon, Ceramic-supported thin film composite membrane for organic solvent nanofiltration, Journal of Membrane Science, 563 (2018) 857-863.
[5] H.-X. Liu, C. Zhao, N. Wang, L. Shu, J. Zhou, S. Ji, J.-R. Li, Nanosheet α-Co(OH)2 composite membranes with ultrathin separation layer for removing dyes from solvent with high flux, Separation and Purification Technology, 207 (2018) 506-513.
[6] S. Rezaei Hosseinabadi, K. Wyns, V. Meynen, R. Carleer, P. Adriaensens, A. Buekenhoudt, B. Van der Bruggen, Organic solvent nanofiltration with Grignard functionalised ceramic nanofiltration membranes, Journal of Membrane Science, 454 (2014) 496-504.
[7] S.R. Hosseinabadi, K. Wyns, V. Meynen, A. Buekenhoudt, B. Van der Bruggen, Solvent-membrane-solute interactions in organic solvent nanofiltration (OSN) for Grignard functionalised ceramic membranes: Explanation via Spiegler-Kedem theory, Journal of Membrane Science, 513 (2016) 177-185.
[8] M. Priske, M. Lazar, C. Schnitzer, G. Baumgarten, Recent Applications of Organic Solvent Nanofiltration, 2015.
[9] M. Amirilargani, M. Sadrzadeh, E.J.R. Sudhölter, L.C.P.M. de Smet, Surface modification methods of organic solvent nanofiltration membranes, Chemical Engineering Journal, 289 (2016) 562-582.
[10] H. Yang, N. Wang, L. Wang, H.-X. Liu, Q.-F. An, S. Ji, Vacuum-assisted assembly of ZIF-8@GO composite membranes on ceramic tube with enhanced organic solvent nanofiltration performance, Journal of Membrane Science, 545 (2018) 158-166.
[11] C.R. Tanardi, A.F.M. Pinheiro, A. Nijmeijer, L. Winnubst, PDMS grafting of mesoporous γ-alumina membranes for nanofiltration of organic solvents, Journal of Membrane Science, 469 (2014) 471-477.
[12] J. Kujawa, S. Al-Gharabli, W. Kujawski, K. Knozowska, Molecular Grafting of Fluorinated and Nonfluorinated Alkylsiloxanes on Various Ceramic Membrane Surfaces for the Removal of Volatile Organic Compounds Applying Vacuum Membrane Distillation, ACS Applied Materials & Interfaces, 9 (2017) 6571-6590.
[13] J. Kujawa, W. Kujawski, Functionalization of Ceramic Metal Oxide Powders and Ceramic Membranes by Perfluoroalkylsilanes and Alkylsilanes Possessing Different Reactive Groups: Physicochemical and Tribological Properties, ACS Applied Materials & Interfaces, 8 (2016) 7509-7521.
[14] J. Kujawa, S. Cerneaux, W. Kujawski, M. Bryjak, J. Kujawski, How To Functionalize Ceramics by Perfluoroalkylsilanes for Membrane Separation Process? Properties and Application of Hydrophobized Ceramic Membranes, ACS Applied Materials & Interfaces, 8 (2016) 7564-7577.
[15] J. Kujawa, W. Kujawski, S. Koter, A. Rozicka, S. Cerneaux, M. Persin, A. Larbot, Efficiency of grafting of Al2O3, TiO2 and ZrO2 powders by perfluoroalkylsilanes, Colloids and Surfaces A: Physicochemical and Engineering Aspects, 420 (2013) 64-73.
[16] C.R. Tanardi, I.F.J. Vankelecom, A.F.M. Pinheiro, K.K.R. Tetala, A. Nijmeijer, L. Winnubst, Solvent permeation behavior of PDMS grafted γ-alumina membranes, Journal of Membrane Science, 495 (2015) 216-225.
[17] A.F.M. Pinheiro, D. Hoogendoorn, A. Nijmeijer, L. Winnubst, Development of a PDMS-grafted alumina membrane and its evaluation as solvent resistant nanofiltration membrane, Journal of Membrane Science, 463 (2014) 24-32.
[18] R.B. Merlet, C.R. Tanardi, I.F.J. Vankelecom, A. Nijmeijer, L. Winnubst, Interpreting rejection in SRNF across grafted ceramic membranes through the Spiegler-Kedem model, Journal of Membrane Science, 525 (2017) 359-367.
[19] M. Amirilargani, R.B. Merlet, A. Nijmeijer, L. Winnubst, L.C.P.M. de Smet, E.J.R. Sudhölter, Poly (maleic anhydride-alt-1-alkenes) directly grafted to γ-alumina for high-performance organic solvent nanofiltration membranes, Journal of Membrane Science, 564 (2018) 259-266.
[20] P.-F. Li, R. Xie, J.-C. Jiang, T. Meng, M. Yang, X.-J. Ju, L. Yang, L.-Y. Chu, Thermo-responsive gating membranes with controllable length and density of poly(N-isopropylacrylamide) chains grafted by ATRP method, Journal of Membrane Science, 337 (2009) 310-317.
[21] C.-W. Chu, Y. Higaki, C.-H. Cheng, M.-H. Cheng, C.-W. Chang, J.-T. Chen, A. Takahara, Zwitterionic polymer brush grafting on anodic aluminum oxide membranes by surface-initiated atom transfer radical polymerization, Polymer Chemistry, 8 (2017) 2309-2316.

[22] C. Sugnaux, L. Lavanant, H.-A. Klok, Aqueous Fabrication of pH-Gated, Polymer-Brush-Modified Alumina Hybrid Membranes, Langmuir, 29 (2013) 7325-7333.
[23] D. He, M. Ulbricht, Tailored "Grafting-From" Functionalization of Microfiltration Membrane Surface Photo-Initiated by Immobilized Iniferter, Macromolecular Chemistry and Physics, 210 (2009) 1149-1158.
[24] M. de Cazes, M.P. Belleville, M. Mougel, H. Kellner, J. Sanchez-Marcano, Characterization of laccase-grafted ceramic membranes for pharmaceuticals degradation, Journal of Membrane Science, 476 (2015) 384-393.
[25] S. Hou, J. Xing, X. Dong, J. Zheng, S. Li, Integrated antimicrobial and antifouling ultrafiltration membrane by surface grafting PEO and N-chloramine functional groups, Journal of Colloid and Interface Science, 500 (2017) 333-340.
[26] O. Burtovyy, V. Klep, T. Turel, Y. Gowayed, I. Luzinov, Polymeric Membranes: Surface Modification by "Grafting to" Method and Fabrication of Multilayered Assemblies, in: Nanoscience and Nanotechnology for Chemical and Biological Defense, American Chemical Society, 2009, pp. 289-305.
[27] J. Campbell, R.P. Davies, D.C. Braddock, A.G. Livingston, Improving the permeance of hybrid polymer/metal-organic framework (MOF) membranes for organic solvent nanofiltration (OSN) - development of MOF thin films via interfacial synthesis, Journal of Materials Chemistry A, 3 (2015) 9668-9674.
[28] E.S. Park, M.N. Kim, I.M. Lee, S.L. Han, J.S. Yoon, Living radical copolymerization of styrene/maleic anhydride, Journal of Polymer Science, Part A: Polymer Chemistry, 38 (2000) 2239-2244.
[29] O. Galioğlu Atici, A. Akar, R. Rahimian, Modification of poly(maleic anhydride-co-styrene) with hydroxyl containing compounds, Turkish Journal of Chemistry, 25 (2001) 259-266.
[30] J. Zhao, S. Jiang, Q. Wang, X. Liu, X. Ji, B. Jiang, Effects of molecular weight, solvent and substrate on the dewetting morphology of polystyrene films, Applied Surface Science, 236 (2004) 131-140.
[31] M. Nielsen, H. Junge, A. Kammer, M. Beller, Towards a Green Process for Bulk-Scale Synthesis of Ethyl Acetate: Efficient Acceptorless Dehydrogenation of Ethanol, Angewandte Chemie International Edition, 51 (2012) 5711-5713.
[32] C. Löser, T. Urit, T. Bley, Perspectives for the biotechnological production of ethyl acetate by yeasts, Applied Microbiology and Biotechnology, 98 (2014) 5397-5415.
[33] H.-G. Franck, J.W. Stadelhofer, Production and uses of toluene derivatives, in: Industrial Aromatic Chemistry: Raw Materials · Processes · Products, Springer Berlin Heidelberg, Berlin, Heidelberg, 1988, pp. 236-264.
[34] H.R. Omran, S.M. El-Marsafy, F.H. Ashour, E.F. Abadir, Economic evaluation of aromatics production, a case study for financial model application in petrochemical projects, Egyptian Journal of Petroleum, 26 (2017) 855-863.
[35] S. Darvishmanesh, J. Degrève, B. Van Der Bruggen, Mechanisms of solute rejection in solvent resistant nanofiltration: The effect of solvent on solute rejection, Physical Chemistry Chemical Physics, 12 (2010) 13333-13342.
[36] S. Darvishmanesh, J. Degrè, B.V.D. Bruggen, Performance of solvent-pretreated polyimide nanofiltration membranes for separation of dissolved dyes from toluene, Industrial and Engineering Chemistry Research, 49 (2010) 9330-9338.
[37] S.R. Hosseinabadi, K. Wyns, A. Buekenhoudt, B. Van der Bruggen, D. Ormerod, Performance of Grignard functionalized ceramic nanofiltration membranes, Separation and Purification Technology, 147 (2015) 320-328.
[38] C.R. Tanardi, A. Nijmeijer, L. Winnubst, Coupled-PDMS grafted mesoporous γ-alumina membranes for solvent nanofiltration, Separation and Purification Technology, 169 (2016) 223-229.

Annex

3

Molecular separation using poly (styrene-co-maleic anhydride) grafted to γ-alumina: surface versus pore modification

A3.1 Results

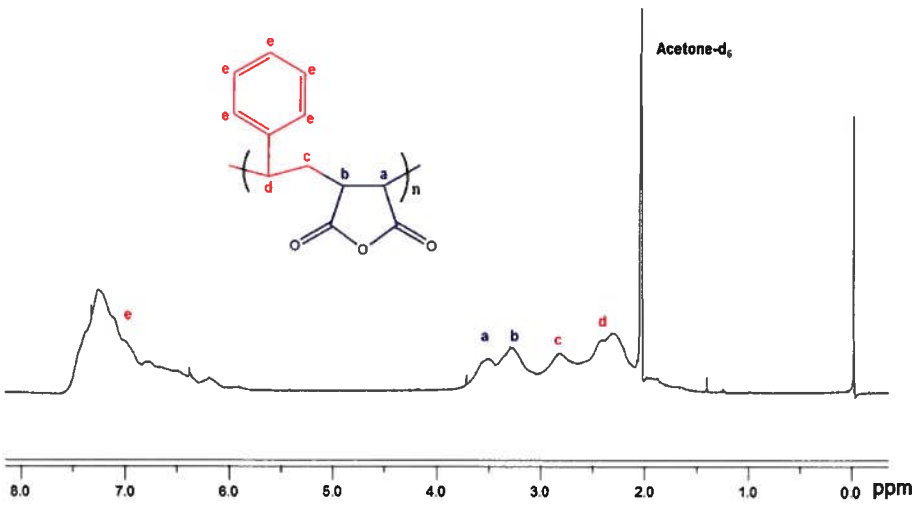

Figure A3.1 ^{1}H-NMR spectrum of S-SMA.

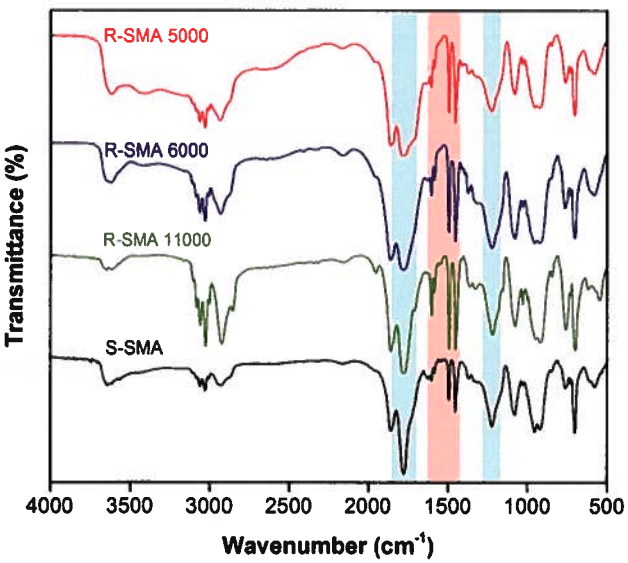

Figure A3.2 FTIR spectra of the different copolymers.

Figure A3.2 shows the FTIR spectra of the copolymers under study. The peak observed at 1453, 1496 and 1500 cm^{-1} can be attributed to the C=C stretching of styrene. The peak at 1225 cm^{-1} is attributed to the C-O-C bond of maleic anhydride. The peaks at 1860, 1781 cm^{-1} are attributed to the stretching vibrations of the carbonyl group and are indicative for an anhydride functionality.

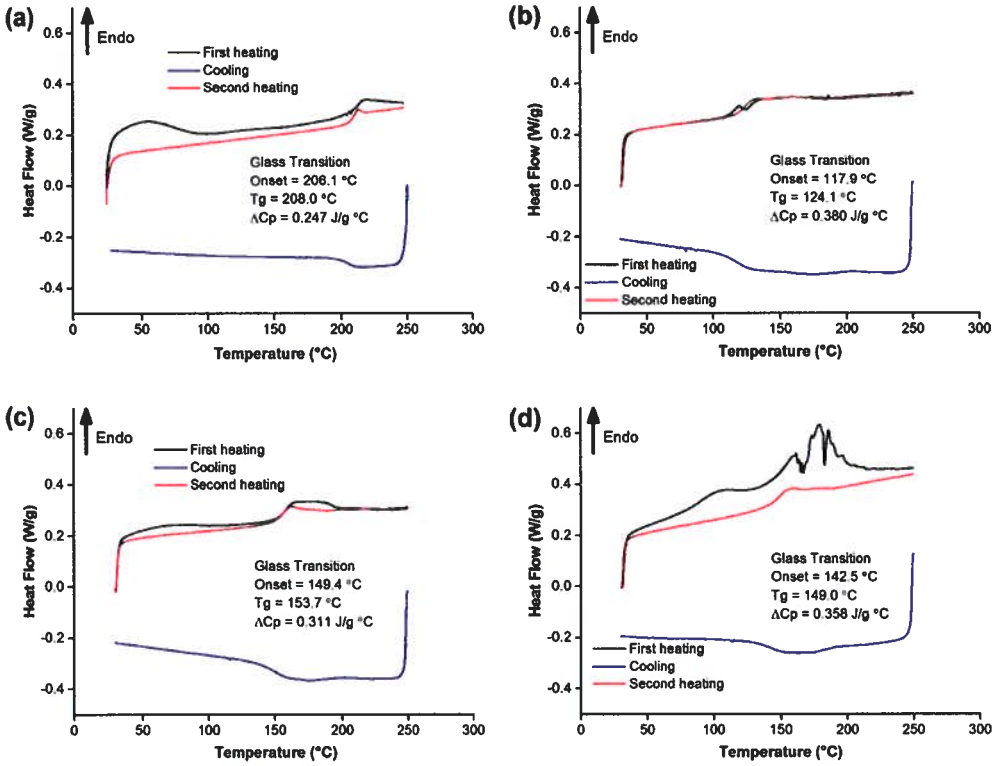

Figure A3.3 ^{1}H-NMR spectrum of P(MA-*alt*-C_{10}). DSC thermograms of different copolymers: (a) S-SMA, (b) R-SMA 11000, (c) R-SMA 6000 and (d) R-SMA 5000.

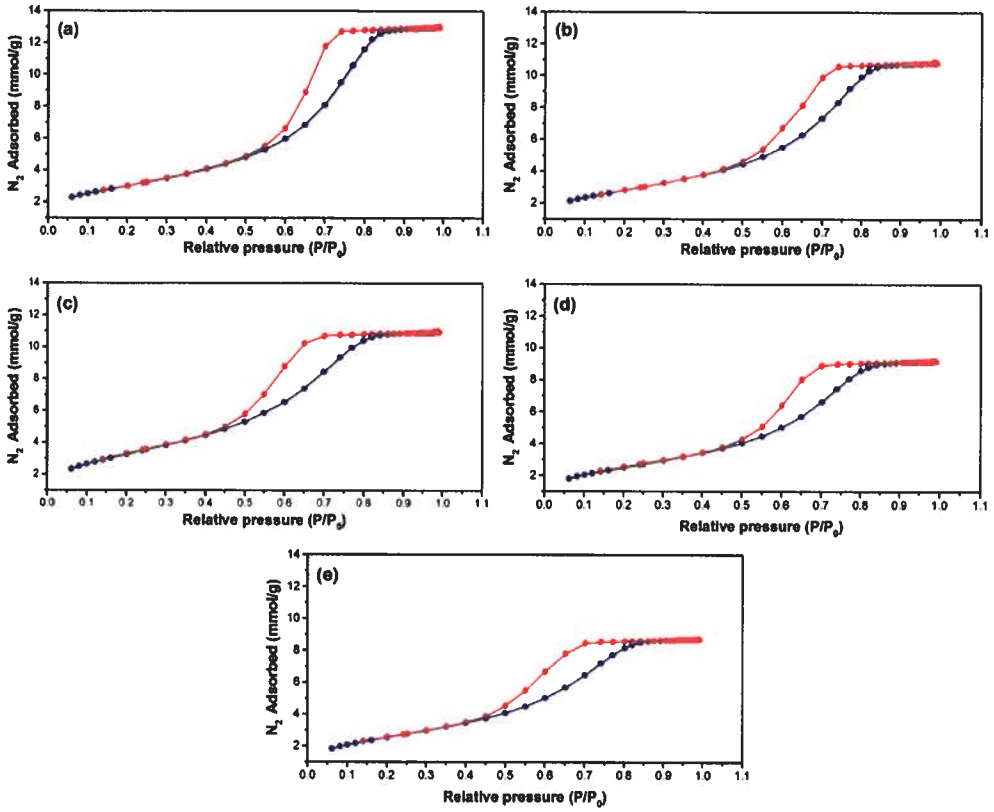

Figure A3.4 N_2 adsorption-desorption isotherm for (a) unmodified flakes, (b) γ-Al_2O_3-*g*-S-SMA, (c) γ-Al_2O_3-*g*-R-SMA 11000, (d) γ-Al_2O_3-*g*-R-SMA 6000 and (e) γ-Al_2O_3-*g*-R-SMA 5000

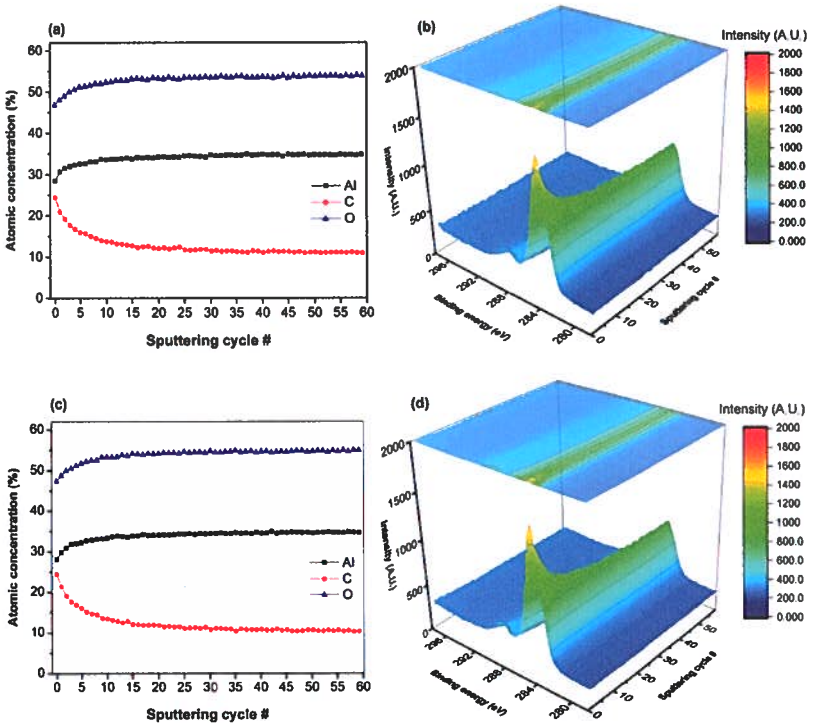

Figure A3.5 XPS atomic concentration depth profile and XPS C1S depth profile analysis of (a,b) γ-Al_2O_3-*g*-S-SMA 6000 and (c,d) γ-Al_2O_3-*g*-R-SMA 5000 membranes.

Table A3.1 Atomic percentage of Al, C and O at sputtering cycle #0 and #59.

	Atomic percentage at sputtering cycle # 0 (%)				Atomic percentage at sputtering cycle # 59 (%) (%)			
Membrane	Al	C	O	C/Al	Al	C	O	C/Al
Unmodified	34.7	7.2	58.0	0.20	38.5	1.9	59.4	0.05
S-SMA	22.9	43.2	33.8	1.88	41.2	4.4	54.4	0.10
R-SMA	27.5	28.1	44.3	1.02	34.6	11.8	53.5	0.34
R-SMA	28.5	24.3	47.1	0.85	34.8	11.1	53.9	0.31
R-SMA	28.1	24.4	47.4	0.86	34.6	10.4	54.9	0.30

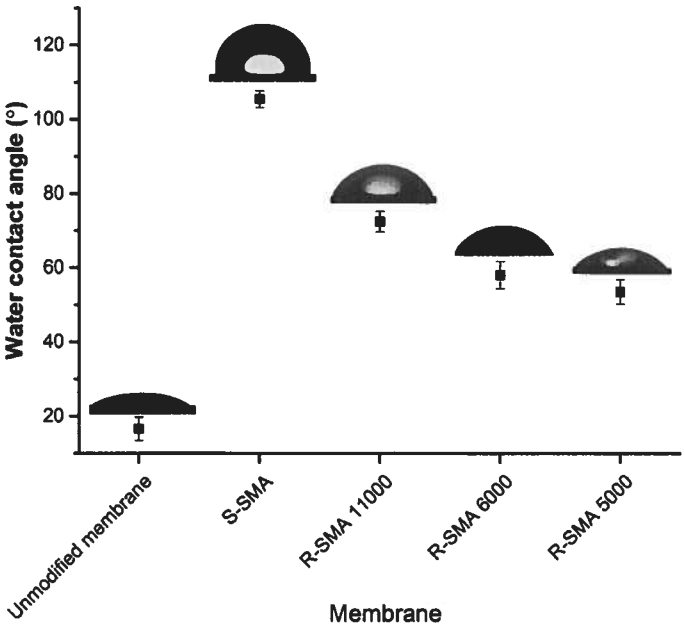

Figure A3.6 Water contact angle data of unmodified and grafted membranes.

Chapter 4

MIL-53(Al) and NH_2-MIL-53(Al) modified α-alumina membranes for efficient adsorption of dyes from organic solvents

This chapter contains parts of the following publication:

M. Amirilargani, R. B. Merlet, P. Hedayati, A. Nijmeijer, L. Winnubst, L. C. P. M. de Smet, E. J. R. Sudhölter, , *J. Chem. Comm*, **(2019)**, 55, 4119-4122.

In this chapter, for the first time MIL-53(Al) and NH_2-MIL-53(Al) modified α-alumina membranes are investigated for adsorption of organic dyes from organic solvents. These new modified membranes show excellent adsorption of high concentration of Rose Bengal dye in methanol and *iso*-propanol solutions. NH_2-MIL-53(Al) modified α-alumina membranes show higher solvent permeability and Rose Bengal dye adsorption capacity compared to MIL-53(Al) modified α-alumina membrane.

4.1 Introduction

Purification of non-aqueous mixtures has recently received much attention due to increased environmental concerns and the search for cleaner and more energy-efficient processes [1-3]. Adsorption processes are key in many chemical industries due to their feasibility, ease of operation and high efficiency. Metal organic frameworks (MOFs) have emerged as a new class of materials due to their special structures, tunable properties and broad range of applications [4]. MOFs are a class of crystalline open structures composed of inorganic units of metal ions or metal clusters as nodes and organic ligands as linkers with potential controllable molecular sieving properties in gas and liquid separations [5-8], owing to their relatively facile tunability of their pore size and pore structure [9, 10]. Among different MOFs, MIL-53 series (MIL stands for Matériaux de l'Institut Lavoisier) have been considered as promising porous materials for organic dyes separation [11-13]. MIL-53 materials represent metal hydroxyterephthalates and are formed from trans bridging of corner-sharing $Me^{3+}O_4(OH)_2$ octahedra, bridged by 1,4-benzenedicarboxylate linkers[14]. They possess a three-dimensional skeleton structure with large pores of *ca.* 0.85 nm in diameter and belong to the class of so-called breathing MOFs, *i.e.* they switch reversibly between large-pore (lp) and narrow-pore (np) configurations upon adsorption and thermal or mechanical stimuli [14-16]. For instance, the pore configuration of NH_2-MIL-53(Al) changes from its np form (pore window area ~ 3.4×16.0 $Å^2$) at low CO_2 pressure to its lp form (pore window area ~ 8.5×12.0 $Å^2$) upon increasing the CO_2 pressure [17]. Most of the research applying MIL-53 for organic dye separation, has tended to focus only on their sieving properties, which do significantly improve the performance for dye separation from organic solvents via the organic solvent nanofiltration (OSN) process. Although extensive research has been carried out on adsorption capacity of MOFs in aqueous media [18-20], only little attention has been paid to their adsorption capacities in organic media. This study therefore sets out to assess the MOF adsorption ability for dye removal from organic solvents.

Based on the above-mentioned considerations, we report now a unique morphology obtained for MIL-53(Al) and NH_2-MIL-53(Al) directly synthesized on α-alumina membranes, resulting in an excellent performance in terms of separating of an organic dye, namely Rose Bengal (RB) from methanol solutions at an extremely high concentration of 200 mg L^{-1}. To the best of our knowledge, this is the first example of a MOF-based membrane adsorber successfully used for highly efficient removal of a hazardous organic dye from organic solvents. This provides a useful system for a wide range of potential applications, including solvent extraction in the pharmaceutical and bio industries.

4.2 Experimental section

4.2.1 Materials

All chemicals were purchased from Sigma-Aldrich, unless otherwise indicated. Aluminum (III) nitrate nonahydrate ($Al(NO_3)_3 \cdot 9H_2O$), terephthalic acid (H_2BDC), 2-aminoterephthalic acid (NH_2-H_2BDC) and acetic acid were used for the MOF preparation. All water used is Milli-Q water. N,N-Dimethylformamide (DMF) and methanol were used for washing the MOF powders. Rose Bengal (RB; $C_{20}H_2Cl_4I_4Na_2O_5$), methanol and *iso*-propanol were used for adsorption experiments. Flat disc-shaped α-alumina membranes (having a diameter of 39 mm, a thickness of 2 mm, and a pore diameter of 80 nm) were purchased from Pervatech B.V., The Netherlands.

4.2.2 Synthesis of MIL-53(Al) and NH_2-MIL-53(Al) seeds

The MIL-53 and NH_2-MIL-53 membranes were prepared on an α-alumina support by the reactive seeding (RS) method, where the alumina support works as metal source reacted with organic ligand to grow a seed layer directly. A typical RS method contains two steps, (i) seed layer growth and (ii) secondary MOF layer growth. For the seed growth, 0.5 g of H_2BDC (3 mmol) or NH_2-H_2BDC (2.7 mmol), 55 ml water and 0.5 ml acetic acid were mixed and stirred vigorously for 15 min. The resulting mixture was further dispersed by sonication for 15 min. Then, the solution was transferred into a Teflon-lined stainless steel autoclave containing an α-alumina support that was placed vertically. The autoclave was sealed and heated at 120 °C for two days and then cooled down to room temperature. The α-alumina membrane reacted with the organic ligand and was rinsed with ethanol three times and dried in an oven at 60 °C for 24 h and further referred to as seed layer membrane.

4.2.3 Synthesis of MIL-53(Al) and NH_2-MIL-53(Al) membranes trough secondary growth

Secondary growth steps for the synthesis of the MIL-53(Al) and NH_2-MIL-53(Al) membranes are slightly different. For the MIL-53(Al) membrane, typically 3.0 g (8.0 mmol) $Al(NO_3)_3 \cdot 9H_2O$ and 0.72 g (4.3 mmol) H_2BDC was dispersed in 55 ml water and then loaded into an autoclave, in which the seed layer membrane was fixed vertically and heated at 160 °C for 24 h. After cooling the autoclave, the MIL-53(Al) membrane was washed with ethanol three times and then dried at 90° C under vacuum.

For the synthesis of the NH_2-MIL-53(Al) membrane, 2.0 g (5.3 mmol) $Al(NO_3)_3 \cdot 9H_2O$ and 0.5 g (2.7 mmol) NH_2-H_2BDC were dispersed in 55 ml water. Again, the resulting mixture was loaded into an autoclave containing a seed layer membrane positioned vertically and was then heated at 80 °C for 72 h. The washing and drying steps are as reported for the MIL-53(Al) membrane.

In addition, the MOF powders synthesized during the second growth step were collected from the bottom of the autoclave. Subsequently, the powders were thoroughly activated in DMF at 140 °C K for 12 h and methanol at 90 °C K for 15 h. The powders were washed with acetone and dried at 120 °C under vacuum.

4.2.4 Characterizations

Materials characterization

To confirm the formation of MIL-53(Al) and NH_2-MIL-53(Al), XRD measurements were carried out. The XRD patterns of the membranes and MOF powders were obtained with a Bruker D8 advance diffractometer by using Co-Kα at room temperature. The measurement covers a scan range of 2θ = 5° to 50° with a scan speed of 0.2 s per step and step size of 0.02° in a continuous scanning mode. XRD peaks were assigned using Diamond Software (Diamond 4.5.2, Crystal Impact GbR, Bonn, Germany) and CCDC data from the Table A4.2. FE-SEM images were acquired to observe the morphology of MOF membranes and powders. The gold-coated samples were places in a Nova NanoSEM 450 (Thermo Fisher Scientific) with an accelerating voltage of 10 kV. TEM analysis was carried out with JEOL JEM-2010 microscope operated at 200 kV. N_2 and CO_2 adsorption isotherms of MOFs particles and membranes were recorded with a Tristar II 3020 (Micromeritics) setup at 77 and 295 K, respectively. Prior to the measurements, at least 150 mg of MOF powder was degassed at 423 K under vacuum for 16 h and subsequently used for the adsorption measurements.

Dye adsorption performance of MIL-53(Al) and NH_2-MIL-53(Al) membranes

Membrane performance was tested in a typical stainless steel dead-end pressure cell at a transmembrane pressure (TMP) of 6 bar at room temperature. The system is pressurized using inert argon. During the filtration, the feed solution was stirred at 100 rpm using a magnetic stirrer. The membrane cell was filled with 240 ml of feed solution per membrane and different samples of 10 ml were collected for each membrane at the permeate side. The membrane permeability was calculated according to Equation [21],

$$\text{Permeability} = \frac{J}{\Delta P} = \frac{V}{\Delta P A t} = [\mathrm{L\,m^{-2}\,h^{-1}bar^{-1}}] \quad (4.1)$$

where J is the solvent flux [L m^{-2} h^{-1}], ΔP is the applied pressure across the membrane [bar], V is the permeate volume [L], A is the effective membrane surface area [m^2] and t is the collecting permeate sample time [h]. The solutes concentration in the permeate ($C_{permeate}$) and initial concentration in the feed (C_{feed}) were measured using a double-beam UV-Vis spectrophotometer (Shimadzu, UV-1800).

4.3 Results and discussions

The Field-Emission Scanning Electron Microscopy (FE-SEM) surface images of the bare and MOF-modified α-alumina are shown in Figure 4.1, clearly showing the unique structures of MIL-53(Al) and NH_2-MIL-53(Al). The MIL-53(Al) layer is formed by closely packed submicron particles, while the NH_2-MIL-53(Al) layer is formed by rather dense and compact packed submicron particles. In addition, Figures 4.1 d and 4.1 f show two different orientations of particles grown from the surface.

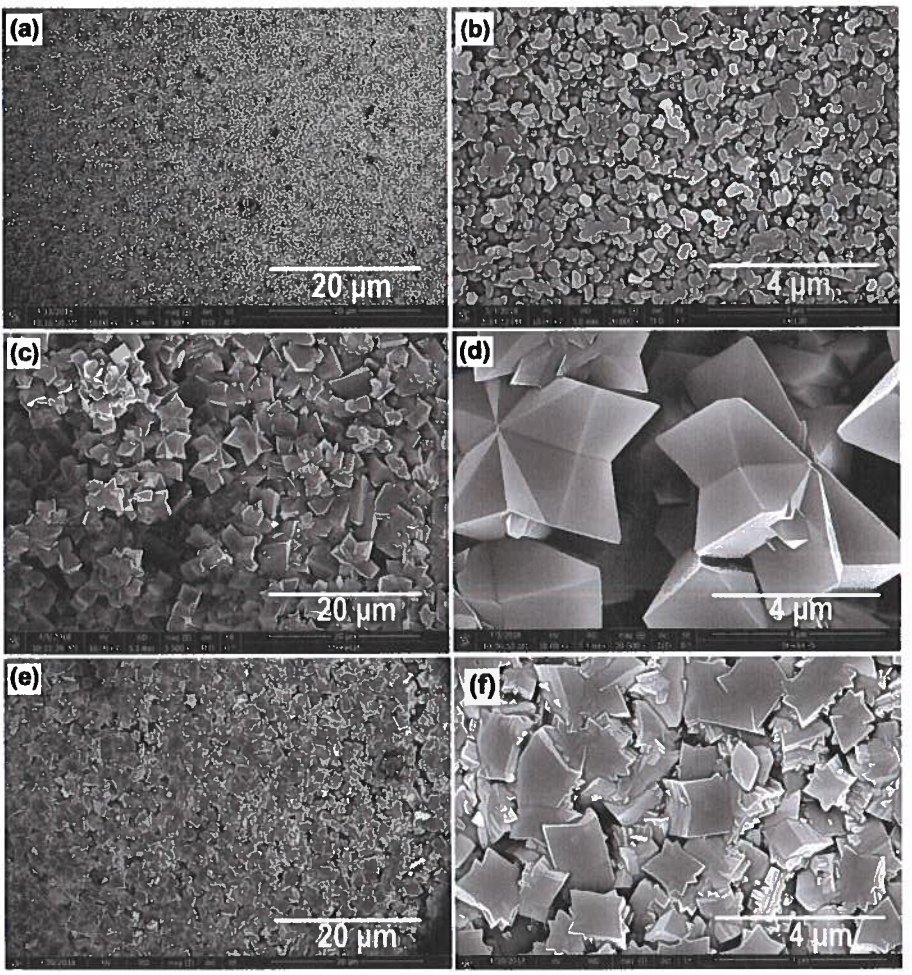

Figure 4.1 Low and high magnification FE-SEM surface images of (a,b) α-alumina, (c,d) MIL-53(Al) and (e,f) NH_2-MIL-53(Al) membranes.

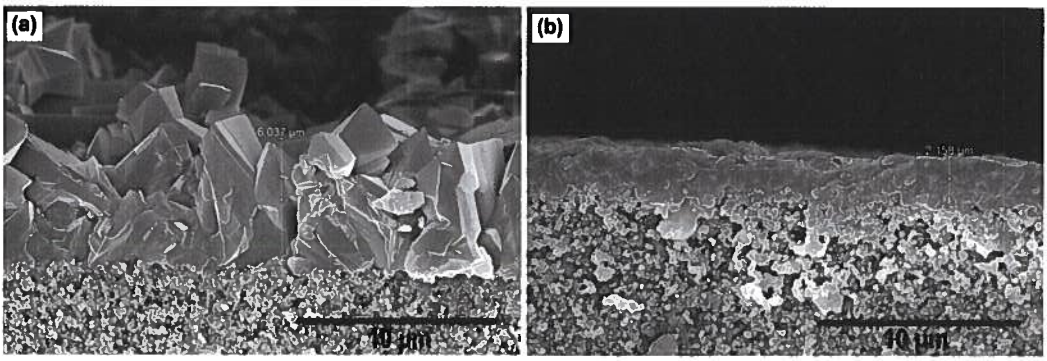

Figure 4.2 Cross-sectional FE-SEM images of (a) MIL-53(Al) and (b) NH_2-MIL-53(Al) membranes on α-alumina support.

Furthermore, the MIL-53(Al) layer does not show any preferred growth direction, while the NH_2-MIL-53(Al) layer is formed by numerous layers of MOFs grown in a layer-by-layer fashion (Figure 4.1 f and A4.1). These differences may be attributed to the different synthesis temperatures that were applied for MIL-53(Al) (160°C) and NH_2-MIL-53 (80 °C). A higher temperature speeds up the crystal growth rate, resulting in larger crystallites [22]. Both MIL-53(Al) and NH_2-MIL-53(Al) layers were well adhered to the α-alumina support, where the MIL-53(Al) layer is almost 3× thicker compared to the NH_2-MIL-53(Al) layer (Figure 4.2). This is in line with the faster crystallization at higher temperature.

The crystal structures obtained from the MOF powders isolated from the bottom of the autoclave and the MOFs synthesized on the alumina membranes were determined by X-ray diffraction (XRD) and the results are shown in Figure A4.3. Good agreement for both MOFs were obtained by comparison with their simulated XRD patterns (Figures A4.4 and A4.5). In both MIL-53(Al) powders and membranes the np and lp configurations seem to coexist. The same behaviour was observed for the NH_2-MIL-53(Al) obtained from the membranes, while the NH_2-MIL-53(Al) powders mainly showed the np structure. Switching between lp and np structurers is observed upon water/solvent uptake, temperature changes or mechanical stress [14, 23-25]. Our result may indicate that some of the solvent molecules trapped in the pores of the MOF- modified membranes remained after the drying step and therefore both np and lp structures do coexist.

Next, we measured the breakthrough curves for adsorption of RB from methanol at initial feed concentrations of 130 mg L^{-1} (Figure 4.3).

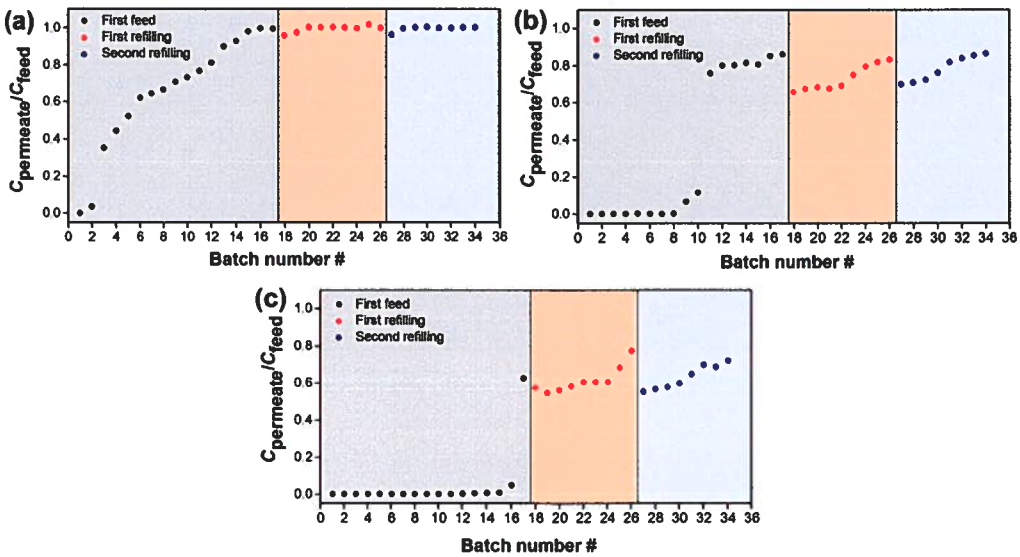

Figure 4.3 Breakthrough curves showing the dynamic adsorption of RB from methanol (130 mgL^{-1}) using (a) α-alumina, (b) MIL-53(Al) and (c) NH_2-MIL-53(Al) modified membranes. The colored region refered to the different filling steps.

The feed side of the membrane cell was filled with 240 mL of solution and different 10 mL batches of permeant were collected from the permeate side. Figure 4.3 a shows the adsorption capacity of the unmodified membrane, which dramatically drops already after the collection of 2 samples (each of 10 mL), while MIL-53(Al) and NH_2-MIL-53(Al) modified membranes showed a much higher adsorption capacity. However, as shown in Figure 4.3 c the NH_2-MIL-53(Al) modified membrane is still far outside the maximal adsorption capacity and after the collection of 17 samples the $C_{permeate}/C_{feed}$ is still ~ 0.6. In order to determine the maximal adsorption capacity, the cell was refilled with a fresh RB/methanol solution to continue the permeation experiments. To our surprise, the observed $C_{permeate}/C_{feed}$ value decreased after each performed refilling steps. This was due to an increase of C_{feed} after each refill. That increase originates from the release of RB bound to the MOF-modified membranes, when the external pressure is reduced. Regeneration of the MOF-modified membranes in this situation is thus very simple and might be of use in future applications. In addition, no significant changes were observed for the NH_2-MIL-53(Al) modified membrane after two refilling steps and even after the collection of 34 samples, the $C_{permeate}/C_{feed}$ remained stable at ~ 0.7.

To find the maximal adsorption capacity and to avoid the release of bound RB to the MOF-modified membranes, filtration experiments were done using now an extremely high

concentration RB in methanol and *iso*-propanol (200 mg L^{-1}). The observed breakthrough curves are shown in Figure 4.4.

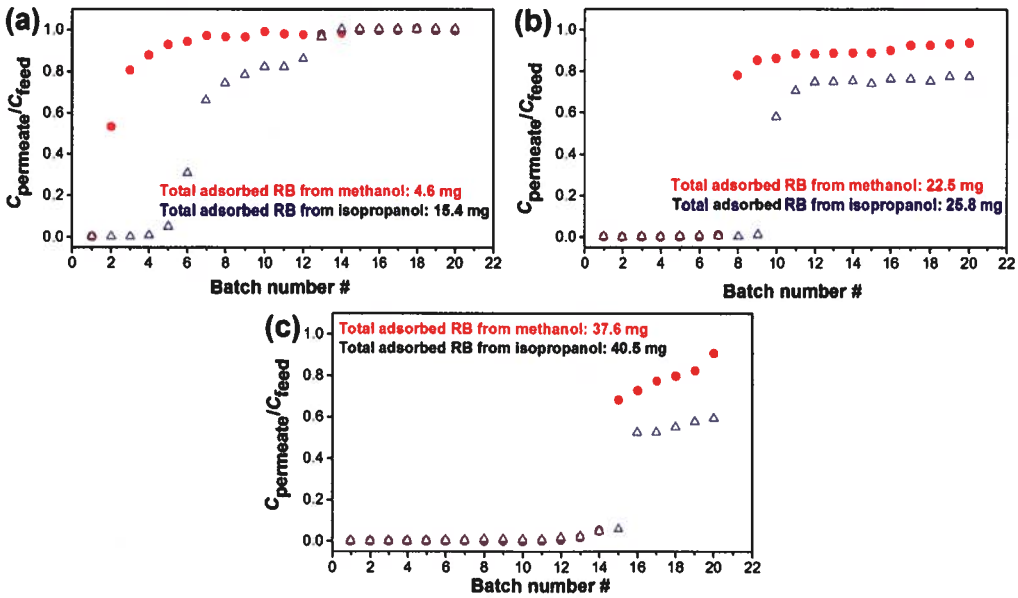

Figure 4.4 Breakthrough curves showing the dynamic adsorption of RB from methanol and *iso*-propanol (200 mgL^{-1}) using (a) α-alumina, (b) MIL-53(Al) and (c) NH_2-MIL-53(Al) membranes.

For the unmodified α-alumina membranes almost no RB is adsorbed from methanol. For the NH_2-MIL-53(Al) modified membranes the amount of adsorbed RB from a methanol solution was nearly 70% higher compared to the amount adsorbed by MIL-53(Al) modified membranes (37.6 *versus* 22.5 mg, respectively, Figures 4.4 b and 4.4 c). For both MOF-modified and unmodified α-alumina membranes the adsorption capacity is slightly higher for RB removal from *iso*-propanol compared to the one of methanol. This is most likely due to the higher viscosity of *iso*-propanol compared to methanol, resulting in a longer contact time of the RB/*iso*-propanol solution and consequently lower *iso*-propanol permeability (Figure 4.5).

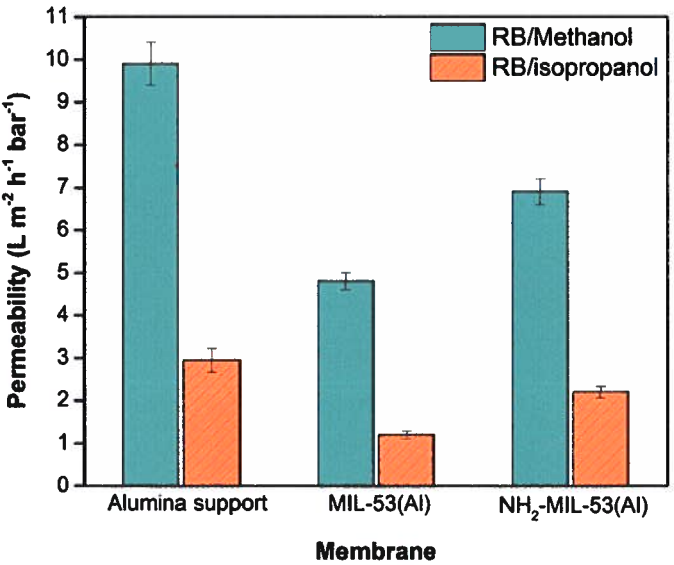

Figure 4.5 Methanol and *iso*-propanol permeability during the dynamic adsorption of RB.

The size of the RB molecule is much larger than the pore sizes within both MOF crystallites, and therefore its adsorption can only occur on the available outer facets of the MOF crystallites (Scheme A4.1) [12]. Since the NH_2-MIL-53(Al) modified membranes are more compact and composed of smaller MOF crystallites compared to the MIL-53(Al) modified membranes (compare Figures 4.1 d and 4.1 f), the adsorption of RB is higher due to a larger available facet area. In addition, zeta potential distribution obtained for the MIL-53(Al) and NH_2-MIL-53(Al) powders dispersed in methanol revealed a slightly positive zeta potential of +0.03 mV for NH_2-MIL-53(Al) compared to -9.25 mV for MIL-53(Al) (Figure A4.10). This slightly more positive charge of NH_2-MIL-53(Al) will contribute to the observed increase of the RB adsorption capacity since that is an anionic dye.

Figure 4.5 shows the solvent permeability of the different investigated membranes during the dynamic adsorption of RB from methanol and *iso*-propanol solutions. The solvent permeabilities of the MOF-modified membranes is lower compared to the unmodified α-alumina membranes, the thinner NH_2-MIL-53(Al) modified membrane still shows a relatively high methanol permeability of 6.9 L m^{-2} h^{-1} bar^{-1}. State-of-the-art ceramic organic solvent nanofiltration membranes show methanol permeabilities in the range between 3.9 - 6.1 L m^{-2} h^{-1} bar^{-1} [26, 27], from which we conclude that our NH_2-MIL-53(Al) modified membranes combine a good RB adsorption with a high permeability.

4.4 Conclusions

In summary, a unique structures of MIL-53(Al) and NH_2-MIL-53(Al) modified α-alumina membranes show a high RB adsorption and an easy release of bound RB, in combination with a high methanol solvent permeability. Additionally, the adsorption capacity of the MOF-modified α-alumina membranes were proportionally related to the available facet area and the surface charge of the MOF coated on the alumina support. NH_2-MIL-53(Al) modified α-alumina membranes composed of smaller MOF crystals highly packed together and slightly positively charge compared to the unmodified α-alumina MIL-53(Al)-modified α-alumina membranes shows higher Rose Bengal adsorption.

References

[1] G. Szekely, M.F. Jimenez-Solomon, P. Marchetti, J.F. Kim, A.G. Livingston, Sustainability assessment of organic solvent nanofiltration: From fabrication to application, Green Chemistry, 16 (2014) 4440-4473.
[2] P. Marchetti, M.F. Jimenez Solomon, G. Szekely, A.G. Livingston, Molecular Separation with Organic Solvent Nanofiltration: A Critical Review, Chemical Reviews, 114 (2014) 10735-10806.
[3] J.F. Kim, G. Szekely, M. Schaepertoens, I.B. Valtcheva, M.F. Jimenez-Solomon, A.G. Livingston, In Situ Solvent Recovery by Organic Solvent Nanofiltration, ACS Sustainable Chemistry & Engineering, 2 (2014) 2371-2379.
[4] D.-M. Chen, J.-Y. Tian, Z.-W. Wang, C.-S. Liu, M. Chen, M. Du, An anionic Na(i)–organic framework platform: separation of organic dyes and post-modification for highly sensitive detection of picric acid, Chemical Communications, 53 (2017) 10668-10671.
[5] Y.-Y. Jia, Y.-H. Zhang, J. Xu, R. Feng, M.-S. Zhang, X.-H. Bu, A high-performance "sweeper" for toxic cationic herbicides: an anionic metal–organic framework with a tetrapodal cage, Chemical Communications, 51 (2015) 17439-17442.
[6] M. Amirilargani, B. Sadatnia, Poly(vinyl alcohol)/zeolitic imidazolate frameworks (ZIF-8) mixed matrix membranes for pervaporation dehydration of isopropanol, Journal of Membrane Science, 469 (2014) 1-10.
[7] G. Liu, V. Chernikova, Y. Liu, K. Zhang, Y. Belmabkhout, O. Shekhah, C. Zhang, S. Yi, M. Eddaoudi, W.J. Koros, Mixed matrix formulations with MOF molecular sieving for key energy-intensive separations, Nature Materials, 17 (2018) 283-289.
[8] A. Sabetghadam, B. Seoane, D. Keskin, N. Duim, T. Rodenas, S. Shahid, S. Sorribas, C.L. Guillouzer, G. Clet, C. Tellez, M. Daturi, J. Coronas, F. Kapteijn, J. Gascon, Metal Organic Framework Crystals in Mixed-Matrix Membranes: Impact of the Filler Morphology on the Gas Separation Performance, Advanced Functional Materials, 26 (2016) 3154-3163.
[9] M. Eddaoudi, J. Kim, N. Rosi, D. Vodak, J. Wachter, M. O'Keeffe, O.M. Yaghi, Systematic Design of Pore Size and Functionality in Isoreticular MOFs and Their Application in Methane Storage, Science, 295 (2002) 469-472.
[10] M. O'Keeffe, O.M. Yaghi, Deconstructing the Crystal Structures of Metal–Organic Frameworks and Related Materials into Their Underlying Nets, Chemical Reviews, 112 (2012) 675-702.
[11] L. Zhu, H. Yu, H. Zhang, J. Shen, L. Xue, C. Gao, B. van der Bruggen, Mixed matrix membranes containing MIL-53(Al) for potential application in organic solvent nanofiltration, RSC Advances, 5 (2015) 73068-73076.
[12] S. Basu, M. Maes, A. Cano-Odena, L. Alaerts, D.E. De Vos, I.F.J. Vankelecom, Solvent resistant nanofiltration (SRNF) membranes based on metal-organic frameworks, Journal of Membrane Science, 344 (2009) 190-198.
[13] S. Sorribas, P. Gorgojo, C. Téllez, J. Coronas, A.G. Livingston, High Flux Thin Film Nanocomposite Membranes Based on Metal–Organic Frameworks for Organic Solvent Nanofiltration, Journal of the American Chemical Society, 135 (2013) 15201-15208.
[14] M. Mihaylov, K. Chakarova, S. Andonova, N. Drenchev, E. Ivanova, A. Sabetghadam, B. Seoane, J. Gascon, F. Kapteijn, K. Hadjiivanov, Adsorption Forms of CO2 on MIL-53(Al) and NH2-MIL-53(Al) As Revealed by FTIR Spectroscopy, The Journal of Physical Chemistry C, 120 (2016) 23584-23595.
[15] L. Chen, J.P.S. Mowat, D. Fairen-Jimenez, C.A. Morrison, S.P. Thompson, P.A. Wright, T. Düren, Elucidating the Breathing of the Metal–Organic Framework MIL-53(Sc) with ab Initio Molecular Dynamics Simulations and in Situ X-ray Powder Diffraction Experiments, Journal of the American Chemical Society, 135 (2013) 15763-15773.
[16] J.Y. Kim, L. Zhang, R. Balderas-Xicohténcatl, J. Park, M. Hirscher, H.R. Moon, H. Oh, Selective Hydrogen Isotope Separation via Breathing Transition in MIL-53(Al), Journal of the American Chemical Society, 139 (2017) 17743-17746.
[17] A. Sabetghadam, X. Liu, M. Benzaqui, E. Gkaniatsou, A. Orsi, M.M. Lozinska, C. Sicard, T. Johnson, N. Steunou, P.A. Wright, C. Serre, J. Gascon, F. Kapteijn, Influence of Filler Pore Structure and Polymer on the Performance of MOF-Based Mixed-Matrix Membranes for CO2 Capture, Chemistry – A European Journal, 24 (2018) 7949-7956.
[18] H. Ting, H.-Y. Chi, C.H. Lam, K.-Y. Chan, D.-Y. Kang, High-permeance metal–organic framework-based membrane adsorber for the removal of dye molecules in aqueous phase, Environmental Science: Nano, 4 (2017) 2205-2214.
[19] C. Li, Z. Xiong, J. Zhang, C. Wu, The Strengthening Role of the Amino Group in Metal–Organic Framework MIL-53 (Al) for Methylene Blue and Malachite Green Dye Adsorption, Journal of Chemical & Engineering Data, 60 (2015) 3414-3422.
[20] Z. Jia, M. Jiang, G. Wu, Amino-MIL-53(Al) sandwich-structure membranes for adsorption of p-nitrophenol from aqueous solutions, Chemical Engineering Journal, 307 (2017) 283-290.

[21] J. Campbell, R.P. Davies, D.C. Braddock, A.G. Livingston, Improving the permeance of hybrid polymer/metal-organic framework (MOF) membranes for organic solvent nanofiltration (OSN) - development of MOF thin films via interfacial synthesis, Journal of Materials Chemistry A, 3 (2015) 9668-9674.
[22] E. Haque, J.H. Jeong, S.H. Jhung, Synthesis of isostructural porous metal-benzenedicarboxylates: Effect of metal ions on the kinetics of synthesis, CrystEngComm, 12 (2010) 2749-2754.
[23] K. Titov, Z. Zeng, M.R. Ryder, A.K. Chaudhari, B. Civalleri, C.S. Kelley, M.D. Frogley, G. Cinque, J.-C. Tan, Probing Dielectric Properties of Metal–Organic Frameworks: MIL-53(Al) as a Model System for Theoretical Predictions and Experimental Measurements via Synchrotron Far- and Mid-Infrared Spectroscopy, The Journal of Physical Chemistry Letters, 8 (2017) 5035-5040.
[24] S. Couck, E. Gobechiya, C.E.A. Kirschhock, P. Serra-Crespo, J. Juan-Alcañiz, A. Martinez Joaristi, E. Stavitski, J. Gascon, F. Kapteijn, G.V. Baron, J.F.M. Denayer, Adsorption and Separation of Light Gases on an Amino-Functionalized Metal–Organic Framework: An Adsorption and In Situ XRD Study, ChemSusChem, 5 (2012) 740-750.
[25] E. Stavitski, E.A. Pidko, S. Couck, T. Remy, E.J.M. Hensen, B.M. Weckhuysen, J. Denayer, J. Gascon, F. Kapteijn, Complexity behind CO2 Capture on NH2-MIL-53(Al), Langmuir, 27 (2011) 3970-3976.
[26] H. Yang, N. Wang, L. Wang, H.-X. Liu, Q.-F. An, S. Ji, Vacuum-assisted assembly of ZIF-8@GO composite membranes on ceramic tube with enhanced organic solvent nanofiltration performance, Journal of Membrane Science, 545 (2018) 158-166.
[27] N.F.D. Aba, J.Y. Chong, B. Wang, C. Mattevi, K. Li, Graphene oxide membranes on ceramic hollow fibers – Microstructural stability and nanofiltration performance, Journal of Membrane Science, 484 (2015) 87-94.

Annex

4

MIL-53(Al) and NH_2-MIL-53(Al) modified α-alumina membranes for efficient adsorption of dyes from organic solvents

A4.1 Results and discussions

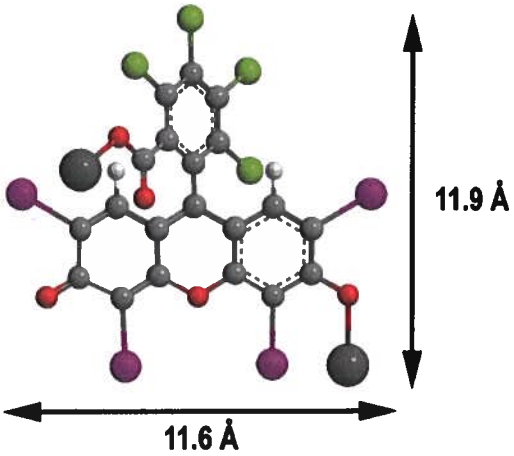

Scheme A4.1 Molecular structure of Rose Bengal (RB) and its overall dimensions.

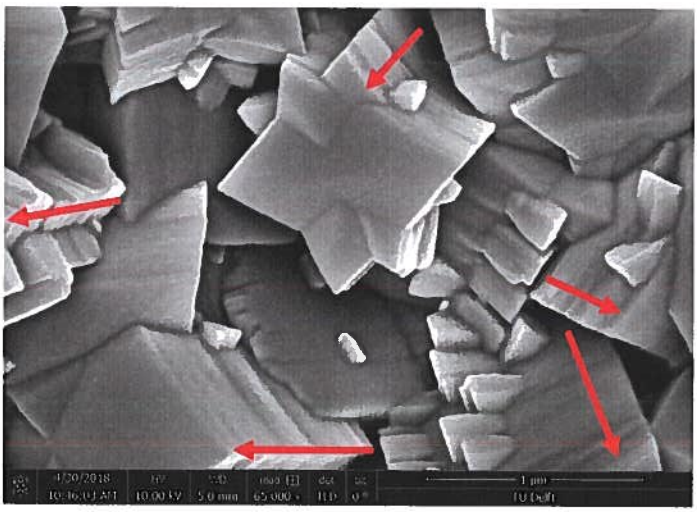

Figure A4.1 High magnification FE-SEM surface images of NH_2-MIL-53(Al) membranes. Arrows indicate the growing directions.

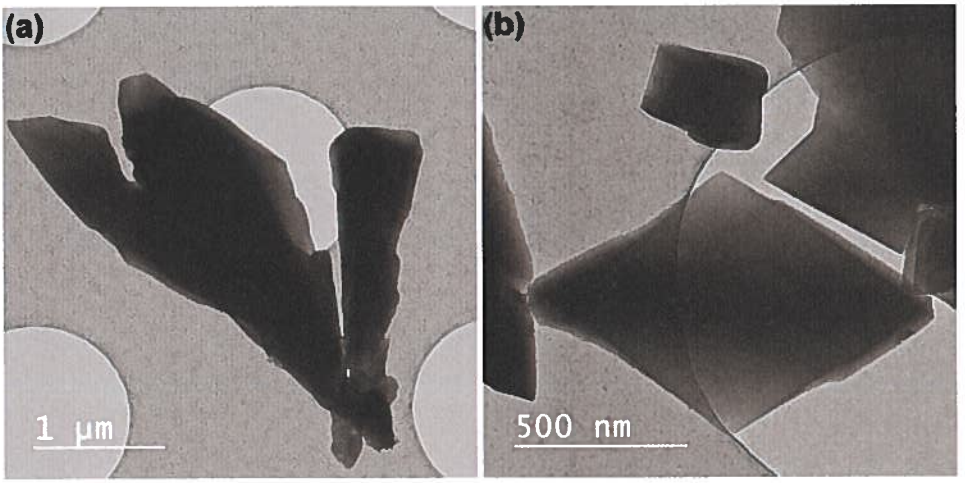

Figure A4.2 TEM images of (a) MIL-53(Al) and (b) NH_2-MIL-53(Al) particles collected from the autoclave.

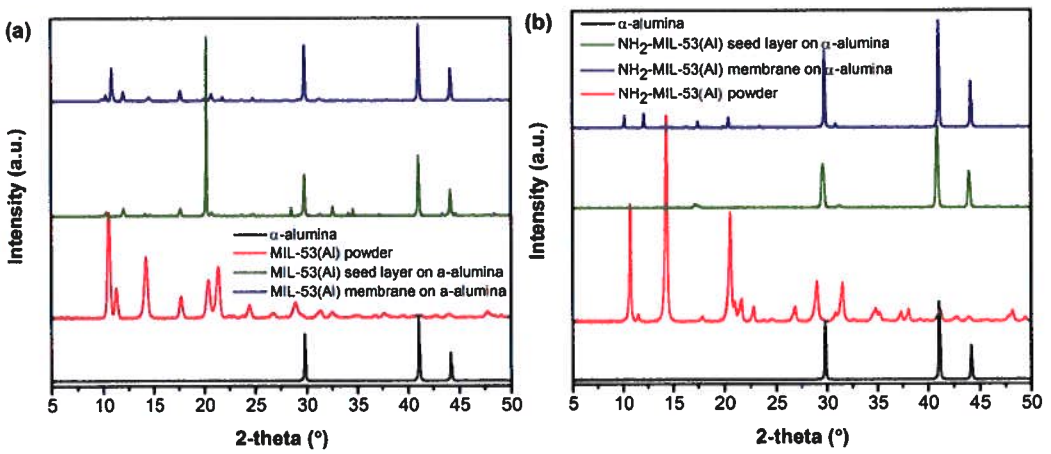

Figure A4.3 XRD patterns of (a) MIL-53(Al) and (b) NH_2-MIL-53(Al) powders and membranes.

Table A4.1 CCDC codes of MOFs used in this study.

MOF	Chemical formula	CCDC	Ref.
MIL-53(Al)	$Al(OH)[O_2C\text{-}C_6H_4\text{-}CO_2]$	lp: 220477, np: 220476	[1]
NH_2-MIL-53(Al)	$Al(OH)[O_2C\text{-}C_6H_3NH_2\text{-}CO_2]$	lp: 847255, np: 847256	[2]

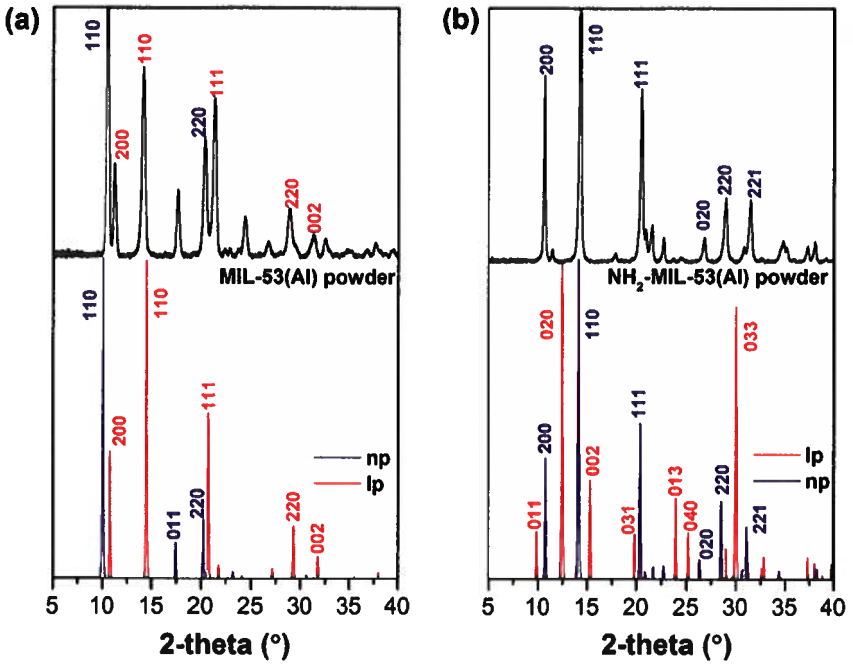

Figure A4.4 Experimental and simulated XRD patterns of (a) MIL-53(Al) and (b) NH_2-MIL-53(Al) powders.

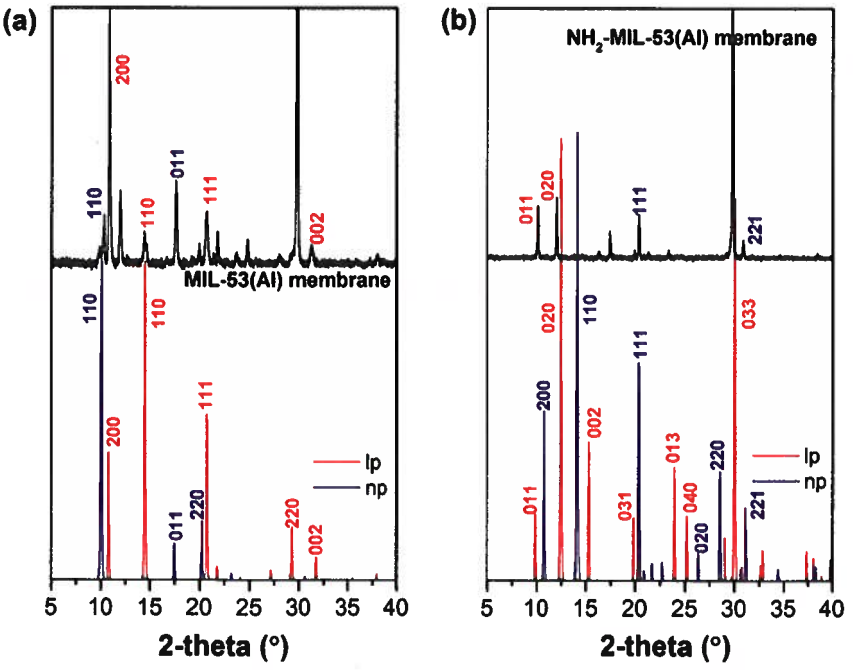

Figure A4.5 Experimental and simulated XRD patterns of (a) MIL-53(Al) and (b) NH_2-MIL-53(Al) membranes.

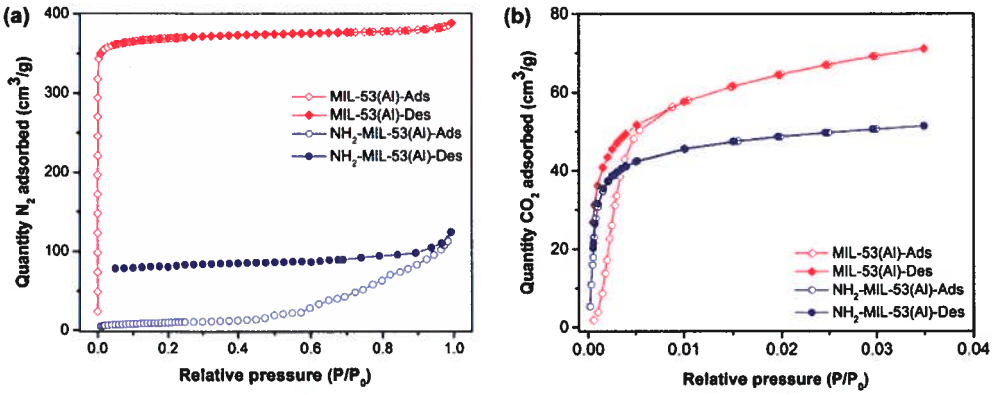

Figure A4.6 Experimental N_2 (a) and CO_2 (b) adsorption (open symbols) and desorption (solid symbols) of MIL-53(Al) and NH_2-MIL-53(Al).

N_2 and CO_2 adsorption-desorption isotherms of MIL-53(Al) and NH_2-MIL-53(Al) powders are presented in Figure A4.6. MIL-53(Al) exhibits a reversible, Type-I N_2 isotherm (Figure A4.6 a), indicating the microporous nature of this material. N_2 could not adsorb in the NH_2-MIL-53(Al) powders as it presents in the np form (Figure A4.4 b) [3, 4]. CO_2 adsorption-desorption isotherms of MI-53(Al) and NH_2-MIL-53(Al) powders at low pressure are in agreement with literature [4].

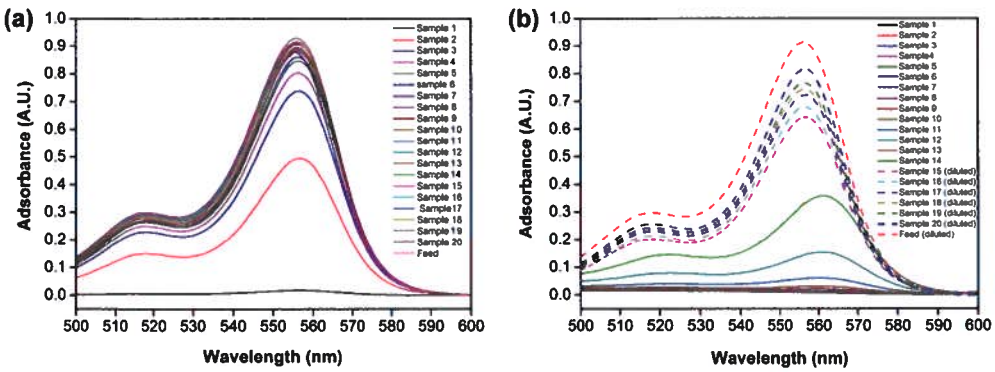

Figure A4.7 UV-vis absorption spectra of RB in methanol of different 10 ml batches of permeate collected for (a) bare α-alumina support and (b) NH_2-MIL-53(Al) membrane. The model feed solution was a 250 ml mixture of RB (200 mg L^{-1}) in methanol. The feed solution and all collected samples and feed were diluted 20 times in Figure A4.7 a while feed solution and samples 15-20 were diluted 20 times in the Figure A4.7 b.

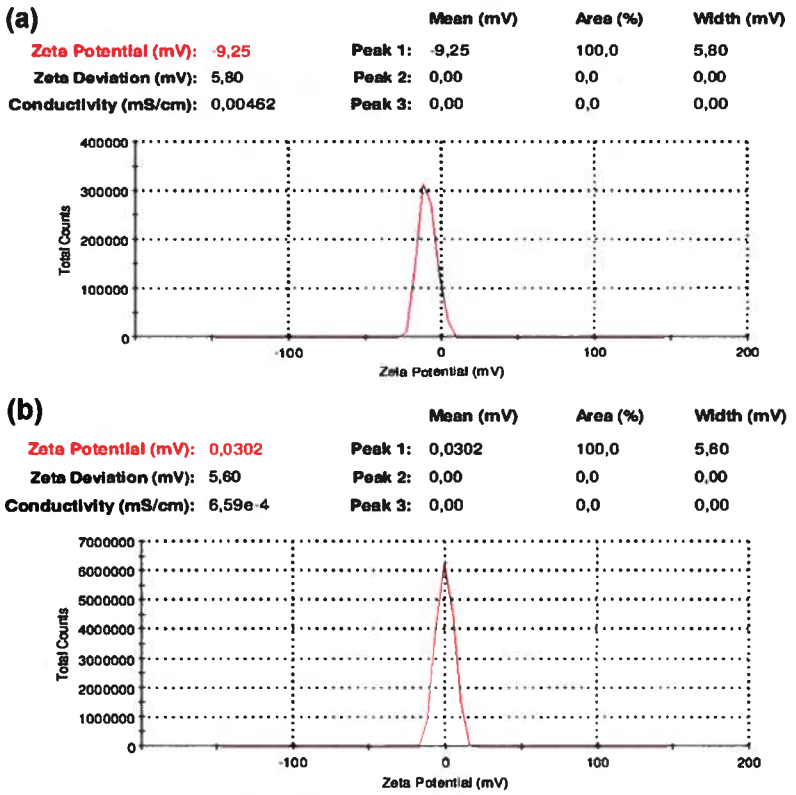

Figure A4.8 The zeta-potential distribution of (a) MIL-53 and (b) NH_2-MIL-53 powders in methanol.

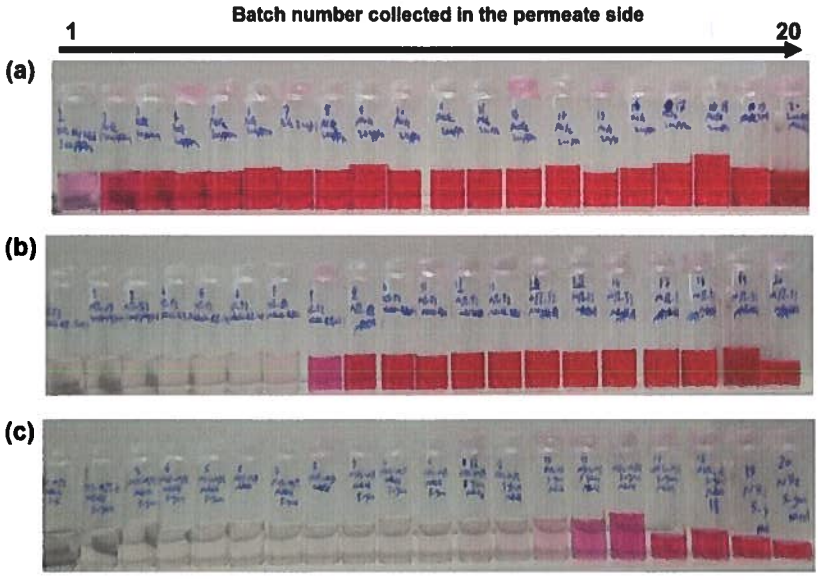

Figure A4.9 Photographs of collected samples at the permeate side of (a) bare α-alumina, (b) MIL-53(Al) and NH_2-MIL-53(Al) membranes tested with RB in methanol (200 mg L^{-1}).

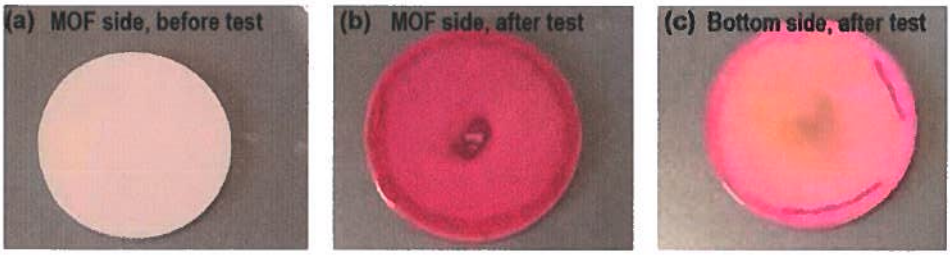

Figure A4.10 Photographs of the NH_2-MIL-53(Al) membrane before and after the filtration test RB in methanol (200 mg L^{-1}).

References

[1] T. Loiseau, C. Serre, C. Huguenard, G. Fink, F. Taulelle, M. Henry, T. Bataille, G. Férey, A Rationale for the Large Breathing of the Porous Aluminum Terephthalate (MIL-53) Upon Hydration, Chemistry – A European Journal, 10 (2004) 1373-1382.
[2] S. Couck, E. Gobechiya, C.E.A. Kirschhock, P. Serra-Crespo, J. Juan-Alcañiz, A. Martinez Joaristi, E. Stavitski, J. Gascon, F. Kapteijn, G.V. Baron, J.F.M. Denayer, Adsorption and Separation of Light Gases on an Amino-Functionalized Metal–Organic Framework: An Adsorption and In Situ XRD Study, ChemSusChem, 5 (2012) 740-750.
[3] L. Bolinois, T. Kundu, X. Wang, Y. Wang, Z. Hu, K. Koh, D. Zhao, Breathing-induced new phase transition in an MIL-53(Al)–NH2 metal–organic framework under high methane pressures, Chemical Communications, 53 (2017) 8118-8121.
[4] E. Stavitski, E.A. Pidko, S. Couck, T. Remy, E.J.M. Hensen, B.M. Weckhuysen, J. Denayer, J. Gascon, F. Kapteijn, Complexity behind CO2 Capture on NH2-MIL-53(Al), Langmuir, 27 (2011) 3970-3976.

Chapter

5

Melamine-based microporous organic framework thin films on an alumina membrane for high-flux organic solvent nanofiltration

This chapter contains parts of the following publication:

M. Amirilargani, G. N. Yokota, G. H. Vermeij, R. B. Merlet, G. Delen, L. D. B. Mandemaker, B. M. Weckhuysen, A. Nijmeijer, L. Winnubst, L. C. P. M. de Smet, E. J. R. Sudhölter, *Submitted to ChemSusChem, Under Review*.

Microporous polymer frameworks have attracted considerable attention to make novel separation layers owing to their highly porous structure, high permeability and excellent molecular separation. Here, we report the fabrication and properties of thin melamine–based microporous polymer networks with a layer thickness of *ca.* 400 nm, supported on an α-alumina support, and show their potential use in organic solvent nanofiltration. The modified membranes show excellent solvent purification performances, such as n-heptane permeability as high as 9.2 L m^{-2} h^{-1} bar $^{-1}$ in combination with a very high rejection of ~99% for organic dyes with molecular weight of ≥ 457 Da. These properties are higher than the majority of the state-of-the-art membranes. We further demonstrate the outstanding long-time operation stability of these membranes. Our work significantly expands the possibilities of using ceramic membranes in organic solvent nanofiltration process.

5.1 Introduction

Purification of organic solvents has received much attention due to the increased environmental concerns and the search for cleaner and more energy-efficient processes [1-4]. Organic solvent nanofiltration (OSN) is an energy-efficient, membrane-based separation process with a high potential to be employed in a wide range of applications [5]. However, the development of high-performance OSN processes is still challenging. Despite the satisfactory rejection of the OSN membranes reported to far, most of them have a relatively low solvent permeability. Reduction of the selective layer thickness is obvious for enhancing the solvent permeability. Such a path length reduction has been applied to graphene-based membranes [3, 6], bilayer polyelectrolyte membranes [7] and interfacially polymerized polyamide membranes [8, 9], all resulting in a significant increase of solvent permeation.

Membranes with molecular sieving properties, originating from the presence of well-ordered and tunable pores are attractive candidates for OSN where a high molecular size selectivity for rejection in combination with a high solvent permeation are required [10, 11]. Microporous materials such as metal organic frameworks (MOFs) [11-14], zeolites [15, 16] and graphene [3, 17, 18] are well-known molecular sieve materials, showing high permeability and selectivity. Recently, a wide range of different porous all organic frameworks have become of interest for investigations in membrane applications. Among these are the porous organic frameworks (POFs) [19, 20], crystalline covalent-organic frameworks (COFs) [10, 21, 22], covalent triazine frameworks (CTFs) [23-25], polymers of intrinsic microporosity (PIMs) [26, 27], porous aromatic frameworks (PAFs) [28-30] and amorphous hyper-crosslinked polymers (AHCPs) [31].

Polycondensation of melamine and aromatic bis-aldehydes results in the formation of a microporous polymer network of aminal bonds. [32, 33]. Schiff base-based POFs have found to be chemically stable in polar and nonpolar organic solvents, in aqueous solution with a wide range of pH (2.0-13.0), even under extreme harsh conditions, like boiling water [34, 35]. Interestingly, recently developed POFs made from melamine and terephthaldehyde, having a mean pore diameter of ~ 5 Å, show very good properties for nanofiltration [36, 37] and gas separation applications [31].

5.2 Experimental section

5.2.1 Materials

All chemicals were purchased from Sigma-Aldrich, unless otherwise indicated. 3-amino propyl triethoxysilane (APTES), Melamine (99%), terephthaldehyde (Reagent Plus, 99%), isophthaldehyde (97%) and dimethyl sulfoxide (anhydrous) were used for membrane fabrication. Sudan Red 7B (*MW*=379 Da), Solvent Green 3 (*MW*=418 Da), Sudan Black B (*MW*=456 Da) and Bromothymol Blue

(*MW* = 624 Da), n-heptane (anhydrous) and toluene (anhydrous) were used for OSN experiments. Flat disc-shaped α-alumina membranes (having a diameter of 39 mm, a thickness of 2 mm, and a pore diameter of 80 nm) were purchased from Pervatech B.V., The Netherlands.

5.2.2 APTES modification of the α-alumina substrate

Prior to the APTES modification, samples were submerged in a 2 M HCl solution (40 ml) for 5 h at room temperature to activate the surface hydroxyl groups [10]. The soaked membranes were then washed several times with milliQ water to reach a neutral pH and dried in a vacuum oven at 70 °C overnight. Afterwards the activated membranes were grafted with a 4 mM solution of APTES in 50 mL of toluene at 105 °C for 3 h under an argon atmosphere. Afterwards, the APTES-modified α-alumina membranes were removed from the solution and were rinsed with toluene and ethanol and then dried in a vacuum oven at 60 °C overnight.

5.2.3 Preparation of the microporous organic frameworks thin films on the APTES-modified α-alumina substrate

The thin microporous polymer networks were prepared via the following, optimized, procedure the APTES-modified α-alumina membranes were immersed in a DMSO solution (50 ml) containing melamine (0.313 g / 2.5 mmol) and terephthaldehyde (0.5 g / 3.75 mmol) or isophthaldehyde (0.5 g / 3.75 mmol). Then the solution was heated at 180 °C for 72 h. Finally, the modified membranes were rinsed with acetone, THF and CH_2Cl_2 for several times and dried in a vacuum oven at 70 °C.

5.2.4 Characterization methods and related measurement protocols

Materials characterization

FE-SEM images were acquired to observe the morphology of membranes and powders. The gold-coated samples were places in a Nova NanoSEM 450 (Thermo Fisher Scientific) with an accelerating voltage of 10 kV. TEM analysis was carried out with JEOL JEM-2010 microscope operated at 200 kV. Fourier transforms infrared (FTIR) spectra of the different POFs particles in KBr tablets were measured using a Nicolet iS50 FTIR (Thermo Fisher Scientific Co., Madison, USA) spectrophotometer in the range of 4000-500 cm^{-1}. Each spectrum was captured by 128 scans at a resolution of 4 cm^{-1}. The thermogravimetric properties of the POF particles were determined by a thermogravimetric analyzer (TGA; Mettler Toledo, TGA/SDTA 851e). The samples were heated under a N_2 atmosphere from 25 to 850 °C at a heating rate of 10 °C min^{-1}. N_2 adsorption-desorption experiments were performed at 77 K for POFs particles, using a Quantachrome Autosorb 1MP apparatus. Pore size distributions were obtained using non-local density-functional theory (NLDFT)

method. The NLDFT pore size distributions were obtained using a NLDFT approach implemented within the demo version of SAIEUS software (www.nldft.com/download/) (Micromeritics, GA) [38, 39]. The standard slit-pore model for N_2 adsorption at 77 K on carbon was selected because it is widely used in experiments to characterize amorphous microporous materials. The L-curve method, which balances the roughness of the solution and soundness of the fit, is implemented in SAIEUS when choosing λ as a user-adjustable parameter. λ = 0 selected for the calculation of pore size distribution.

Photo-induced force microscopy (PiFM) measurements were performed using a VistaScope from Molecular Vista, Inc. Topography and PiFM images (5 x 5 μm^2, 256 x 256 pixels) were taken in dynamic non-contact mode using NCHAu tips (Nanosensors) with a scan speed of 0.4 Hz. A Block Engineering tunable quantum cascade laser (QCL) was used as mid-IR source. Detection of the topography signal was tuned to the second mechanical mode, while the IR signal detection was tuned to the first mechanical mode of the AFM cantilever. By using independent eigenmodes for detection, simultaneous collection of topography and the PiFM signal was realized. Near-field infrared spectroscopy measurements were performed with an approximate lateral resolution of 10 nm and probing depth of 30 nm [40]. 30× averaged infrared point spectra were within the AFM topography images (indicated by markers). AFM-IR spectra were taken in the 1970-775 cm^{-1} range with a resolution of 2 cm^{-1} and a spectrum acquisition time of 750 ms. All spectral data was corrected for the laser source power profile. To this end, the laser power profile was measured in IR direct detection mode at 200 µm above the surface. AFM-IR images were analyzed using Gwyddion software, spectral data was analyzed using Surface Works software.

OSN experiment procedure

Membrane performance was tested in a typical stainless steel dead-end pressure cell at a transmembrane pressure (TMP) of 6 bar at room temperature. The system is pressurized using inert argon. The effective area of each membrane was 8.9 cm^2 and at least three independently prepared membranes of each type were investigated. The reported results are the mean values of these measurements. The model solutions for the rejection measurement had a concentration of 20 mg L^{-1} of Sudan Red 7B, Solvent Green 3, Sudan Black B or Bromothymol Blue in either toluene or n-heptane solution. During the filtration, the feed solution was stirred at 200 rpm using a magnetic stirrer to minimize concentration polarization near the membrane surface. The membrane cell was filled with 100 ml of feed solution per membrane and 50 ml of the permeate was collected for each membrane at the permeate side (i.e., 50% recovery). The membrane permeability was calculated according to Equation 1 [41],

$$\text{Permeability} = \frac{J}{\Delta P} = \frac{V}{\Delta P A t} = [\mathrm{L\,m^{-2}\,h^{-1}bar^{-1}}] \qquad (5.1)$$

where J is the solvent flux [L m^{-2} h^{-1}], ΔP is the applied pressure across the membrane [bar], V is the permeate volume [L], A is the effective membrane surface area [m^2] and t is the collecting permeate sample time [h]. The dye solute rejections (*R*) were calculated from the solutes concentration in the permeate (C_p) and initial concentration in the feed (C_f), using Equation 2 [41]:

$$R = \left(1 - \frac{C_p}{C_f}\right) \times 100\% \qquad (5.2)$$

Dye concentrations at the permeate side were measured using a double beam UV-Vis spectrophotometer (Shimadzu, UV-1800).

5.3 Results and discussions

The α-alumina, with an average pore diameter of 80 nm, was first modified with 3-aminopropyl trimethoxy silane (APTES), to promote covalent linkage of the *in-situ* prepared POF in the subsequent step (Figure 5.1). In more detail, this step involves a polycondensation on top of the amine-functionalized α-alumina membrane using melamine and terephthaldehyde (*i.e.*, benzene 1,4-dicarboxaldehyde) to make a melamine-terephthaldehyde (MT) POF thin film. To study the effect of the *bis*-aldehyde's structure on the morphology and the performance of the thin membrane, we also used *iso*-phthaldehyde (*i.e.* benzene 1,3-dicarboxaldehyde) as a POF building block to synthesize a melamin-*iso*-phthaldehyde (MI) POF thin film. The polycondensation reaction resulted in a light yellow coloration of the α-alumina membrane, which remained after thoroughly washing with THF and acetone (Figure 5.2 a).

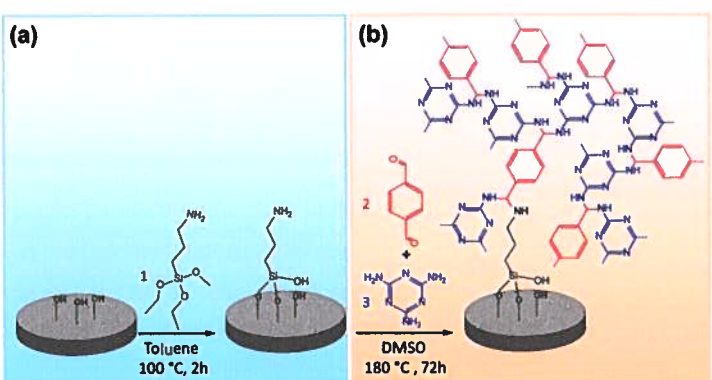

Figure 5.1 Schematic representation of (a) APTES grafting onto the α-alumina membrane, (b) *in-situ* synthesis of melamine-terephthaldehyde microporous polymer networks (MT POF) on the APTES-modified α-alumina membrane. Molecules 1-3 are APTES, terephthaldehyde and melamine, respectively.

Next, the POF-modified membranes were investigated by both surface and cross-sectional field-emission scanning electron microscopy (FE-SEM) and compared to the images obtained from the unmodified, bare membranes.

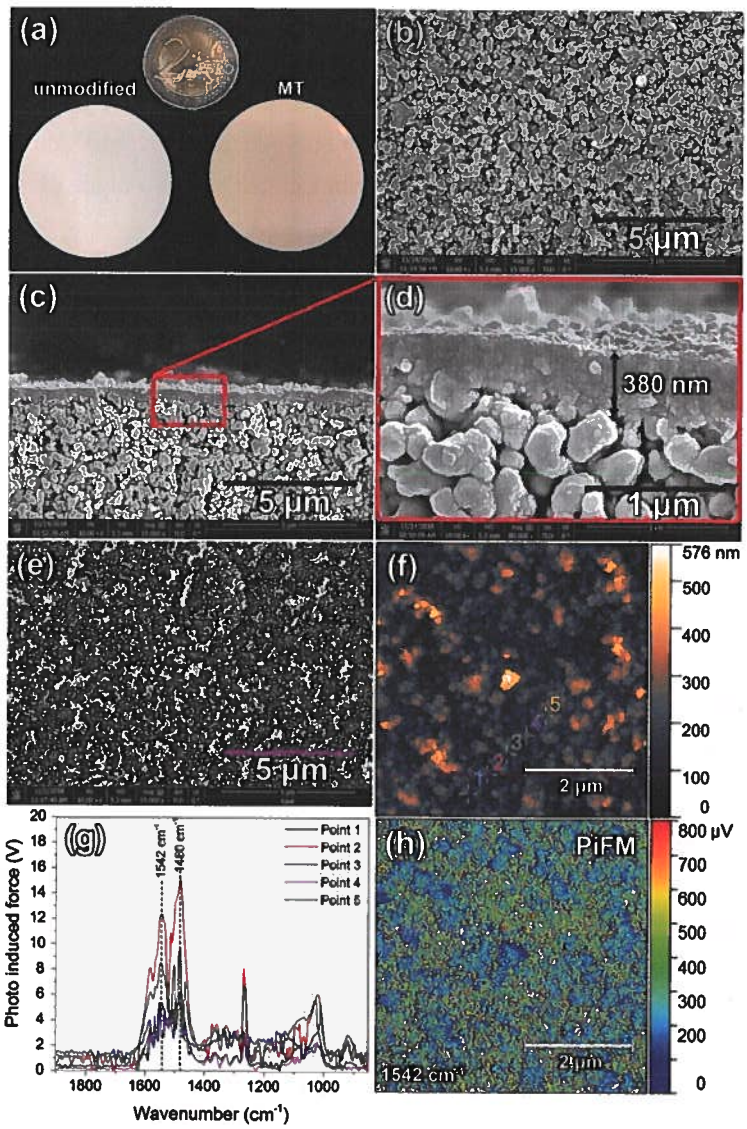

Figure 5.2 a) Photographs of unmodified and MT POF-modified α-alumina membranes. b) Surface FE-SEM image of unmodified membrane. c) Low-magnification cross-section FE-SEM image, d) high-magnification cross-section FE-SEM image, e) Surface FE-SEM, f) 3D AFM surface image, g) Surface FT-IR analysis and h) FT-IR image of MT POF-modified α-alumina membrane.

For the unmodified α-alumina membrane the FE-SEM image of the surface (Figure 5.2 b) shows the typical surface morphology, reflecting closely packed micro-sized α-alumina particles, while it can

be clearly seen that the membrane surface morphology changed upon the POF-formation. The cross-sectional images (Figure 5.2 c and 5.2 d) show a thin 'blanket' of the MT POF, with a thickness of *ca.* 400 nm. For the membranes modified with MI POFs the cross-sectional FE-SEM image displays a similar morphology and a thickness of ~ 450 nm.

To learn more about the (network) structure of the synthesized POF layer, the MT POF-modified α-alumina membranes were also characterized by an emerging tip-sensed AFM-IR technology, namely, photo-induced force microscopy (PiFM). In PiFM-IR, a pulsed laser source induces a dipole in the POF layer and consequently a mirror dipole is induced in the AFM tip, which is translated into FT-IR spectral data [40, 42, 43].

The 3D surface morphology of the MT POF-modified α-alumina membrane shows a rather dense structure of the membrane surface, whereas the POF particles are clearly visible at the surface as shown in Figure 5.2 f. We have chosen randomly five points at the surface for the FT-IR analysis and the results are presented in Figure 5.2 g. The obtained FT-IR spectra all manifest two strong bands at 1480 and 1542 cm^{-1}, which are attributed to the semicircle and quadrant stretching of the triazine ring in the POF structure, respectively. These are similar peaks to the ones observed from the FT-IR analysis of the MT POF powders (Figure A5.4), indicating a certain level of similarity in the chemical structure of the POF films and the collected POF powders. As can be seen in the FT-IR map taken at 1542 cm^{-1}, as well as the point analysis (Figure 5.2 h), the POF thin film is homogeneously dispersed at the surface of an α-alumina support.

Once the presence of the thin MT-POF films was confirmed, their solvent stability is among the most important factors having a crucial impact as it can cause severe swelling or even dissolution of the membrane materials, resulting in loss of separation performance. Therefore, we have examined the stability of the POF powders when dispersed in toluene and n-heptane for a period of maximal 4 weeks. Since no changes from the FT-IR spectra were observed in time (Figure A5.4), we conclude that these POFs are stable in contact with these solvents.

From N_2 adsorption-desorption experiments on the POF powders, the BET surface was determined to be 520 $m^2\ g^{-1}$ for the MT POF and 598 $m^2\ g^{-1}$ for MI POF. Using non-local density-functional theory (NL-DFT) method the pore diameter of ~ 5 and 4 Å were calculated for the corresponding POFs (Figure A5.5), indicating their microporous structure.

To date there has been little success to make membranes showing high solvent permeability in combination with a high solute rejection for non-polar organic solvents, such as toluene and n-heptane. These solvents have tremendous applications and are therefore ideal choices for OSN performance tests using different molecular weight dyes [44, 45]. We have investigated OSN performance of the MT and MI POF-modified α-alumina membranes using a solution of toluene and n-heptane containing 20 mg L^{-1} Sudan Red 7B (*MW* = 379 Da), Solvent Green 3 (*MW* = 418 Da),

Sudan Black B (*MW* = 456 Da) and Bromothymol Blue (*MW* = 624 Da) (Scheme A5.1 and Table A5.1).

The results of the measured rejection of the organic dyes and the solvent permeability are shown in Figure 5.3. For the MT and MI POF-modified α-alumina membranes (Figure 5.3) and toluene as the solvent, a solute rejection of ≥ 90% was found for Solvent Green 3, Sudan Black B, and Bromothymol Blue, while Sudan Red 7B shows a rejection of ~50%. In n-heptane as the solvent the results are very similar, although the rejections found for Solvent Green 3 and Sudan Red 7B were found to be somewhat lower. In both cases the solvent permeability remains high, *i.e.*, 6 – 8 L m^{-2} h^{-1} bar^{-1}. For n-heptane the permeability is always found a few percent higher compared to toluene (Figure 5.3), which can be well understood by the difference in the solvent dynamic viscosity (0.37 mPa s and 0.59 mPa s for n-heptane and toluene, respectively) and their kinetic diameters (4.3 Å [46] *vs.* 5.8 Å [47], respectively).

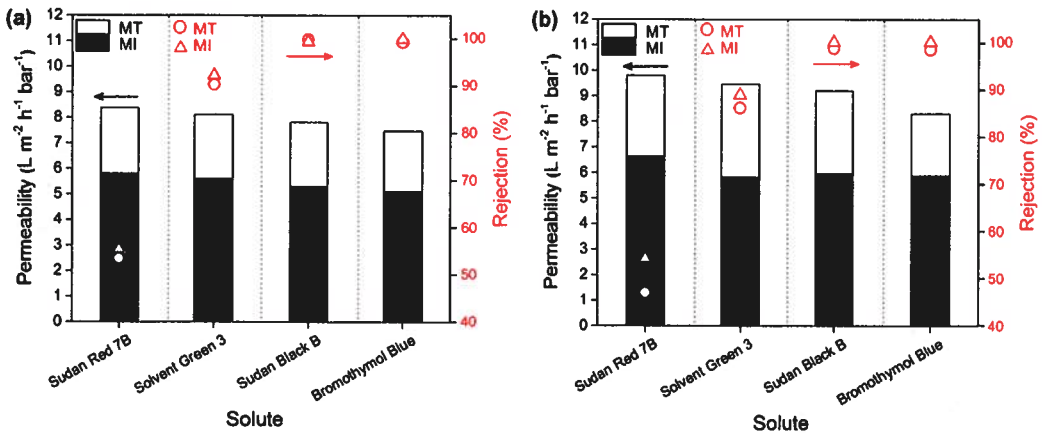

Figure 5.3 Solvent permeability (columns) and solute rejection (red markers) for MT and MI POF-modified α-alumina membranes in (a) toluene and (b) n-heptane.

From Figure 5.3 it can also be clearly seen that the solvent permeability found for the MI POF-modified α-alumina membranes is lower than the one found for the MT POF-modified α-alumina membranes. This is attributed to a ~ 50 nm thicker MI POF compared with MT POF layer and a somewhat denser structure of the MI POF-modified α-alumina membrane (Figure A5.6). Both POF-modified membranes show very high rejections (≥ 90%) of solute molecules of a *MW* ≥ 418 Da in toluene, while the rejection in heptane of Solvent Green 3 with a *MW* of 418 Da is 86 and 89% for MT and MI POFs-modified α-alumina membranes. It is important to note that the pore sizes of the POF-modified membranes are expected to be lower than the size of a Solvent Green 3 molecule. Unfortunately, effective solute diameters, which can be calculated in different ways, are not always accessible. For instance to calculate the Stokes diameter, the solute diffusivity in each solvent is

needed [48]. Nevertheless, from the solute molecular weight point of view, our results signify that the molecular weight cut-off (MWCO) of our membranes to be determined around 460 Da.

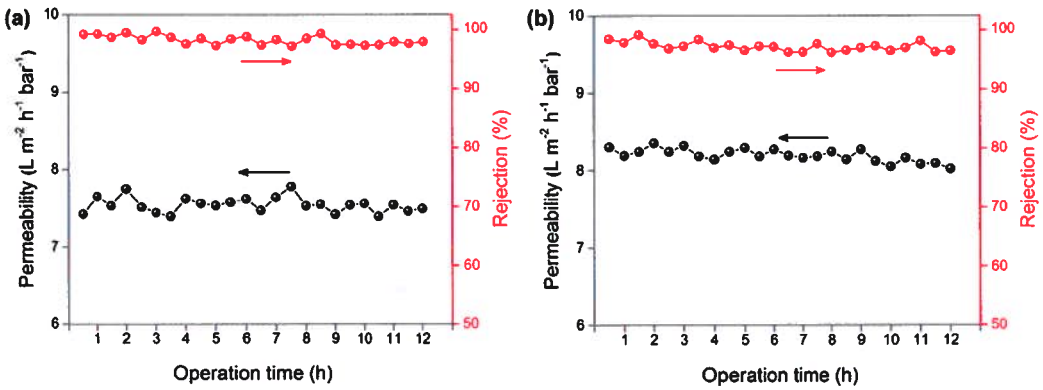

Figure 5.4 long-time OSN tests of 20 mg L^{-1} (a) Bromothymol Blue/toluene and (b) Bromothymol Blue/n-heptane using a MT POF-modified α-alumina membrane.

The long-term stability of the MT membrane was characterized by measuring the toluene and n-heptane permeability and Bromothymol Blue rejection (Figure 5.4). Both remained highly constant during 12 h of measurement indicating a solvent stability of the POF membranes for this system.

Finally, we compared our new MT POF-modified α-alumina membranes for separation of Sudan Black B from toluene and n-heptane with reported functionalized ceramic membranes and the commercially available polymeric STARMEM 122 membranes. For all these systems the observed rejections are plotted against their respective permeabilities in Figure 5.5.

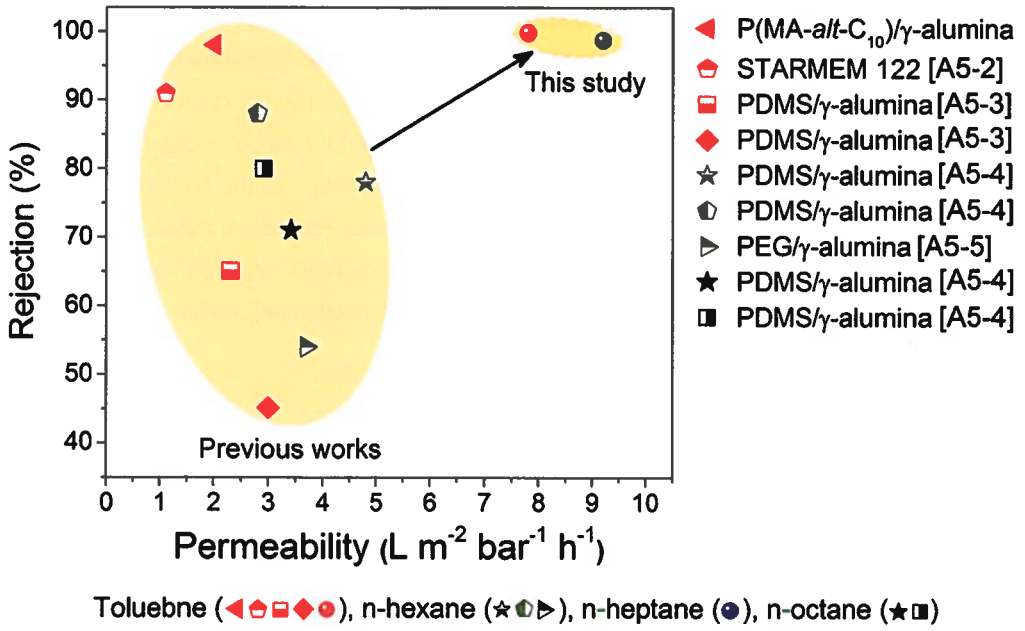

Figure 5.5 Comparison of the OSN performance for the separation of Sudan black B of MT POF-modified α-alumina membrane with state-of-the-art ceramic and commercially polymeric STARMEM 122 membranes (for details see Table A5.2).

It is evident that the rejection and permeability properties of our system are exceptionally high compared to those of the other systems. This is a direct consequence of the thickness of only 380 nm of the POF layer on the α-alumina supporting membrane of thickness of 2 mm. The other modified ceramic membranes, such as the ones shown in Figure 5.5, are all based on a 3-5 μm thick layer of γ-alumina modified with different functionalization agents on a 2 mm porous α-alumina. In other words, our layers are about 10 times thinner.

5.4 Conclusions

In summary, for the first time, a facile and efficient membrane modification approach to develop a continuous and defect-free melamine-based microporous organic frameworks selective layer for OSN applications is reported. Because of the formation of such thin layers (only 360 nm thick), the obtained membranes showed a much higher organic solvent permeability compared with other state-of-the-art ceramic membranes. A maximum toluene permeability of 7.8 L m^{-2} h^{-1} bar^{-1} was obtained with a MT membrane, which permeability is ~ 2.5 times higher than the best reported ceramic membranes so far. In addition, due to their microporosity, the POF membranes showed excellent rejection values for the organic dyes with a *MW* > 418 Da. Furthermore, the POF

membranes showed excellent solvent stability with no change in solvent permeation and solute rejection after 12 h of continuous solvent filtration. The superior performance coupled with the high solvent stability of this new POF-based membrane, could render the use of POF membranes made on an alumina substrate is an attractive choice for purification of non-polar organic solvents where most of the investigated polymeric membranes failed. Furthermore, as the library of building blocks for (functionalized) organic frameworks is vast and continuously increasing, the tunability possibilities is expected to further increase, paving the way for a wider integration of these framework in the field of high-performance OSN applications, addressing various molecular separations.

References

[1] G. Szekely, M.F. Jimenez-Solomon, P. Marchetti, J.F. Kim, A.G. Livingston, Sustainability assessment of organic solvent nanofiltration: From fabrication to application, Green Chemistry, 16 (2014) 4440-4473.
[2] P. Marchetti, M.F. Jimenez Solomon, G. Szekely, A.G. Livingston, Molecular Separation with Organic Solvent Nanofiltration: A Critical Review, Chemical Reviews, 114 (2014) 10735-10806.
[3] Q. Yang, Y. Su, C. Chi, C.T. Cherian, K. Huang, V.G. Kravets, F.C. Wang, J.C. Zhang, A. Pratt, A.N. Grigorenko, F. Guinea, A.K. Geim, R.R. Nair, Ultrathin graphene-based membrane with precise molecular sieving and ultrafast solvent permeation, Nature Materials, 16 (2017) 1198.
[4] B. Liang, H. Wang, X. Shi, B. Shen, X. He, Z.A. Ghazi, N.A. Khan, H. Sin, A.M. Khattak, L. Li, Z. Tang, Microporous membranes comprising conjugated polymers with rigid backbones enable ultrafast organic-solvent nanofiltration, Nature Chemistry, 10 (2018) 961-967.
[5] M. Amirilargani, R.B. Merlet, A. Nijmeijer, L. Winnubst, L.C.P.M. de Smet, E.J.R. Sudhölter, Poly (maleic anhydride-alt-1-alkenes) directly grafted to γ-alumina for high-performance organic solvent nanofiltration membranes, Journal of Membrane Science, 564 (2018) 259-266.
[6] L. Huang, J. Chen, T. Gao, M. Zhang, Y. Li, L. Dai, L. Qu, G. Shi, Reduced Graphene Oxide Membranes for Ultrafast Organic Solvent Nanofiltration, Advanced Materials, 28 (2016) 8669-8674.
[7] N. Joseph, J. Thomas, P. Ahmadiannamini, H. Van Gorp, R. Bernstein, S. De Feyter, M. Smet, W. Dehaen, R. Hoogenboom, I.F.J. Vankelecom, Ultrathin Single Bilayer Separation Membranes Based on Hyperbranched Sulfonated Poly(aryleneoxindole), Advanced Functional Materials, 27 (2017) 1605068-n/a.
[8] S. Karan, Z. Jiang, A.G. Livingston, Sub–10 nm polyamide nanofilms with ultrafast solvent transport for molecular separation, Science, 348 (2015) 1347-1351.
[9] Z. Jiang, S. Karan, A.G. Livingston, Water Transport through Ultrathin Polyamide Nanofilms Used for Reverse Osmosis, Advanced Materials, 30 (2018) 1705973.
[10] H. Fan, J. Gu, H. Meng, A. Knebel, J. Caro, High-Flux Membranes Based on the Covalent Organic Framework COF-LZU1 for Selective Dye Separation by Nanofiltration, Angewandte Chemie International Edition, 57 (2018) 4083-4087.
[11] J. Hou, P.D. Sutrisna, Y. Zhang, V. Chen, Formation of Ultrathin, Continuous Metal–Organic Framework Membranes on Flexible Polymer Substrates, Angewandte Chemie International Edition, 55 (2016) 3947-3951.
[12] K. Huang, B. Wang, S. Guo, K. Li, Micropatterned Ultrathin MOF Membranes with Enhanced Molecular Sieving Property, Angewandte Chemie International Edition, 57 (2018) 13892-13896.
[13] H. Wang, S. He, X. Qin, C. Li, T. Li, Interfacial Engineering in Metal–Organic Framework-Based Mixed Matrix Membranes Using Covalently Grafted Polyimide Brushes, Journal of the American Chemical Society, 140 (2018) 17203-17210.
[14] J.Y. Chan, H. Zhang, Y. Nolvachai, Y. Hu, H. Zhu, M. Forsyth, Q. Gu, D.E. Hoke, X. Zhang, P.J. Marriot, H. Wang, Incorporation of Homochirality into a Zeolitic Imidazolate Framework Membrane for Efficient Chiral Separation, Angewandte Chemie International Edition, 57 (2018) 17130-17134.
[15] M.Y. Jeon, D. Kim, P. Kumar, P.S. Lee, N. Rangnekar, P. Bai, M. Shete, B. Elyassi, H.S. Lee, K. Narasimharao, S.N. Basahel, S. Al-Thabaiti, W. Xu, H.J. Cho, E.O. Fetisov, R. Thyagarajan, R.F. DeJaco, W. Fan, K.A. Mkhoyan, J.I. Siepmann, M. Tsapatsis, Ultra-selective high-flux membranes from directly synthesized zeolite nanosheets, Nature, 543 (2017) 690.
[16] P.-S. Huang, C.H. Lam, C.-Y. Su, Y.-R. Chen, W.-Y. Lee, D.-M. Wang, C.-C. Hua, D.-Y. Kang, Scalable Wet Deposition of Zeolite AEI with a High Degree of Preferred Crystal Orientation, Angewandte Chemie International Edition, 57 (2018) 13271-13276.
[17] P.R. Kidambi, G.D. Nguyen, S. Zhang, Q. Chen, J. Kong, J. Warner, A.-P. Li, R. Karnik, Facile Fabrication of Large-Area Atomically Thin Membranes by Direct Synthesis of Graphene with Nanoscale Porosity, Advanced Materials, 30 (2018) 1804977.
[18] G. Wei, X. Quan, S. Chen, H. Yu, Superpermeable Atomic-Thin Graphene Membranes with High Selectivity, ACS Nano, 11 (2017) 1920-1926.
[19] X. Zou, G. Zhu, Microporous Organic Materials for Membrane-Based Gas Separation, Advanced Materials, 30 (2018) 1700750.
[20] Y. Cheng, Y. Ying, S. Japip, S.-D. Jiang, T.-S. Chung, S. Zhang, D. Zhao, Advanced Porous Materials in Mixed Matrix Membranes, Advanced Materials, 30 (2018) 1802401.
[21] D.B. Shinde, G. Sheng, X. Li, M. Ostwal, A.-H. Emwas, K.-W. Huang, Z. Lai, Crystalline 2D Covalent Organic Framework Membranes for High-Flux Organic Solvent Nanofiltration, Journal of the American Chemical Society, 140 (2018) 14342-14349.
[22] V.A. Kuehl, J. Yin, P.H.H. Duong, B. Mastorovich, B. Newell, K.D. Li-Oakey, B.A. Parkinson, J.O. Hoberg, A Highly Ordered Nanoporous, Two-Dimensional Covalent Organic Framework with Modifiable Pores, and Its Application in Water Purification and Ion Sieving, Journal of the American Chemical Society, 140 (2018) 18200-18207.

[23] Y. Wang, J. Li, Q. Yang, C. Zhong, Two-Dimensional Covalent Triazine Framework Membrane for Helium Separation and Hydrogen Purification, ACS Applied Materials & Interfaces, 8 (2016) 8694-8701.
[24] L.-C. Lin, J. Choi, J.C. Grossman, Two-dimensional covalent triazine framework as an ultrathin-film nanoporous membrane for desalination, Chemical Communications, 51 (2015) 14921-14924.
[25] Y.P. Tang, H. Wang, T.S. Chung, Towards High Water Permeability in Triazine-Framework-Based Microporous Membranes for Dehydration of Ethanol, ChemSusChem, 8 (2015) 138-147.
[26] P. Gorgojo, S. Karan, H.C. Wong, M.F. Jimenez-Solomon, J.T. Cabral, A.G. Livingston, Ultrathin Polymer Films with Intrinsic Microporosity: Anomalous Solvent Permeation and High Flux Membranes, Advanced Functional Materials, 24 (2014) 4729-4737.
[27] A. Sabetghadam, X. Liu, A.F. Orsi, M.M. Lozinska, T. Johnson, K.M.B. Jansen, P.A. Wright, M. Carta, N.B. McKeown, F. Kapteijn, J. Gascon, Towards High Performance Metal–Organic Framework–Microporous Polymer Mixed Matrix Membranes: Addressing Compatibility and Limiting Aging by Polymer Doping, Chemistry – A European Journal, 24 (2018) 12796-12800.
[28] C.H. Lau, K. Konstas, A.W. Thornton, A.C.Y. Liu, S. Mudie, D.F. Kennedy, S.C. Howard, A.J. Hill, M.R. Hill, Gas-Separation Membranes Loaded with Porous Aromatic Frameworks that Improve with Age, Angewandte Chemie International Edition, 54 (2015) 2669-2673.
[29] C.H. Lau, X. Mulet, K. Konstas, C.M. Doherty, M.-A. Sani, F. Separovic, M.R. Hill, C.D. Wood, Hypercrosslinked Additives for Ageless Gas-Separation Membranes, Angewandte Chemie International Edition, 55 (2016) 1998-2001.
[30] X. Wu, M. Shaibani, S.J.D. Smith, K. Konstas, M.R. Hill, H. Wang, K. Zhang, Z. Xie, Microporous carbon from fullerene impregnated porous aromatic frameworks for improving the desalination performance of thin film composite forward osmosis membranes, Journal of Materials Chemistry A, 6 (2018) 11327-11336.
[31] X. Gao, X. Zou, H. Ma, S. Meng, G. Zhu, Highly Selective and Permeable Porous Organic Framework Membrane for CO2 Capture, Advanced Materials, 26 (2014) 3644-3648.
[32] M.G. Schwab, B. Fassbender, H.W. Spiess, A. Thomas, X. Feng, K. Müllen, Catalyst-free Preparation of Melamine-Based Microporous Polymer Networks through Schiff Base Chemistry, Journal of the American Chemical Society, 131 (2009) 7216-7217.
[33] P. Puthiaraj, Y.-R. Lee, S. Zhang, W.-S. Ahn, Triazine-based covalent organic polymers: design, synthesis and applications in heterogeneous catalysis, Journal of Materials Chemistry A, 4 (2016) 16288-16311.
[34] J. Pan, S. Jia, G. Li, Y. Hu, Organic Building Block Based Microporous Network SNW-1 Coating Fabricated by Multilayer Interbridging Strategy for Efficient Enrichment of Trace Volatiles, Analytical Chemistry, 87 (2015) 3373-3381.
[35] O.S. Taskin, S. Dadashi-Silab, B. Kiskan, J. Weber, Y. Yagci, Highly Efficient and Reusable Microporous Schiff Base Network Polymer as a Heterogeneous Catalyst for CuAAC Click Reaction, Macromolecular Chemistry and Physics, 216 (2015) 1746-1753.
[36] C. Wang, Z. Li, J. Chen, Z. Li, Y. Yin, L. Cao, Y. Zhong, H. Wu, Covalent organic framework modified polyamide nanofiltration membrane with enhanced performance for desalination, Journal of Membrane Science, 523 (2017) 273-281.
[37] C. Li, S. Li, L. Tian, J. Zhang, B. Su, M.Z. Hu, Covalent organic frameworks (COFs)-incorporated thin film nanocomposite (TFN) membranes for high-flux organic solvent nanofiltration (OSN), Journal of Membrane Science, 572 (2019) 520-531.
[38] G. Kupgan, T.P. Liyana-Arachchi, C.M. Colina, NLDFT Pore Size Distribution in Amorphous Microporous Materials, Langmuir, 33 (2017) 11138-11145.
[39] A.M. Puziy, O.I. Poddubnaya, B. Gawdzik, M. Sobiesiak, Comparison of heterogeneous pore models QSDFT and 2D-NLDFT and computer programs ASiQwin and SAIEUS for calculation of pore size distribution, Adsorption, 22 (2016) 459-464.
[40] D. Fu, K. Park, G. Delen, Ö. Attila, F. Meirer, D. Nowak, S. Park, J.E. Schmidt, B.M. Weckhuysen, Nanoscale infrared imaging of zeolites using photoinduced force microscopy, Chemical Communications, 53 (2017) 13012-13014.
[41] J. Campbell, R.P. Davies, D.C. Braddock, A.G. Livingston, Improving the permeance of hybrid polymer/metal-organic framework (MOF) membranes for organic solvent nanofiltration (OSN) - development of MOF thin films via interfacial synthesis, Journal of Materials Chemistry A, 3 (2015) 9668-9674.
[42] G. Delen, Z. Ristanović, L.D.B. Mandemaker, B.M. Weckhuysen, Mechanistic Insights into Growth of Surface-Mounted Metal-Organic Framework Films Resolved by Infrared (Nano-) Spectroscopy, Chemistry – A European Journal, 24 (2018) 187-195.
[43] L.D.B. Mandemaker, M. Filez, G. Delen, H. Tan, X. Zhang, D. Lohse, B.M. Weckhuysen, Time-Resolved In Situ Liquid-Phase Atomic Force Microscopy and Infrared Nanospectroscopy during the Formation of Metal–Organic Framework Thin Films, The Journal of Physical Chemistry Letters, 9 (2018) 1838-1844.

[44] L.M. Sharaf, M.M. El Nady, Application of Light Hydrocarbon (C7+) and Biomarker Analyses in Characterizing Oil from Wells in the North and North Central Sinai, Egypt, Petroleum Science and Technology, 24 (2006) 607-627.
[45] H.-G. Franck, J.W. Stadelhofer, Production and uses of toluene derivatives, in: Industrial Aromatic Chemistry: Raw Materials · Processes · Products, Springer Berlin Heidelberg, Berlin, Heidelberg, 1988, pp. 236-264.
[46] H.H. Funke, A.M. Argo, C.D. Baertsch, J.L. Falconer, R.D. Noble, Separation of close-boiling hydrocarbons with silicalite zeolite membranes, Journal of the Chemical Society, Faraday Transactions, 92 (1996) 2499-2502.
[47] C.D. Baertsch, H.H. Funke, J.L. Falconer, R.D. Noble, Permeation of Aromatic Hydrocarbon Vapors through Silicalite−Zeolite Membranes, The Journal of Physical Chemistry, 100 (1996) 7676-7679.
[48] S. Darvishmanesh, J. Degrève, B. Van Der Bruggen, Mechanisms of solute rejection in solvent resistant nanofiltration: The effect of solvent on solute rejection, Physical Chemistry Chemical Physics, 12 (2010) 13333-13342.

Annex

5

Melamine-based microporous organic framework thin films on an alumina membrane for high-flux organic solvent nanofiltration

A5.1 Results and discussions

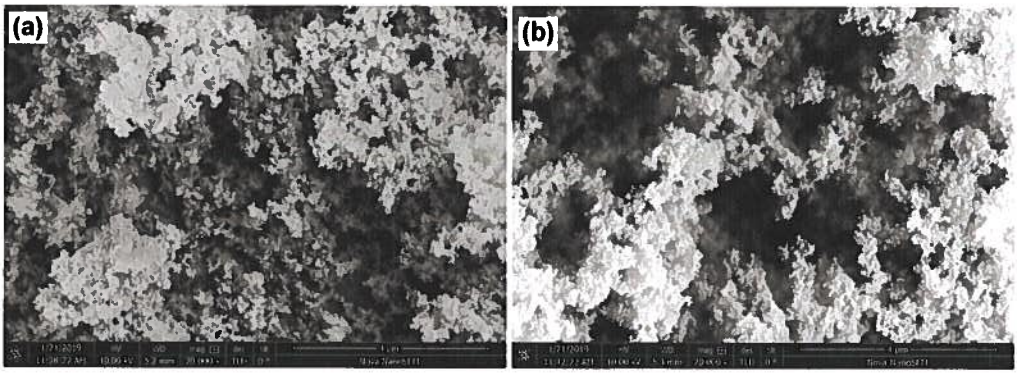

Figure A5.1 FE-SEM images from the (a) MT and (b) MI particles collected from the reaction vessel.

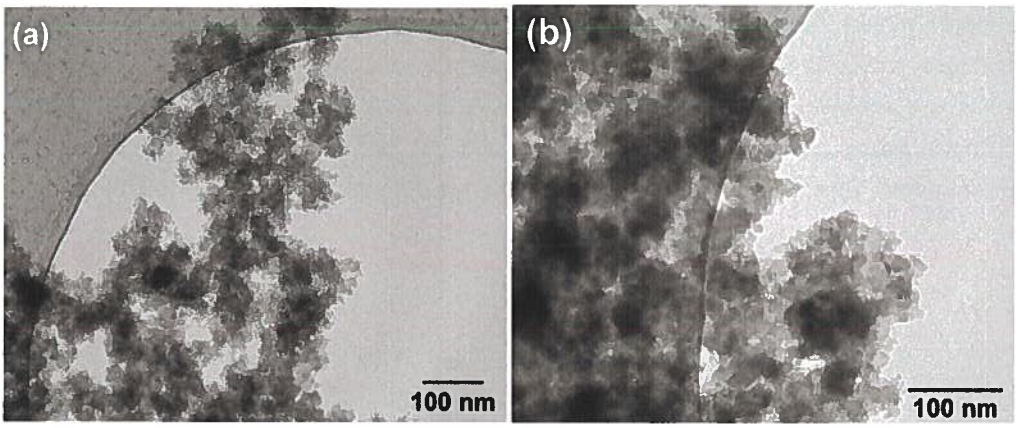

Figure A5.2 TEM images of (a) MT and (b) MI particles collected from the reaction vessel.

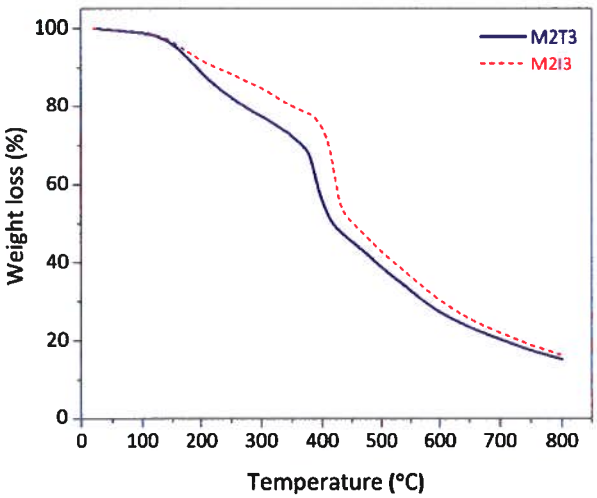

Figure A5.3 TGA curves of the (blue solid) MT and (red dash) MI particles collected from the reaction vessel.

Representative TGA curves of MT and MI particles show that although they have the same weight loss at 800 °C, the MT particles showed faster weight loss after 150 °C. As, we discussed in the main text, the chance of hydrogen bonding between the NH_2 groups of the melamine reacted with isophthaldehyde is higher than terephthaldehyde and this resulted in more compact structure with narrower pores. Thus, the MI particles showed lower rate of weight loss between 150 to ~ 650 °C.

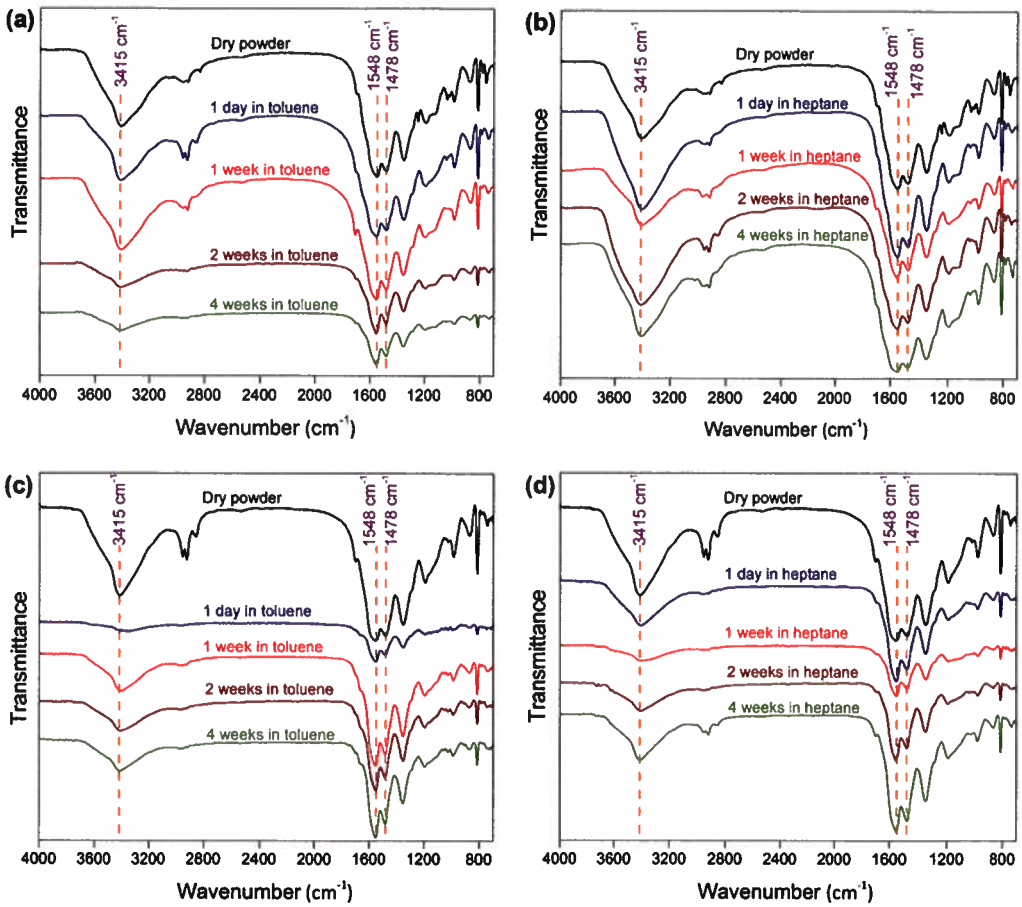

Figure A5.4 FTIR spectra of as synthesized and after stability test of MT particles in (a) toluene and (b) n-heptane and MI particles in (c) toluene and (d) n-heptane.

The presence of the characteristic peaks corresponding to the quadrant and semicircle stretching of the triazine ring at 1548 and 1478 cm^{-1}, respectively, confirms the successful incorporation of melamine into the POF structure via the aminal linkage as no feature band for the imine group at ~ 1600 cm^{-1} is observed. The band at 3419 cm^{-1} is attributed to the stretching vibration of N-H. The POFs particles showed excellent solvent stability no changes observed in the characteristic bands even after 4 weeks of soaking in toluene and n-heptane.

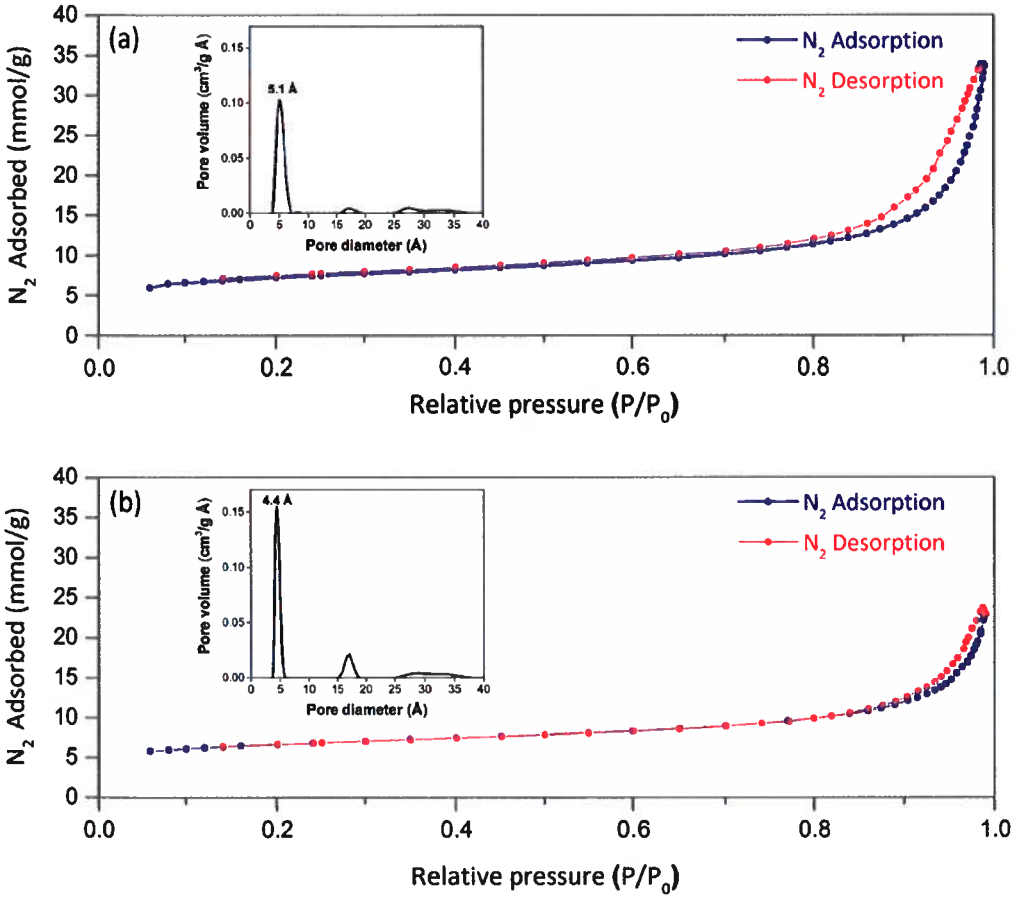

Figure A5.5 N_2 adsorption-desorption isotherm and pore size distribution of the (a) MT and (b) MI particles.

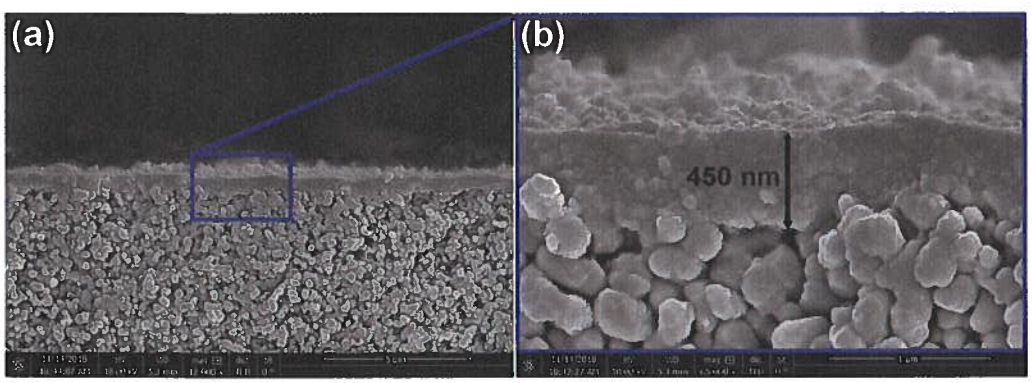

Figure A5.6 (a) MT and (b) MI particles. (a) Low and (b) high magnification cross-section FE-SEM images of MI POF-modified α-alumina membrane.

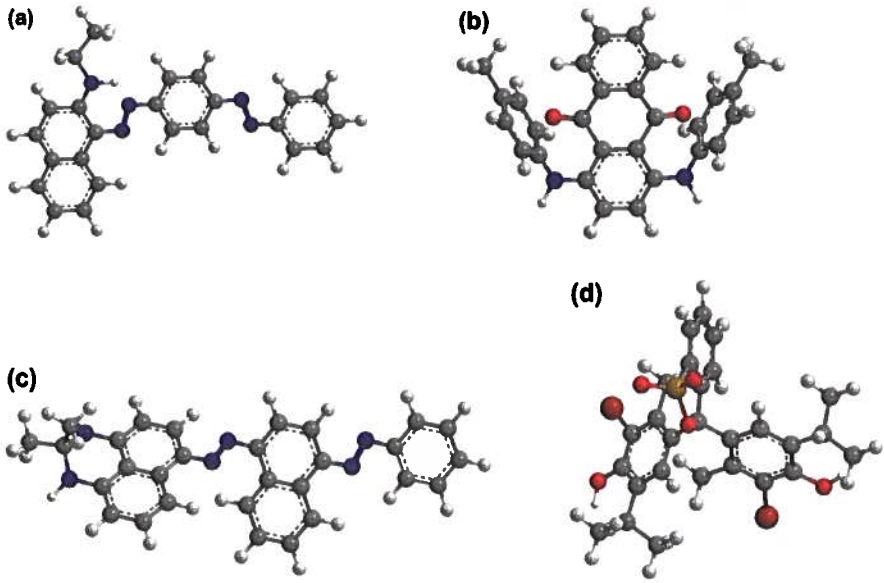

Scheme A5.1 Chemical structure of (a) Sudan Red 7B, (b) Solvent Green 3, (c) Sudan Black B and (d) Bromothymol Blue.

Table A5.1 Physical properties of the organic dyes used for OSN experiment.

Dye	λ_{max} (nm)	MW (g mol^{-1})	Van der Waals volume ($Å^3$)*
Sudan Red 7B	538	379.4	347
Solvent Green 3	637	418.4	377
Sudan Black B	577	456.5	407
Bromothymol Blue	402	624.3	465

* Note: van der Waals volume was measured by Marvin Sketch version 19.8 (ChemAxon, LLC).

Table A5.2 Performance comparison of MT POF-modified α-alumina membrane with ceramic and ATARMEM 122 polymeric membranes for Sudan Black B separation from organic solvents

Membrane	Solvent	Solute	Permeability ($L\ m^2\ h^{-1}\ bar^{-1}$)	Rejection (%)	Reference
γ-alumina-grafted C_{10}	Toluene	SB	2.0	98	[1]
STARMEM 122	Toluene	SB	1.1	91	[2]
PDMS grafted γ-alumina	Toluene	SB	2.3	65	[3]
PDMS grafted γ-alumina	Toluene	SB	3.0	45	[3]
PDMS grafted γ-alumina	n-hexane	SB	4.8	78	[4]
PDMS grafted γ-alumina	n-hexane	SB	2.8	88	[4]
PEG grafted γ-alumina	n-hexane	SB	3.7	54	[5]
PDMS grafted γ-alumina	n-octane	SB	3.4	71	[4]
PDMS grafted γ-alumina	n-octane	SB	2.9	80	[4]
MT POF-modified α-alumina	Toluene	SB	7.8	99	This study
MT POF-modified α-alumina	n-heptane	SB	9.2	98	This study

References

[1] M. Amirilargani, R.B. Merlet, A. Nijmeijer, L. Winnubst, L.C.P.M. de Smet, E.J.R. Sudhölter, Poly (maleic anhydride-alt-1-alkenes) directly grafted to γ-alumina for high-performance organic solvent nanofiltration membranes, Journal of Membrane Science, 564 (2018) 259-266.
[2] S. Darvishmanesh, J. Degrè, B.V.D. Bruggen, Performance of solvent-pretreated polyimide nanofiltration membranes for separation of dissolved dyes from toluene, Industrial and Engineering Chemistry Research, 49 (2010) 9330-9338.
[3] C.R. Tanardi, A. Nijmeijer, L. Winnubst, Coupled-PDMS grafted mesoporous γ-alumina membranes for solvent nanofiltration, Separation and Purification Technology, 169 (2016) 223-229.
[4] R.B. Merlet, C.R. Tanardi, I.F.J. Vankelecom, A. Nijmeijer, L. Winnubst, Interpreting rejection in SRNF across grafted ceramic membranes through the Spiegler-Kedem model, Journal of Membrane Science, 525 (2017) 359-367.
[5] C.R. Tanardi, R. Catana, M. Barboiu, A. Ayral, I.F.J. Vankelecom, A. Nijmeijer, L. Winnubst, Polyethyleneglycol grafting of γ-alumina membranes for solvent resistant nanofiltration, Microporous and Mesoporous Materials, 229 (2016) 106-116.

Chapter

6

Summary and Outlook

6.1 Summary

Organic solvent nanofiltration (OSN) is an energy-efficient and sustainable pressure-driven separation process in which the membrane forms the core of the unit. Despite all the progress made in this field, the implementation of OSN membranes in industry is still very slow. The most challenging target in the design of an OSN process is to enhance the physical/chemical resistance of the applied membranes while maintaining their high permeation and selective separation properties, especially for non-polar solvents. Currently OSN membranes need to be further developed to be applied successfully in industrial plants. This goal cannot be achieved without acquiring the knowledge of surface science and surface modification in order to make membranes with the desired performance. The focus of this PhD thesis is therefore on the exploration of novel, facile and efficient methods for the surface modification of porous ceramic substrates to fabricate OSN membranes with excellent performance compared to current existing state-of-the-art ceramic membranes.

This thesis is divided into four different parts, where part I (**Chapter 1**) serves as an introductory reading for OSN membranes and surface modification techniques, highlighting the important factors influencing the performance of OSN membranes and the recent advancements made in the synthesis and surface modification of ceramic OSN membranes. Part II (**Chapters 2 and 3**) describe new techniques for the direct covalent grafting of alumina membranes for OSN applications and a comparison is made between surface *and* pore modification. In part III (**Chapter 4**) Metal Organic Framework (MOF)-based membranes are investigated for the efficient adsorption of organic dyes. Finally, part IV (**Chapter 5**) reports a method for the fabrication of thin Porous Organic Frameworks (POFs) membranes as a selective layer on top of the supporting ceramic alumina membranes, including an investigation for OSN applications. A more detailed summary of each Chapter in this thesis is presented below.

In **Chapter 2**, different poly (maleic anhydride-*alt*-1-alkenes), using the alkenes 1-hexene, 1-decene, 1-hexadecene, and 1-octadecene, were used for the direct covalent grafting to γ-alumina membranes. Nucleophilic attack of the surface hydroxyl groups of the γ-alumina membranes on the carbonyl of the anhydride moieties starts the ring opening of the maleic anhydride (MA) units to form an ester bond with the surface and a remaining carboxylic acid group attached to the copolymer chain. The best OSN performance was obtained by the membranes grafted with poly (maleic anhydride-*alt*-1-decene). Although only the surface of the γ-alumina membranes were grafted by the applied polymers, and no pore shrinkage was found, the observed differences in OSN performance could be explained on the basis of the difference in the molecular weight (M_w) of the applied copolymers.

Chapter 3, compares the surface *versus* pore modification of the poly (maleic anhydride-*co*-styrene)-grafted on γ-alumina membranes. In this chapter, four different

copolymers of poly (maleic anhydride-*co*-styrene) were used for the direct grafting to the γ-alumina membranes: a high M_w alternating copolymer of MA and styrene (St) was synthesized and used for the direct grafting to the γ-alumina membrane; three commercially available low M_w random copolymers of St and MA were also investigated. It was shown that the covalent grafting mechanism is independent from the alternating or random character of the applied copolymers. Grafted copolymers with the highest M_w showed a higher permeability and a higher solute rejection compared to the lower M_W copolymers. The higher M_w copolymers mostly modify the surface, while the lower M_W copolymers also enter the pores of the γ-alumina membranes. Due to this additional pore grafting, the solvent permeability experiences a higher resistance. The shrinked pores are still relatively large as deduced from the observed solute rejections. These rejections are found to be larger for the surface grafted γ-alumina membrane if the M_W of the applied copolymer is higher.

The observed remarkable organic dye adsorption capacity of MIL-53(Al) and NH_2-MIL53(Al) MOFs modified α-alumina membranes are presented in **Chapter 4**. Both MOFs were synthesized directly on top of the α-alumina ceramic support. It was shown that a higher solvent permeability and a higher adsorption of Rose Bengal was obtained for NH_2-MIL53(Al) compared to MIL-53(Al). This work shows for the first time the very significant organic dye adsorption properties of MOF-based membranes in organic solvents. To date, all the research reported in this field connects the found separation performances with rejection and ignores any adsorption. It is therefore strongly recommended to investigate such membranes for their adsorption properties.

In **Chapter 5**, thin films of a melamine-based microporous polymer networks, *i.e.* melamine-terephthaldehyde (MT) and melamine-*iso*-phthaldehyde (MI) with a layer thickness of *ca.* 400 nm, was fabricated on top of α-alumina membranes. The combination of thin layers and the highly microporous polymeric network contribute to the found high and improved permeabilities and similar solute rejections in comparison to most polymeric membranes. The MT-modified α-alumina membrane showed a molecular weight cut-off (MWCO) of ~ 460 g mol^{-1} with a permeability of 7.8 and 9.2 L m^2 h^{-1} bar^{-1} for toluene and n-heptane, respectively. It is shown that the superior performance coupled with the high solvent stability, the use of POF-based membranes is a highly attractive choice for purification of non-polar organic solvents and it is expected to open new avenues in the applications of OSN.

In summary, this research shows different approaches for the surface modification of ceramic membranes to be applied in organic solvent purification. The modified membranes were used in harsh and aggressive media of polar and non-polar organic solvents and they showed excellent solvent stability during a long-period of the filtration process. The work illustrates the importance of the precise molecular engineering of the selective layer in order to attain highly permeable OSN membrane with remarkable solute rejection.

6.2 General remarks and outlook

Organic syntheses are generally performed in organic solvents and their high added value products need to be separated from the organic solvents used. The costs for separation and recovery of the organic solvents used are a significant fraction of the overall costs. OSN is a relatively young pressure driven-based filtration technology that allows size exclusion-based separation of solutes having a molecular weight (M_W) between 50-2000 g mol^{-1}. This separation technique might be cost effective in future solute and solvent separations and recovery processes. OSN consumes less energy than conventional solvent purification techniques based on distillation and evaporation [1]. Chemically stable membranes showing good solvent permeabilities and solute rejections are therefore needed.

In this thesis, different methods of surface modifications of both γ- and α-alumina ceramic membranes have been investigated for organic solvent purification. For the first time, direct grafting of polymers onto the mesoporous γ-alumina membranes was employed (Chapters 2 and 3). Grafting of the γ-alumina membranes via different maleic anhydride (MA)-based copolymers enabled us to simplify the surface modification process of the ceramic membranes by eliminating a pre-treatment step. This could be a significant step toward for industrial use of ceramic membranes for OSN applications as their preparation has become simpler. In addition, we showed to be able to tune between surface grafting and pore grafting by changing the molecular weight of the applied copolymers (Chapter 3). This observation is valid for ceramic membranes with different pore sizes, *i.e.* a defect-free surface grafting will result in a more permeable membrane with higher rejections, because the solvent permeability is inversely proportional to the thickness of the selective layer. Modification inside the pores was shown to be possible only near the pore entrances. This hardly effects the solute rejections and only retards the permeability.

In Chapter 5 the results obtained from the thin melamine-based microporous organic frameworks synthesized directly on top of the α-alumina membrane are described. Better control of the microporosity and thickness of the grafted polymeric organic framework are needed, in combination with simplification of the synthesis procedure. For instance, covalent organic frameworks (COFs), which provide an inherent porosity with well-defined pore aperture, ordered channel structures, a large surface area and excellent thermal and chemical stability can be applied on top of the porous ceramic support to make high-performance ceramic-based OSN membranes.

To date, most of the efforts in the field of ceramic OSN membranes were primarily focused on pore modification via grafting and other functionalization techniques rather than ultrathin film formation on top of the ceramic supports. The latter is more efficient to develop membranes that can withstand the harsh operating conditions, *i.e.* high temperatures and extreme pH, while preserving both selectivity and permeability at reasonable levels. Therefore synthesizing ultrathin selective

layers (at the nanometer scale) on top of the ceramic membrane can attain a great deal of attention for future research. Moreover, employing the modification techniques *together*, such as, *e.g.* ultrathin film formation and nanoparticle incorporation on top of the porous ceramic supports will result in membranes with no typical trade-off between the permeability and solute rejection that exists with the conventional OSN membranes.

In addition to the experimental aspects of the surface modification of ceramic-based OSN membranes, the development of their characterization and testing techniques are needed. For instance, knowing and understanding the precise depth of the prepared selective layer will help in the future molecular engineering of such membranes by selecting the proper functionalization agents. In addition, molecular modelling of the ceramic OSN membranes and computer simulations of their permeability, rejection and adsorption properties need to be developed to improve our understanding of their properties and helping us to guide to directions of research and applications.

Finally, apart from the development of new experimental methods for the fabrication of high-performance OSN membranes, simplifying the currently available techniques facilitates the use of ceramic-based OSN membranes at industrial scales. For instance, applying modification techniques that do not need specific (oxygen-free of high-temperature) conditions and can be easily performed under atmospheric condititons at room temperature will significantly reduce the total cost of the fabrication step. This opens new windows towards efficient and cost-effective preparation of OSN membranes which are highly interesting from the scaling-up point of view.

References

[1] G. Szekely, M.F. Jimenez-Solomon, P. Marchetti, J.F. Kim, A.G. Livingston, Sustainability assessment of organic solvent nanofiltration: From fabrication to application, Green Chemistry, 16 (2014) 4440-4473.

Chapter

6

Samenvatting

6.2 Samenvatting

Nanofiltratie van organische oplosmiddelen (Organic Solvent Nanofiltration, OSN) is een energiezuinige en ook duurzame scheidingsmethode, die gebaseerd is op een drukgradiënt, waarin het membraan een centrale functie vervult. Ondanks alle vooruitgang die gemaakt is op dit gebied, verloopt de toepassing van deze techniek in de industrie echter langzaam. De grootste uitdaging bij het ontwerpen van OSN-processen is het verbeteren van de fysische/chemische stabiliteit van de membranen, zonder daarbij eigenschappen zoals een hoge permeatie en selectiviteit aan te tasten door de aanwezigheid van apolaire oplosmiddelen. De huidige OSN-membranen moeten dus verder ontwikkeld worden om succesvol toegepast te kunnen worden in industriële installaties. Om dit doel te verwezenlijken, is meer kennis nodig van de oppervlakte-eigenschappen en oppervlaktemodificatie, zodat membranen met de gewenste eigenschappen gemaakt kunnen worden. De focus van dit proefschrift ligt dan ook op het onderzoeken van nieuwe, eenvoudige en efficiënte methoden voor de oppervlaktemodificatie van poreuze, keramische membranen om OSN-membranen te maken met uitzonderlijke prestaties in vergelijking tot de huidige 'state-of-the-art' keramische membranen.

Dit proefschrift is bestaat uit vier onderdelen, waarvan deel I (**Hoofdstuk 1**) dient als een inleiding in OSN-membranen en oppervlaktemodificatiemethoden, waarin de factoren die van invloed zijn op de eigenschappen van OSN-membranen worden besproken als ook de recente vorderingen op het gebied van oppervlaktemodificatiemethoden voor keramische membranen. Deel II (**Hoofdstukken 2 en 3**) beschrijven nieuwe technieken voor de directe covalente hechting aan aluminiumoxide membranen voor OSN en maakt onderscheid tussen het modificeren van het membraanoppervlak en de membraanporien. In deel III (**Hoofdstuk 4**) worden membranen, die gebaseerd zijn op 'Metal Organic Frameworks' (MOFs), onderzocht op de efficiënte adsorptie van organische kleurstoffen. Tot slot wordt in deel IV (**Hoofdstuk 5**) de fabricage van membranen van dunne 'Porous Organic Frameworks' (POFs) als selectieve toplaag op keramische aluminiumoxide membranen besproken. Deze membranen worden getest voor OSN-toepassingen. Een meer gedetailleerde samenvatting van elk hoofdstuk uit dit proefschrift is hieronder weergegeven.

In **Hoofdstuk 2** worden verschillende poly (maleïnezuuranhydride-*alt*-1-alkenen), waaronder de alkenen 1-hexeen, 1-deceen, 1-hexadeceen en 1-octadeceen, gebruikt voor de directe covalente koppeling aan γ-alumina membranen. Nucleofiele aanval door de hydroxyl groepen aan het γ-alumina oppervlak op de carbonyl groep van de anhydride groepen initieert de opening van de maleïnezuuranhydride (MA) ring, waarbij een esterbinding met het oppervlak wordt gevormd, en een overgebleven carbonzuurgroep verbonden aan de copolymeer keten. De beste resultaten werden verkregen met poly (maleïnezuuranhydride-*alt*-deceen). Hoewel alleen het oppervlak van de γ-alumina membranen gemodificeerd werd met de gebruikte polymeren en er geen vernauwing van de porieen werd gevonden, konden de waargenomen

resultaten goed verklaard worden op basis van het verschil in molecuulgewicht (M_w) van de gebruikte copolymeren.

Hoofdstuk 3 vergelijkt de oppervlaktemodificatie versus poriemodificatie met poly (maleïnezuuranhydride-*co*-styreen) aan γ-alumina membranen. Vier verschillende copolymeren van poly (maleïnezuuranhydride-co-styreen) worden gebruikt voor de directe hechting aan de γ-alumina membranen: een hoog M_w alternerend copolymeer van MA en styreen (St) werd gesynthetiseerd en gebruikt voor directe hechting aan het γ-alumina membraan; drie commercieel verkrijgbare laag M_w 'random' copolymeren van St en MA werden ook onderzocht. Het blijkt dat t het covalente hechtingsmechanisme onafhankelijk is van het alternerende of 'random' karakter van de gebruikte copolymeren. De copolymeren met het hoogste M_w laten een hogere permeatie en een hogere rejectie zien in vergelijking tot de lagere M_w copolymeren. De hoger M_w copolymeren modificeren voornamelijk het oppervlak, terwijl de lagere M_w copolymeren ook de poriën van de γ-alumina membranen kunnen modificeren. Als gevolg van deze extra porieenmodificatie ondervindt de permeatie van oplosmiddelen een hogere weerstand. Deze porieenmodificatie heeft echter vrijwel geen invloed op de rejectie van de opgeloste stoffen. Rejecties nemen toe door hoger M_w copolymeren te gebruiken.

De opmerkelijke adsorptiecapaciteit van organische kleurstoffen aan MIL-53(Al) en NH_2-MIL-53(Al) MOFs gemodificeerde α-alumina membranen wordt gepresenteerd in **Hoofdstuk 4**. Beide MOFs werden gesynthetiseerd direct bovenop het α-alumina membraan. Er werd aangetoond dat de permeatie van oplosmiddelen en de adsorptie van Rose Bengal groter was voor NH_2-MIL53(Al) vergeleken met MIL-53(Al). Dit werk toont voor het eerst aan dat er een significante adsorptie is voor organische kleurstoffen bij deze MOF-gebaseerde membranen. Tot op heden werd in vergelijkbaar onderzoek de waargenomen scheidingsprestaties uitsluitend met rejectie verbonden, en adsorptie geheel buiten beschouwing gelaten. Het is daarom sterk aan te raden deze membranen Ook te onderzoeken op deze adsorptie eigenschappen.

In **Hoofdstuk 5** wordt de fabricage beschreven van dunne films van microporeuze 'Polymer Organic Frameworks' (POFs), namelijk melamine-tereftaalaldehyde (MT) en melamine-iso-ftaalaldehyde (MI), met een filmdikte van ca. 400 nm, direct op α-alumina membranen. De combinatie van een deze dunne laag en een sterk microporeus polymeernetwerk draagt bij aan de gevonden hoge en verbeterde permeatie en vergelijkbare rejecties van de opgeloste stoffen in relatie tot de meeste polymere membranen. De MT-gemodificeerde α-alumina membranen toonden een molecuulgewichts-afkappunt (MWCO) van ~ 460 g mol^{-1} met een permeatie van 7.8 en 9.2 L m^2 h^{-1} bar^{-1} voor tolueen en n-heptaan, respectievelijk. De superieure prestaties in combinatie met de hoge stabiliteit in de gebruikte oplosmiddelen maakt het gebruik van POF-gebaseerde membranen een aantrekkelijke

keuze voor het zuiveren van apolaire organische oplosmiddelen, en er wordt verwacht dat dit nieuwe deuren opent naar de toepassing van OSN.

Samengevat toont dit onderzoek de verschillende benaderingen voor de oppervlaktemodificatie van keramische membranen voor toepassing in de zuivering van organische oplosmiddelen. De gemodificeerde membranen werden gebruikt in sterke en agressieve media van zowel polaire als apolaire organische oplosmiddelen, waarbij excellente stabiliteit werd aangetoond bij langdurig gebruik in filtratieprocessen. Dit werk benadrukt het belang van het nauwkeurige moleculaire ontwerpen en maken van de selectieve laag om OSN membranen te verkrijgen met een hoge permeatie en een opmerkelijke rejectie van de opgeloste stoffen.

Acknowledgement

"Happiness lies not in finding what is missing, but in finding what is present."

Tara Brach

Now, by looking to the past four years and coming to the end of this thesis, I would like to thank all the nice people along the way.

Firstly, I want to express my deep gratitude to my promotor, Prof. Dr. Ernst Sudhölter. Thank you Ernst, for all scientific and non-scientific discussions we had, constructive feedback, your trust letting me to have freedom to conduct my research independently and your constructive criticism. I have learned a lot from your wisdom and deep insights into science. A very warm thank you to Dr. Louis de Smet for your comments and efforts in improving my writing skills. I am still using your useful writing tips that are continuously updated. I started my PhD work with writing a comprehensive review paper that was a nice collaboration between TU Delft and my old friend, Dr. Mohtada Sadrzadeh from University of Alberta. Mohtada, I thank you for your help and I hope that we continue our collaborations in future.

During my PhD research I worked in close collaboration with people from University of Twente. I would like to thank Prof. Dr. Arian Nijmeijer, Prof. Dr. Louis Winnubst and Mr. Renaud Merlet for your feedback and thoughtful discussions. Arian and Louis, I truly enjoyed working with you and have learned a lot from your vision on the world of membranes. Louis, I greatly enjoyed all the discussions and regular meetings with you. Arian, I am still explaining to the people why we should use the term of permeability instead of permeance in liquid filtration. Renaud, thank you for all the measurements and feedback I received from you.

Completion of this PhD research would not be possible without the guidance and technical assistance of our technicians. Duco, thanks for helping me to construct my set-up and for your critical view on many subjects. Bart, thank you for developing the LabVIEW software for recording the weight of the balance in my experimental set-up, and letting me know how to use the XPS machine, and also for your great help for measuring my samples. Hozanna, I greatly appreciate your help and support to train me to work with the FE-SEM and FIB-SEM. Ben, thank you for showing me how to work with XRD and doing DSC analysis on my samples. Marcel, I thank you for your help and guidance to use the AFM. Willy, thank you for your kind and help in adsorption measurement and detailed data explanations. Further, I would like to say a big thank you to our secretaries in the OMI group; Els, Caroline and Karin. Thanks for all the administrative assistance, keeping us organised.

I had the chance to work with smart bachelor and master students during my PhD research that I would like to thank them. Pegah, you were a talented bachelor student that really was passionate to learn more and understand in detail. Thanks to your hard working that resulted in a publication. Gijs, you did a great master project and I am so happy that I had the opportunity to guide you. I would like

to say a big thank you for your fresh ideas, challenging questions and help in translating the summary of my thesis in Dutch. Giovana, you did a great job in your master project and I thank you for your efforts.

OMI was a rather small and great research group. Thank you Sumit, Hamid, Pierre, Rajeev, Lukasz, Anping, Laura, Liangyong , Nienke, Nick, Stijn and Naveen for the awesome time in the OMI.

I would like to express my deepest appreciation to my family. My achievement, if any, will always be yours and words are not able to express the real gratefulness I feel to you. First of all, I would like to say a big thank you to my father and mother for their unconditional love, encouraging me in all of my pursuits and by inspiring me to follow my dreams. Maman, Baba thank you for teaching me that my job in life is to learn, to be happy and to understand myself, only then I could know and understand others.

Anahid, *azizam*, my love and my best friend, it is impossible to put on words your great, pure and unconditional love and supports during the past years. You have been extremely supportive of me throughout this entire way. Now, that I look back I see it was not possible to stand on this point without you. I am so glad and grateful to have you in my life.

List of Publications

Publications of Mohammad Amirilargani (source: Scopus, last assessed Sep 2019)

Total 22 peer-reviewed publications, 2 unpublished manuscripts

M. Amirilargani, G. N. Yokota, G. H. Vermeij, R. B. Merlet, G. Delen, L. D. B. Mandemaker, B. M. Weckhuysen, A. Nijmeijer, L. Winnubst, L.C.P.M. de Smet, E.J.R. Sudhölter, Melamine-based microporous organic framework thin films on an alumina membrane for high-flux organic solvent nanofiltration, *Submitted.*

R. Merlet, N. Kyriakou, **M. Amirilargani,** E.J.R. Sudhölter, L.C.P.M. de Smet, A. Nijmeijer, M. Pizzoccaro-Zilamy, L. Winnubst, A new, green thioether-based cross-linked membrane for nanofiltration applications, *Submitted.*

1. **M. Amirilargani**, R.B. Merlet, L. Chu, A. Nijmeijer, L. Winnubst, L.C.P.M. de Smet, E.J.R. Sudhölter, Molecular separation using poly (styrene-*co*-maleic anhydride) grafted to γ-alumina: Surface versus pore modification, *J. Membr. Sci.* 15 **(2019)** 298.

2. **M. Amirilargani**, R.B. Merlet, P. Hedayati, A. Nijmeijer, L. Winnubst, L.C.P.M. de Smet, E.J.R. Sudhölter, MIL-53(Al) and NH_2-MIL-53(Al) membranes on α-alumina for highly efficient removal of Rose Bengal from organic solvents, *Chem. Comm.* 55 **(2019)** 4119.

3. R.B. Merlet, **M. Amirilargani**, L.C.P.M. de Smet, E.J.R. Sudhölter, A. Nijmeijer, L. Winnubst, Growing to shrink: nano-tunable polystyrene brushes inside 5 nm mesopores, *J. Membr. Sci.* 572 **(2019)** 632.

4. **M. Amirilargani**, R.B. Merlet, A. Nijmeijer, L. Winnubst, L.C.P.M. de Smet, E.J.R. Sudhölter, "Poly (maleic anhydride-alt-1-alkenes) directly grafted to γ-alumina for high-performance organic solvent nanofiltration membranes", *J. Membr. Sci.* 564 **(2018)** 259.

5. **M. Amirilargani**, M. Sadrzadeh, E.J.R. Sudhölter, L. de Smet, "Surface modification methods of organic solvent nanofiltration membranes", *Chem. Eng. J.* 289 **(2016)** 562.

Before this thesis

6. **M. Amirilargani**, T. Mohammadi, B. Sadatnia, "Novel poly (vinyl alcohol)/multiwalled carbon nanotubes nanocomposite membranes for pervaporation dehydration of isopropanol: poly(sodium 4-styrenesulfonate) as a functionalization agent", *Ind. Eng. Chem. Res.* 53 **(2014)** 12819.

7. **M. Amirilargani**, B. Sadatnia, Poly (vinyl alcohol)/zeolitic imidazolate frameworks (ZIF-8) mixed matrix membranes for pervaporation dehydration of isopropanol, *J. Membr. Sci.* 469 **(2014)** 1.

8. A. Ghadimi, **M. Amirilargani**, T. Mohammadi, N. kasiri, B. Sadatnia, Preparation of alloyed poly(ether block amid)/poly(ethylene glycol diacrylate) membranes for separation of CO_2/H_2 (syngas application), *J. Membr. Sci.* 458 **(2014)** 14.

9. **M. Amirilargani**, A. Ghadimi, M. Ahmadzadeh Tofighy, T. Mohammadi, Effects of poly (allylamine hydrochloride) as a new functionalization agent for preparation of poly vinyl alcohol/multiwalled carbon nanotubes membranes, *J. Membr. Sci.* 447 **(2013)** 315.

10. **M Amirilargani**, A Sabetghadam, T Mohammadi, Polyethersulfone/polyacrylonitrile blend ultrafiltration membranes with different molecular weight of polyethylene glycol: preparation, morphology and antifouling properties, *Polym. Adv. Tech.* 23 **(2012)** 398.

11. **M. Amirilargani**, T. Mohammadi, Synthesis and characterization of asymmetric polyethersulfone membranes: effects of concentration and polarity of nonsolvent additives on morphology and performance of the membranes, *Polym. Adv. Tecl.* 22 **(2011)** 962.

12. M. Sadrzadeh, **M. Amirilargani**, K. Shahidi, T. Mohammadi, Pure and Mixed gas permeation through a composite polydimethylsiloxane membrane, *Polym. Adv. Technol.* 22 **(2011)** 586.

13. **M. Amirilargani**, T. Mohammadi, E. Saljoughi, Improvement of permeation performance of polyethersulfone (PES) ultrafiltration membranes via addition of Tween-20, *J. App. Polym. Sci.* 115 **(2010)** 504.

14. **M. Amirilargani**, M. Sadrzadeh, T. Mohammadi, Synthesis and characterization of polyethersulfone membranes, *J. Polym. Res.* 17 **(2010)** 363.

15. **M. Amirilargani**, T. Mohammadi, E. Saljoughi, M.R. Moghbeli, Effect of coagulation bath temperature and Polyvinylpyrrolidone content on asymmetric polyethersulfone membranes, *Polym. Eng. Sci.* 50 **(2010)** 885.

16. E. Saljoughi, **M. Amirilargani**, T. Mohammadi, Effect of PEG additive and coagulation bath temperature on the morphology, permeability and thermal/chemical stability of asymmetric CA membranes, *Desalination* 262 **(2010)** 72.

17. E. Saljoughi, **M. Amirilargani**, T. Mohammadi, Asymmetric cellulose acetate dialysis membranes: Synthesis, characterization, and performance, *J. App. Polym. Sci.* 116 **(2010)** 2251.

18. **M. Amirilargani**, T. Mohammadi, E. Saljoughi, Effects of Tween 80 concentration as a surfactant additive on morphology and permeability of flat sheet polyethersulfone (PES) membranes, *Desalination* 249 **(2009)** 837.

19. **M. Amirilargani**, T. Mohammadi, Effects of PEG on Morphology and Permeation Properties of Polyethersulfone Membranes, *Sep. Sci. Technol.* **44 (2009)** 3854.

20. **M. Amirilargani**, T. Mohammadi, Preparation and characterization of asymmetric polyethersulfone (PES) membranes, *Polym. Adv. Technol.* 20 **(2009)** 993.

21. M. Sadrzadeh, **M. Amirilargani**, K. Shahidi, T. Mohammadi, Gas permeation through a synthesized composite PDMS/PES membrane, *J. Membr. Sci.* 342 **(2009)** 236.

22. E. Saljoughi, **M. Amirilargani**, T. Mohammadi, Effect of poly(vinyl pyrrolidone) concentration and coagulation bath temperature on the morphology, permeability and thermal/chemical stability of asymmetric CA membranes, *J. App. Polym. Sci.* 111 **(2009)** 2537.

Selected Presentations

Nanotunable & versatile OSN membranes | Amersfoort , The Netherlands, ISPT annual event, **Poster, 13.11.2018**

Maleic anhydride based copolymers grafted to γ-alumina for organic solvent nanofiltration: Importance of the copolymer structure | Valencia, Spain, Euromembrane 2018, **Oral and Poster, 11.07.2018**

Highly selective organic solvent nanofiltration membranes by grafting alternating copolymers to γ-alumina | Twente, The Netherlands, Netherlands Process Technology Symposium (NPS 15), **Oral, 30.05.2018**

Directly grafted copolymer on γ-alumina membranes for organic solvent nanofiltration: effects of copolymer structure | San Francisco, USA, International Congress on Membranes and Membrane Processes (ICOM 2017), **Oral, 01.08.2017**

Organic solvent nanofiltration with copolymer functionalized γ-alumina membranes | Saint Petersburg, Russia, 6th International Conference on Organic Solvent Nanofiltration, **Oral, 05.06.2017**

Modular Functionalized Ceramic Nanofiltration Membranes | Amersfoort , The Netherlands, ISPT day, **Poster, 14.11.2017**

About the Author

Mohammad Amirilargani was born in Noshahr, a small town in north province of Mazandaran in Iran. After obtaining his high school diploma in mathematics and physics, he continued his studies in Chemical Engineering at University of Mazandaran. After graduation from bachelor study, he was accepted in the national entrance exam to start his master study in Tehran to continue his passion about the Chemical Engineering. He got his MSc degree from Iran University of Science and Technology (IUST) with the thesis title of "Preparation, Characterization and Performance of Polymeric Microfiltration Membranes".

After his graduation, he joined Research Institute of Petroleum Industry as a *Research and Development (R&D) Engineer*. After two years, he moved to Petrochemical Research and Technology Company and started his work as a *Product Development Engineer*.

In 2015 and after moving to the Netherlands, he accepted the offer to start his PhD study under the supervision of Prof. Dr. Ernst Sudhölter and Dr. Louis de Smet in Department of Chemical Engineering at Delft University of Technology (TU Delft). His PhD project was part of the research program entitled "Modular Functionalized Hybrid Organic-Inorganic Membranes" and was conducted within the framework of the Institute for Sustainable Process Technology (ISPT) and is jointly financed by the Netherlands Organization for Scientific Research (NWO) and ISPT. This PhD project was in close collaboration with the Inorganic Membranes Group at University of Twente and aimed to develop novel hybrid polymeric-ceramic membranes which withstand in harsh and aggressive media such as polar/non-polar organic solvents and its outcome is presented in this thesis.

During his PhD study he won two prestigious awards. He won the Elias Klein Founder's Award from North American Membrane Society (NAMS) and Travel Award from European Membrane Society (EMS).

From June to September 2019, he worked for 3 months as a *Researcher* at Wetsus, European Centre for Water Excellence and from September 2019 he joined European Membrane Institute (EMI) as a *Researcher*.